Rosalie Dawn McKay

Experimental and modelling study of subsea oil releases

Focusing on small leaks from an aging oilfield off the Norwegian Continental Shelf

NTNU
Kunnskap for en bedre verden

Rosalie Dawn McKay

Experimental and modelling study of subsea oil releases

Focusing on small leaks from an aging oilfield off the Norwegian Continental Shelf

NTNU

Norwegian University of
Science and Technology

Abstract

With advances in exploration and extraction technology, oilfields that would otherwise have been ready for decommission are expected to produce oil for many more years. While beneficial to extract as much resource as possible from existing fields, this prolonged usage also increases the potential for oil leaks from aging pipelines. These pipeline leaks can produce high velocity conditions that emit plumes of small droplets of oil, gas and produced water. This is in contrast to large diameter blowouts where much larger droplets are expected. The exit parameters and resulting size distribution of oil droplets have a significant impact on the fate of oil in the environment.

Using the SINTEF MiniTower in conjunction with a silhouette camera, the droplet size distributions for discharge conditions representative of small diameter, high velocity leaks of oil and produced water were obtained. These distributions were then used to empirically optimize the coefficients, A 8.5 and B 7.68, for use in droplet size prediction with the Modified Weber algorithm. These optimized coefficients predicted larger droplet sizes than the previously reported values, for small diameter, high velocity releases. A series of pipeline leaks and blowouts operating under different seasonal and release conditions were generated with the SINTEF oil spill modelling simulation tool, OSCAR. The Njord field was selected as a proxy for mature oilfields along the Norwegian Continental Shelf. The releases modelled produced thin and spread out surface slicks, which limited the effectiveness of response methods. The low surface oil thickness limited shoreline oiling, and the formation of tarballs would not be expected. This makes the Njord field an unlikely candidate source for oil pollution samples collected in the Frøya municipality region during an excursion in 2017. This fieldwork was carried out as part of the course Marine Organic Environmental Chemistry KJ3050 as a requisite of the Environmental Toxicology and Chemistry Master program at NTNU. Experimental and modelling studies are necessary to ensure appropriate monitoring and contingency planning for maturing oilfields.

Acknowledgements

Table of Contents

List of Abbreviations

Abbreviation	Meaning
NCS	Norwegian Continental Shelf
OSCAR	Oil Spill Contingency and Response
GOR	Gas to oil ratio
GC/FID	Gas chromatography/flame ionization detector
GC/MS	Gas chromatography/mass spectrometry
PAH	Polycyclic aromatic hydrocarbon
SilCam	Silhouette Camera
LabView	LabView systems engineering software
LISST-100	Laser In-Situ Scattering and Transmissiometry
ROV	Remotely operated vehicle
ECD	Equivalent Circular Diameters
NOFO	Norsk Oljevernforening For Operatørselskap
NVODS	National Virtual Ocean Data System
IUCN	International Union for Conservation of Nature
NTNU	Norwegian University of Science and Technology
MSENVITOX	Master of Science in Environmental Toxicology and Chemistry
KJ3050	NTNU Master course, Marine Organic Environmental Chemistry

List of Symbols

Symbol	Explanation
We	Weber number
U	Exit velocity
D	Orifice diameter
σ	Interfacial tension
ρ	density
Re	Reynolds number
μ	Dynamic velocity
Oh	Ohnesorge
c	Constant of proportionality
d	Droplet diameter
α	Constant of proportionality
ε	Turbulent dissipation rate
A	Empirical factor
V_i	Viscosity number
B	Empirical factor
We^*	Modified Weber number
Q	Volume flow
A_N	Nozzle cross section
ν	Kinematic viscosity
M	Momentum flux
n	Gas volume fraction
g	Acceleration of gravity
g'	Reduced gravity
Fr	Exit Froude number
P	Pixel size
π	pi
D_{min}	Minimum quantifiable diameter

List of Figures

List of Tables

1 Introduction

The transport of oil through the marine environment is complex, and understanding it is essential for the identification and mitigation of the human, economic and environmental risks associated with coastal oil activities. The Deepwater Horizon accident on April 20, 2010 released more than 779 million litres of oil over the course of 87 days (McNutt et al., 2011). While this spill represents the worst case scenario, such occurrences are rare (Vinnem, 2014). Far more likely is the occurrence of small leaks, particularly in aging subsea infrastructure (Jernelöv, 2010); the National Research Council of the United States estimates that the worldwide accidental release of oil from pipelines is 12000 to 37000 tonnes per year (National Research Council Transportation Research Board, 2003). Oil spills may lead to injuries or fatalities and impact the environment; they are costly to both the reputation and financial gain of the responsible party (Jernelöv, 2010). Oil companies in the Norwegian Sea are therefore invested in ensuring the environmental and workplace safety of their installations (Tinmannsvik et al., 2011; Vinnem, 2014).

1.1 New life to old fields: lifespan extension on the Norwegian Continental Shelf

The Ministry of Petroleum and Energy in Norway oversees that all recoverable oil is removed from a field before decommissioning takes place (Norsk Petroleum, 2019). This ensures efficient use of infrastructure and resources, with many factors leading to the extended use of existing facilities. Such as, the reservoir produces more oil than initially estimated, advancements in technique allow greater extraction, or the ability to link to another reservoir (Palkar and Markeset, 2012).

The production life of an oilfield begins with very high yields of oil, which then steeply decline as the field matures (Höök and Aleklett, 2008). In order to recover the remaining oil, water or gas injection are often used in order to increase pressure and displace oil out of the reservoir. A common strategy to increase yields on the Norwegian Continental Shelf (NCS) is water injection (Norwegian Petroleum Directorate, 2019). With many fields on the NCS entering a mature stage of production, the balance between the environmental impact of building new infrastructure while

1

minimizing the risk of failure of aging facilities must be maintained. The sea is a harsh environment and facilities face significant weathering. Both experimental and modelling studies are necessary to predict the behaviour of potential leak scenarios from aging structures in order to develop appropriate monitoring and contingency strategies.

1.2   Oil droplets and their fate in the environment

Oil droplets formed as a result of deepsea releases of oil and gas will have different fates in the environment relative to their size. Droplets larger than 5mm will reach the surface within a couple of hours from a depth of 1000m, whereas droplets down to 0.5mm may take up to a day to travel the same distance (Brandvik et al., 2013; Johansen, 2003). Droplets below 100μm may remain in the water for weeks to months before surfacing (Brandvik et al., 2013). Other factors may cause these fine droplets to remain submerged for greater periods of time, such as, turbulent mixing, density stratification and cross flows (Johansen, 2003).

Therefore, the size distribution of oil droplets is a predictor for the behaviour of an oil spill. It determines the surface thickness, area and location, as well as, the water column concentrations. The presence of oil at the surface may have operational, safety and environmental impacts (French-McCay, 2009, 2002; Johansen et al., 2003a; Makatounis et al., 2017). Concerns over flash point or a sensitive shoreline ecosystem in the vicinity are examples. Droplets that remain suspended in the water column may have implications for toxicity to sea life, and dissolution and biodegradation rates (North et al., 2015; Socolofsky et al., 2015).

The size distribution of droplets is determined by the release conditions. The outlet diameter, release velocity, oil properties, water and gas ratios, and physical parameters (pressure, temperature) impact the droplet formation (Brandvik et al., 2015a; Johansen, 2003; Wang et al., 2018). In turn, the droplets then interact with the environmental conditions, such as currents and depth, which determine their fate (Johansen, 2003; Johansen et al., 2015; Socolofsky et al., 2015). A typical mature oil field on the NCS would expect a large amount of surface spreading due to high percentages of water in the reservoir, predicting thin surface slicks.

1.3 Leak detection

One of the main concerns arising from using aging infrastructure is that resulting leaks may not be detectable with current monitoring techniques and technology (Kishawy and Gabbar, 2010; Leifer et al., 2012). As opposed to large scale blowouts, small leaks may occur from pinhole sized exit holes (less than 10mm) and can have large exit velocities. This leads to very thin surface oil slicks or none at all, which can be difficult to detect, particularly on rough seas (Brekke and Solberg, 2005). Very small, thin surface slicks may go undetected for long periods of time (Gajbhiye and Kam, 2008).

1.4 Oil Spill Modelling

Modelling is used to make predictions of the behaviour of potential oil spills, this is important for allocation of recovery resources and strategies for monitoring and prevention (Reed et al., 1999; Spaulding, 2017; Vinnem, 2014). Most modern models use a Lagrangian approach for the transport processes of oil droplets by advection, dispersion, wind, wave and currents; with individual algorithms for fate, such as surface, atmosphere, dissolution, biodegradation, water column, sediment, and shoreline (Spaulding, 2017). Many of the algorithms used are empirically based (Chen and Yapa, 2007). The SINTEF OSCAR simulation tool employs the Modified Weber equation, using constants derived from SINTEF laboratory studies in the Tower Basin and the DeepSpill experiment (Brandvik et al., 2013; Johansen et al., 2013). This equation is expected to best fit the conditions from which it is derived (Johansen et al., 2003a).

The OSCAR simulation tool takes in to account the composition and properties of the oil, oil weathering, oceanographic conditions and response. Resulting in a simulation tool able to predict the fate and effects of oil released in the marine environment.

1.5 Introduction to the Njord field

The Njord oil field is located off the western coast of Norway, Figure 1-1. Production began in 1997 and was originally intended to operate for 16 years. The Njord field was shut down in 2016

for extensive platform upgrades in order to extend production into the nearby Hyme, Bauge and Fenja fields. The recent upgrades will extend the extraction lifetime well in to 2040 (Offshore Technology, n.d.).

Figure 1-1 Location of the Njord field. Image obtained from Google Maps (n.d.).

The extension of operation of the Njord field is a common trend for aging oilfields on the NCS. This highlights the need to study the outcomes of leaks from aging infrastructure. Possible scenarios include high pressure small and medium pipeline leaks with lower GOR liquid, and blowouts with greater percentages of produced water and gas. A blowout from a mature field would not be expected to have consequences with the severity of the Deepwater Horizon accident, as the pressure of the reservoir is much lower and much of the oil has already been removed. These represent general estimations of the possible scenarios expected along the NCS and are not meant to be specific to the Njord field.

The focus of this study is to look at possible leak and blowout scenarios that may be expected of a typical aging oilfield on the NCS. Experiments are carried out to optimize the algorithm used to predict small, high velocity leaks. An assessment is made as to whether the Njord field is a possible

source of oil pollution samples collected along the coast of Frøya, outside of the Trondheim fjord, in September 2017. These samples were collected during participation in the course Marine Organic Environmental Chemistry, KJ3050, which is a requisite of the MSENVITOX Master of Environmental Toxicology and Chemistry program at NTNU.

2 Theory

This section provides a discussion on factors affecting oil as it is transported through the marine environment following release from a well blowout or pipeline leak. Several mathematical relations exist to describe the droplet formation in a turbulent jet and those relevant for this study are presented.

2.1 Deepsea versus shallow blow out

The depth of the release is one of the main factors for the fate of oil and gas in the marine environment.

In a shallow blowout, gases will behave as ideal gases as a result of lower pressure and higher temperature. This results in a more buoyant plume; all of the gas, oil and entrained water will rise quickly to the surface. An outward horizontal flow at the surface is established by the surfacing entrained water, spreading the oil to a relatively homogenous surface slick, see figure 2-1 (Johansen, 2003). In this case, the droplet size will have an impact on the spreading and distribution of the resulting oil slick.
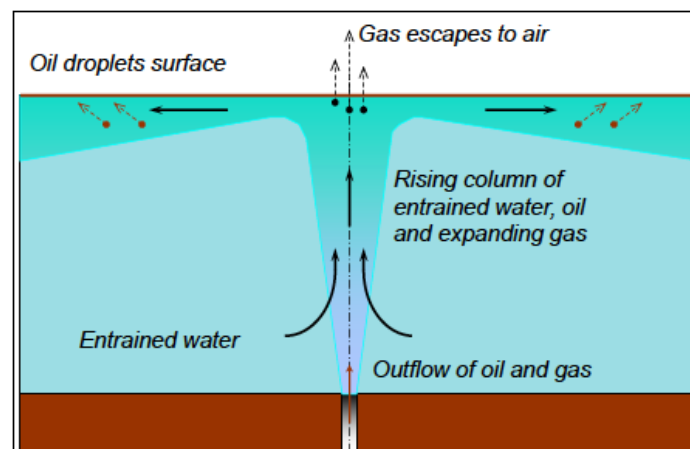
Figure 2-1 The outflow of oil and gas with entrained water from a shallow release, spreading oil on the surface. Illustration from Johansen (2003).

Due to the increased pressures and lower temperatures, deepsea releases behave differently than those in shallow waters (Johansen, 2003). The discharged oil plume will be less buoyant due to

the compression of gas, nonideal gas behaviour and the potential for substantial dissolution of gas into the water. The reduced buoyancy of the deepwater plume increases its likelihood of becoming trapped in density stratifications or bent over by cross currents. When this happens, gas bubbles and oil droplets will separate from the plume according to their own terminal velocities (Brandvik et al., 2013). Large droplets which have a higher velocity, travel quickly to the surface, forming an oil slick just above or near the discharge site. The smaller droplets have a lower velocity and thus stay with the plume for a longer period of time before rising. Some of the smallest droplets may not surface at all and will be subject to vertical turbulent mixing, enhancing dissolution and biodegradation (Reed et al., 1999). This results in a fairly complex distribution of the oil in the water column as droplets rise to the surface (figure 2-2).
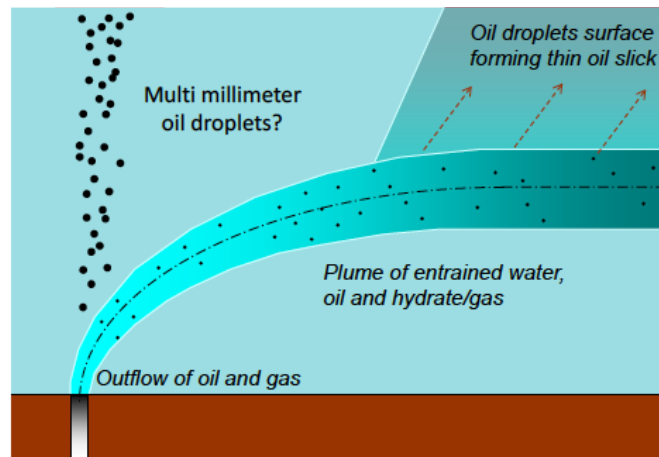
Figure 2-2 The separation of oil droplets from a plume bent in a crossflow. Illustration from Johansen (2003).

2.2 Oil Chemistry

Oil is a complex mixture of substances and the combined properties affect its behaviour at sea. The following is a discussion of composition, properties and weathering at sea.

2.2.1 Composition

Crude oils are comprised of thousands of different chemical components. The composition varies from oil to oil, and can differ among oil samples collected from the same field at different times. The distribution of chemical components imparts the physical properties to an oil and therefore affects how the oil behaves in the environment. Figure 2-3 illustrates the division of crude oil into

the main chemical groups. The majority of crude oil consists of hydrocarbons; from simple, volatile gases up to large molecules comprising over 100 carbon atoms. These include saturated and unsaturated molecules of linear, branched or cyclic structures (Brandvik and Daling, 2015).

```
                                          ┌──────────────────┐
                              ┌──────────▶│ n-alkanes, iso-  │
                   ┌─────────┐│           │ alkanes          │
                   │Paraffins│┤           └──────────────────┘
                   └─────────┘│           ┌──────────────────┐
                  ╱            └──────────▶│ Waxes (20+ carbon│
   ┌────────────┐╱                        │ atoms)           │
   │Hydrocarbons│                         └──────────────────┘
   └────────────┘             ┌──────────┐┌──────────────────┐
  ╱        │    ╲             │Naphthenes├┤ cycloalkanes     │
 ╱         │     ╲            └──────────┘│ containing 1+    │
┌─────────┐│      ╲                       │ saturated rings  │
│Crude oil│       ╲          ┌──────────┐ └──────────────────┘
└─────────┘│       ╲─────────│Aromatics │ ┌──────────────────┐
  ╲        │                 └──────────┘ │ unsaturated cyclic│
   ╲  ┌──────────────┐       ┌──────────┐ │ hyddrocarbons    │
    ╲ │ Hetroatomic  │───────│ Resins   │ └──────────────────┘
      │ organics     │       └──────────┘ ┌──────────────────┐
      └──────────────┘                    │ large polar      │
               ╲                          │ molecules, may   │
                ╲         ┌────────────┐  │ have surface-    │
                 ╲────────│Asphaltenes │  │ active           │
                          └────────────┘  │ properties, NSOs │
                                          └──────────────────┘
                                          ┌──────────────────┐
                                          │ condensed        │
                                          │ polycyclic aromatic│
                                          │ compounds        │
                                          └──────────────────┘
```
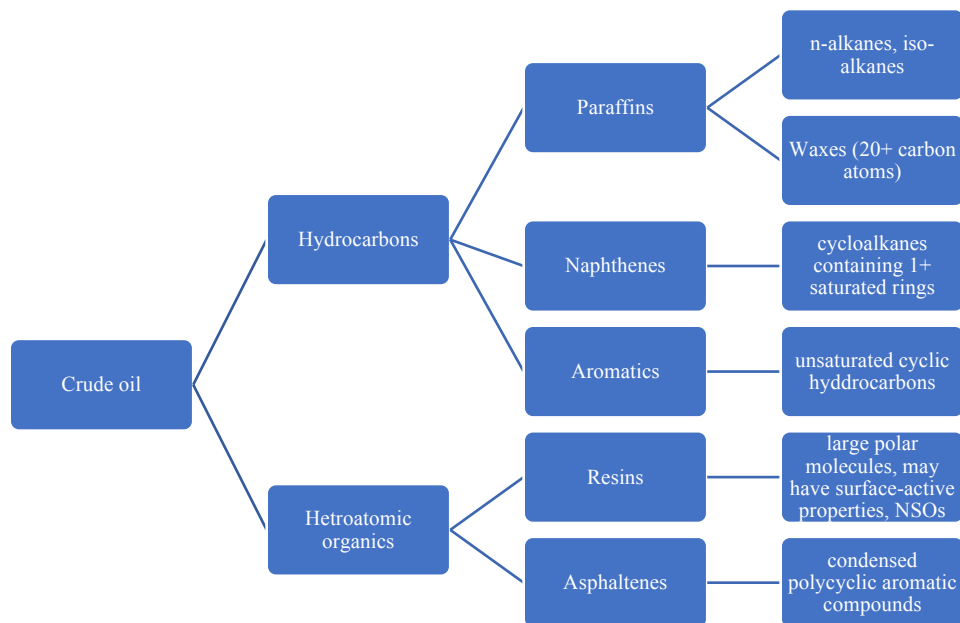
Figure 2-3 Crude oil composition. Adapted from Brandvik and Daling (2015).

Hydrocarbons can be divided in to three main groups, paraffins, naphthenes and aromatics. Paraffins include straight chain (n-alkanes) and branched chain (iso-alkanes) aliphatic compounds. Waxes, typically n-alkanes with 20 or more carbon atoms, are an important subgroup of paraffins, as they may precipitate out at low temperatures, which increases the pour point of the oil (Brandvik and Daling, 2015). Naphthenes are cycloalkanes containing one or more saturated rings; 5 and 6 membered rings are the most common. The rings may have paraffinic side chains. Aromatics consist of unsaturated, cyclic hydrocarbons which may also have paraffinic side chains.

In addition to the pure hydrocarbons discussed above, some compounds in crude oil may contain heteroatoms, including oxygen, nitrogen, sulphur and some trace metals such as vanadium or nickel. Resins tend to be large, with molecular weights ranging from 700-1000 g/mol, and are relatively polar (Brandvik and Daling, 2015). They may possess surface-active properties which have implications for interactions with water, especially in the formation of water-in-oil emulsions. Examples include carboxylic acids, sulphoxides and phenol-like compounds. Asphaltenes are large molecules consisting of condensed polycyclic aromatic compounds, with 6-20 aromatic rings

and side chains. Their molecular weights can range from 1000-10000 g/mol (Brandvik and Daling, 2015). This is a broad and complex group of chemicals with implications for the viscosity and density of the oil.

2.2.1.1   Oil spill fingerprinting

The combination of chemicals in oil result in unique chemical signatures that can be identified using qualitative and quantitative techniques. GC/FID and GC/MS chromatograms of a spilled oil and possible candidate oils can be compared in a qualitative manner, particularly for assessing the degree of weathering (ASTM, 1990; Bayona et al., 2015). A quantitative approach uses relative or absolute concentration measurements of chromatographic peaks, usually PAHs and biomarkers, followed by a statistical or numerical analysis of these parameters (Daling et al., 2002; Stout et al., 2005). Sometimes internal standards are added to aid in quantification (ASTM, 2000). PAHs and biomarkers are often used because of their resistance to weathering and characteristic distributions which may be unique to oils from a certain region or reservoir. Biomarkers are naturally occurring, stable hydrocarbons that occur in crude oils and most petroleum products.

2.2.2   Crude oil properties

The composition of an oil leads to different properties that are measured in the laboratory. The distillation curve, evaporative loss, density, viscosity, pour point and flash point have important implications for contingency planning and oil spill response.

The boiling point and boiling range are used to determine the relative distribution of oil components as a function of the molecular weight or of chemical composition. A distillation curve is obtained by measuring the amount of oil distilled as a function of the boiling point. Evaporative loss is used to approximate the weathering at sea over time. Figure 2-4 shows the distillation curves and evaporative loss for a selection of Norwegian oils.
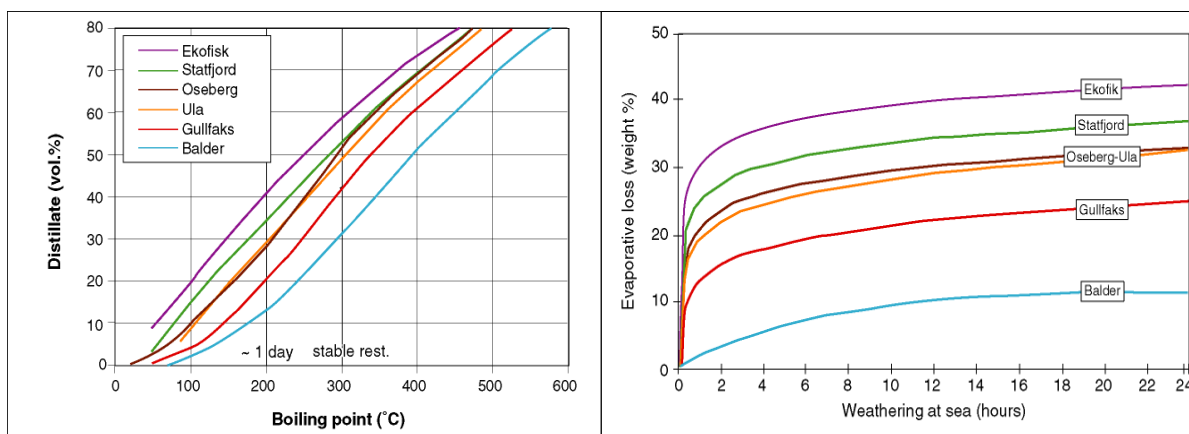
Figure 2-4 Distillation curve (left) and calculated evaporative loss at sea (right) of 6 Norwegian Crude oils. Figures obtained from Brandvik and Daling (2015).

The ratios of different components will affect oil properties like density, viscosity and pour point. Crude oils high in low molecular weight paraffinic compounds tend to be of lower density. While high molecular weight aromatic, naphthenic and asphaltenic crudes will have higher densities. The viscosity is the inner friction or resistance to flow, and varies with temperature. It has an impact on the ability of the oil to spread on the sea surface. High viscosity oils may have high asphaltene content. The density and viscosity impact the efficacy of boom and skimmer use. The pour point is a laboratory measure in which oil is cooled without disturbance and ceases to flow when subjected to a slight disturbance (Brandvik and Daling, 2015). As the oil is cooled, wax crystals precipitate. The higher the wax content of the oil, the higher the pour point. Highly paraffinic oils may have pour points in excess of 30°C and may become semi-solid at sea (Brandvik and Daling, 2015). Low viscosity, naphthenic crude oils can have pour points well below -40°C (Brandvik and Daling, 2015). This can be due to the absence of paraffinic components altogether or due to the presence of low molecular weight naphthenic components that are able to keep wax components in solution. Increased pour-point due to evaporation will decrease the dispersibility of an oil. The density, viscosity and pour point will increase over time as the oil weathers.

Flash point is the lowest temperature at which the vapour generated by heating an oil can be ignited by flame. This is dependent on the low molecular weight composition of the oil and will increase over time as the oil is subject to evaporation at sea. This is primarily a measure of the hazard for explosion and fire during storage and transport of the oil (Brandvik and Daling, 2015).

2.2.3 Weathering

Weathering processes produce changes to the physical and chemical properties of crude oil, resulting in changes to the oil's behaviour at sea. The degree of weathering is influenced by the original physical and chemical properties of the oil, the environmental conditions (waves, wind, sunlight, temperature) and the water properties (current, temperature, salinity, density, oxygen, bacteria, nutrients, presence of particles). Weathering rates are usually highest immediately after a spill. An overview of the main weathering processes is shown in figure 2-5.
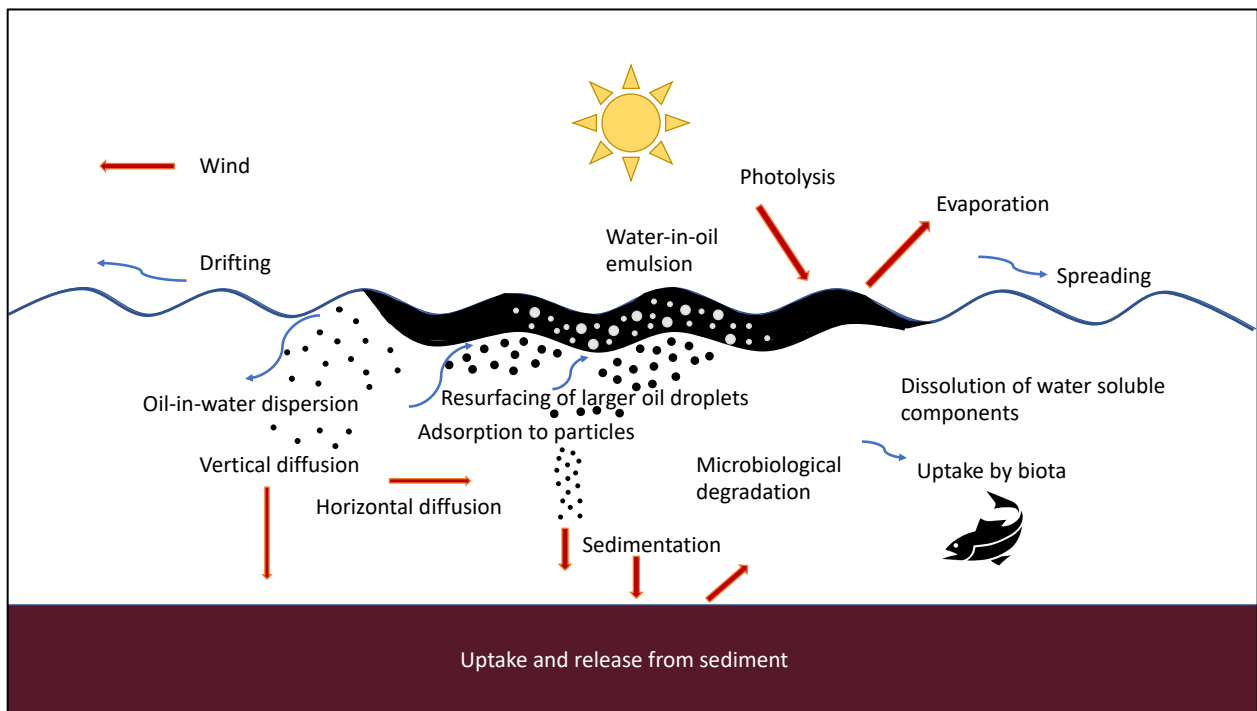
Figure 2-5 Illustration of the weathering processes acting on a marine oil spill. Adapted from Brandvik and Daling (2015).

One of the most important processes that removes oil from the surface is evaporation (Brandvik and Daling, 2015). As oil spreads over the water surface, the lightest components will evaporate. The evaporation rate is a function of the relative number of lighter components of the oil itself, the wind speed, sea temperature and thickness of the oil film. An important consequence of evaporation is how it changes the composition of the remaining oil, leaving behind the heavier components. This causes the density and viscosity to change over time. The pour point will also increase with the loss of volatiles. This concentrates the wax components, leading to precipitation.

However, the crude oil may remain liquid at the sea surface depending on other factors, such as wave action. Flash point also rapidly increases as more of the volatile and inflammable components dilute in to the air. Therefore, the risk of fire and explosion will decrease over time unless the spill is renewed with fresh crude. Heavy wind, causing faster evaporation and diffusion, will also increase the flash point.

Dissolution competes with evaporation as the smaller components, such as aromatics like benzene and toluene, dissolve to some extent (Reddy et al., 2012). These compounds are also volatile and evaporate quickly; evaporation tends to be much faster than dissolution. The heavier hydrocarbon components are essentially insoluble. Water solubility has only a minor effect on the total removal of oil from sea surface, becoming more important as the degree of natural dispersion increases (Brandvik and Daling, 2015). However, the soluble aromatic compounds are toxic to fish and spills that create high localized concentrations of these compounds can have significant effects to marine organisms.

Sea water contains microorganisms that metabolise oil components. Rapid increases in the number of these bacteria in the water surrounding an oil spill is noted when conditions are favourable (Brandvik and Daling, 2015). The rate of biodegradation is increased with higher concentrations of nitrogen, phosphate and oxygen, as well as, warmer temperatures. Straight chain saturated hydrocarbons are the most easily broken down. Different bacteria will prefer specific components, and most crude components can eventually be broken down with the exception of asphaltenes. Biodegradation only occurs at the interface of oil and water. Therefore, oil stranded above the tide zone will degrade very slowly and may remain for many years. Oil trapped in sediments will degrade slowly due to the lack of oxygen and nutrients (Prince et al., 2002). The formation of droplets by natural or chemical dispersion will increase the surface area and the rate of biodegradation.

Some oil components, aromatics in particular, are slowly oxidized under sunlight. This photo-oxidation contributes to the stability of water-oil emulsions and has an influence on the persistence of oils on the surface (Brandvik and Daling, 2015). After a long period of weathering at sea, tar-balls may form. Highly weathered and dense oils may disappear from the surface and later return.

This is mainly a function of the sea conditions, density and viscosity of the oil or water-oil emulsion. Very few crudes have a density higher than sea water (1.024 Kg/L) even after extensive weathering or emulsification. This means minimal crude is expected to sink but if droplets adhere to other particles they may sink to the sediment (Loh et al., 2014).

Water in oil emulsification is an important process for oils remaining on the sea surface. Surface-active compounds in the oil and the presence of breaking waves result in the oil taking up water and increasing the viscosity (Brandvik and Daling, 2015). The more weathered an oil becomes, the more natural dispersion and evaporation are decreased. Resins, waxes and asphaltenes can increase the stability of an emulsion. This can affect recovery methods as water greatly increases the volume of the oil for recovery, or reduces the ability to disperse or burn the oil. Very viscous oil emulsions will reduce the efficacy of skimmers (Brandvik and Daling, 2015).

Turbulence in the water column determines the horizontal and vertical motion of droplets emitted to the water column from a subsea release. Breaking waves can break surface oil up in to droplets and mix them in to the water column. These processes are known as natural dispersion. Chemical dispersants enhance the dispersion rate by decreasing the interfacial tension between oil and water (Brandvik and Daling, 1998). This results in smaller droplets that are more likely to remain in the water column than rise and coalesce on the surface. Oils are chemically dispersible at sea surface temperatures 10-15°C below their pour-point (Brandvik and Daling, 2015).

Spreading is often the dominant process during the initial stages of an oil spill but decreases with time (Brandvik and Daling, 2015). High density, viscosity and pour point will decrease spreading. Current, wind and waves become the dominant conditions acting on spreading as time goes on. Oil slicks will have thickness variations as a result of wind direction and elongate in the direction of the driving forces. Zones of convergence and divergence result in areas of thicker and thinner oil on the surface; with wind and currents causing drifting.

Oil at sea faces many simultaneous processes that alter its composition, properties and distribution. Laboratory, modelling and field studies help to understand this behaviour.

2.3 Breakup Regimes

The competition between cohesive and disruptive forces lead to the breakup of an oil plume or jet into droplets (Masutani and Adams, 2000). Jet velocity and fluid properties are the main factors leading to the breakup of the jet in to droplets. When release velocities are small, liquids released will emerge as large pendant droplets near the exit nozzle, figure 2-6 (a). This is known as the Rayleigh Regime where surface tension forces are dominant and a monodispersion of droplets larger than the exit nozzle diameter result (Masutani and Adams, 2000). When the velocity is increased, the influence of surface tension decreases as hydrodynamic forces from the relative velocities of the jet and surrounding fluid determines the breakup, the discrete droplets develop into a laminar jet. The break up into droplets of this laminar jet occurs a certain distance from the nozzle, figure 2-6 (b). A narrow range of relatively large droplets result. As the velocity is further increased, the breakup point will move further away from the nozzle until a point when it begins to move back closer to the release nozzle, figure 2-6 (c) and (d). Two instability mechanisms operate at the same time: the jet surface becomes unstable to short wavelength disturbances and produces fine droplets near the nozzle, while the core jet persists in continuous laminar flow and breaks up further downstream into larger droplets (Masutani and Adams, 2000). This results in a polydispersion of droplets. Finally, further velocity increases result in atomization, with the fluid breaking into a fine mist, figure 2-6 (e).
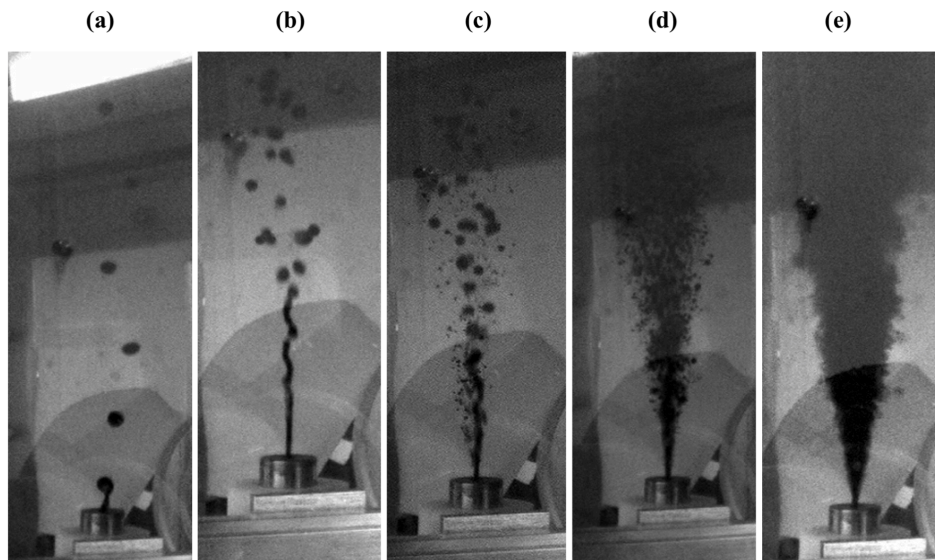
Figure 2-6 Illustration of oil jet breakup regimes from Masutani and Adams (2000). The jet velocity increases from left to right.

2.4 Dimensionless numbers

A series of dimensionless numbers have been created to describe the general relationships of the forces acting on droplets during the breakup of a liquid jet.

The Weber number (We) is the ratio of disruptive momentum (hydrodynamic) forces to restorative interfacial tension forces (Johansen et al., 2015). The lower the Weber number, the more dominant is the surface tension of the fluid.

$$We = \frac{\rho U^2 D}{\sigma} \tag{1}$$

U = the exit velocity
D = the orifice diameter
σ = the interfacial tension (oil-water)
ρ = density

The Reynolds number (Re) is the ratio of the inertial force (in the direction of flow) to the viscous force (against flow) (Masutani and Adams, 2000). It can be used to predict whether the flow will be laminar or turbulent. When viscous forces dominate, slow flow and low Re, the flow is likely laminar as the force is great enough to keep particles in line. When inertial forces are dominant, faster flow and larger Re, the flow is turbulent.

$$Re = \frac{\rho U D}{\mu} \tag{2}$$

μ = the dynamic viscosity of the jet fluid

The Ohnesorge number (Oh) compares the viscous forces with the inertial and surface tension forces. It relates the tendency for a droplet to either stay together or break apart.

$$Oh = \frac{\mu}{(\rho \sigma D)^{\frac{1}{2}}} \tag{3}$$

The Ohnesorge number is a combination of the Reynolds and Weber numbers:

$$Oh = \frac{We^{\frac{1}{2}}}{Re} \tag{4}$$

Experimental results can be described by dimensionless Ohnesorge versus Reynolds number plots to establish general relationships, figure 2-7 (Masutani and Adams, 2000). However, additional factors such as ambient fluid density (and other properties) or the initial state of the jet can also affect the breakup and are not accounted for in these numbers (Brandvik et al., 2014b).
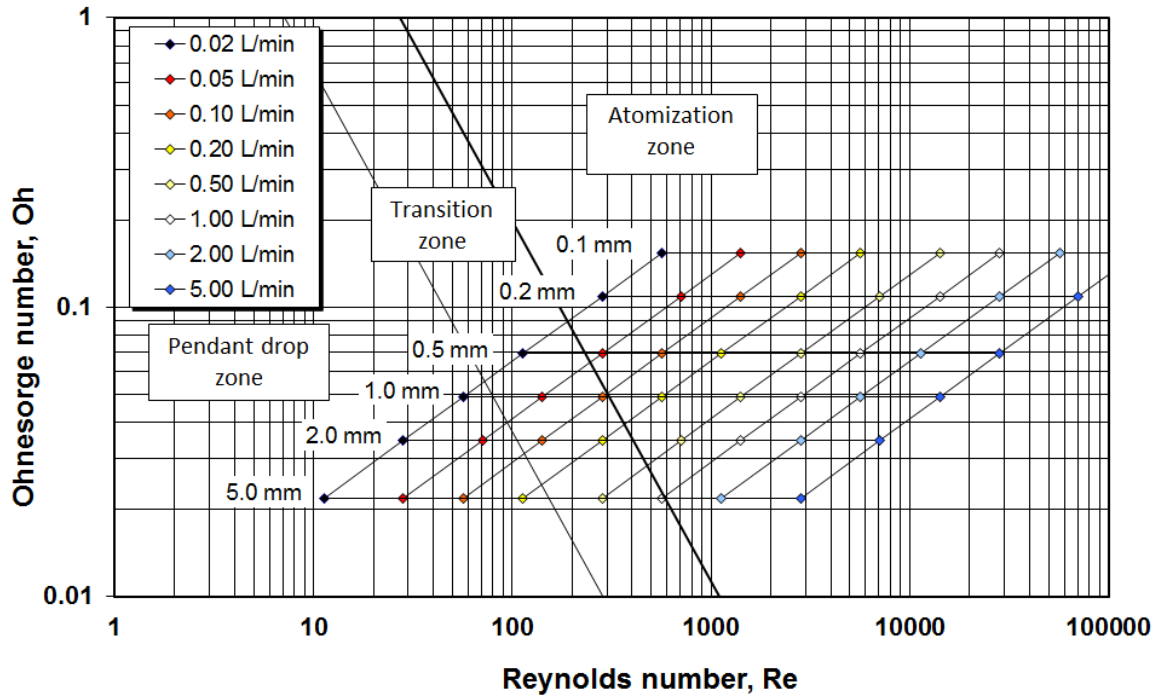
Figure 2-7 Ohnesorge vs. Reynolds number plot. The diagonal lines dividing the three different release regimes have constant Weber numbers. The line dividing the Transitional and Atomizing zone has a Weber number of 324. Diagram from Brandvik et al. (2014).

Different regions on the graph describe different levels of turbulence. There is a boundary between pendant drop and transitional flows, as well as, between turbulent (atomization) and transitional flows (figure 2-7). These boundaries are found to have a linear relationship of:

$$Oh = cRe^{-1} \tag{5}$$

c = constant of proportionality

Because

$$Oh = cRe^{-1} \quad (6) \qquad \text{and} \qquad Oh = \frac{We^{\frac{1}{2}}}{Re} \quad (7) \qquad \text{we get} \qquad We = c^2 \quad (8)$$

The two boundaries in figure 2-7 are lines for constant Weber number ($We = c^2$). This can be useful for setting experimental conditions for the desired system.

2.4.1 Modified Weber scaling

Hinze (1955) proposed that the maximum stable droplet size, d_{max}, in stationary turbulence is given by:

$$d_{max} = \alpha \left(\frac{\sigma}{\rho} \right)^{\frac{3}{5}} \varepsilon^{-\frac{2}{5}} \tag{9}$$

α = a constant of proportionality

ρ = the density continuous phase (water)

ε = the turbulent dissipation rate

σ = the interfacial tension (oil-water)

However, as ε decreases with distance from the nozzle exit in a turbulent round jet, the maximum stable droplet size increases during the time needed for droplets to complete the break up process. Using experimental data, Martínez-Bazán et al. (2002) found that this turbulent round jet dissipation rate scales with the relative downstream distance $\frac{X}{D}$. Providing this relationship for the exit dissipation rate (Martínez-Bazán et al., 2002):

$$\varepsilon_0 \sim \frac{U^3}{D} \tag{10}$$

The corresponding equation for the maximum droplet size becomes

$$\frac{d_{max}}{D} = AWe^{-\frac{3}{5}} \tag{11}$$

A = empirical factor depending on the relative break up length $\frac{X}{D}$

The exit Weber number is $We = \frac{\rho U^2 D}{\sigma}$ and the law is valid when the breakup is limited by the interfacial tension of the jet liquid (Johansen et al., 2013).

Internal viscous stress in fluid droplets may also impact break up (Hinze, 1955; Wang and Calabrese, 1986). Wang and Calabrese (1986) presented the dimensionless viscosity number, V_i, to account for these stresses:

$$V_i = \frac{\mu U}{\sigma} \tag{12}$$

This can also be expressed in terms of the Weber and Reynolds number:

$$V_i = \frac{We}{Re} \tag{13}$$

Wang and Calabrese (1986) found that for small viscosity numbers ($V_i \rightarrow 0$), droplet breakup was governed by the Weber number. For large viscosity numbers, ($V_i \gg 1$), the Reynolds scaling will apply.

For cases where both interfacial tension and viscous stress are influencing the break up, they derived the following semi-empirical equation:

$$\frac{d_{50}}{D} = A We^{-3/5} [1 + B V_i \left(\frac{d_{50}}{D}\right)^{\frac{1}{3}}]^{3/5} \tag{14}$$

Any diameter can be chosen, eg. the volume median diameter, d_{50}
B = empirical coefficient

For large viscosity number values, $V_i \gg 1$ The above equation can be approximated as:

$$(d_{50}/D)^{4/5} = A We^{-\frac{3}{5}} (B V_i)^{3/5} \tag{15}$$

Because the viscosity number is the ratio of the Weber and Reynolds number:

$$\frac{d_{50}}{D} = A^{5/4} B^{3/4} Re^{-3/4} \tag{16}$$

$$\frac{d_{50}}{D} = C Re^{-3/4} \tag{17}$$

For small viscosity number values, $V_i \rightarrow 0$

$$\frac{d_{50}}{D} = A We^{-\frac{3}{5}} \tag{18}$$

As the V_i increases and eventually becomes very large, equation 14 gradually changes from Weber number scaling to a Reynolds number scaling. V_i numbers will generally be small in oil jet breakup, however, large numbers can result with the application of chemical dispersants as the interfacial tension can be decreased by several orders of magnitude (Johansen et al., 2013).

In Tower tank experiments, Johansen et al. (2013) found that the Weber number scaling did not hold true for a large number of experimental conditions, with especially large deviations for samples mixed with dispersants. They proposed a modified Weber number with correction for the viscosity effect, defined as:

$$We^* = \frac{We}{\left[1 + BV_i \left(\frac{d_{50}}{D}\right)^{\frac{1}{3}}\right]} \qquad (19)$$

Using this definition, the relative droplet size can be expressed as the Modified Weber scaling:

$$\frac{d_{50}}{D} = AWe^{*-\frac{3}{5}} \qquad (20)$$

2.4.2 Effects of gas void fractions

Contrary to most oil jet experiments, which typically involve a single fluid (eg. Crude oil) into water, subsea releases involve complex discharges of oil with gas, often mixed with production water. These multiphase flows result in different conditions, from bubbly (continuous oil phase) to slug (alternating sections of oil and gas) to mist (oil droplets suspended in gas) flows. Flow conditions are influenced by the velocities of the fluids. Deep subsea releases are most likely to be bubbly flow with oil as the continuous phase (Lima Neto et al., 2008).

Lima Neto et al. (2008) describe a bubbly water jet with the superficial water velocity:

$$U_W = \frac{Q_W}{A_N} \qquad (21)$$

U_w = superficial water velocity

Q_w = the volume flow of water

A_N = the nozzle cross section corresponding to a nozzle diameter D, $\quad A_N = \frac{\pi D^2}{4}$

Substituting in to the Reynolds equation:

$$Re_W = \frac{U_W D}{v_W} \tag{22}$$

Where v_W = kinematic viscosity of water, $v_W = \frac{\mu}{\rho}$

This, however, is the definition for a water only jet, it does not account for a bubbly jet with gas with the same water flow. The water only velocity may be substituted with a velocity obtained from the conservation of momentum flux in order to account for the volume flow and density of the second phase.

$$M = (\rho_W Q_W + \rho_G Q_G)U_{W+G} \tag{23}$$

M = exit momentum flux of the bubbly water jet

G/W subscripts for gas/water

$$M_T = \rho_W Q_T U_T \tag{24}$$

$$Q_T = A_N U_T \tag{25}$$

M_T = momentum flux of an 'equivalent' single phase water jet

U_T = effective water velocity (velocity of a single phase water jet producing the same momentum flux as the bubbly water jet)

Gas has a much smaller density than water, we neglect its contribution to the momentum flux, then $M_T = M$ will imply:

$$U' = \frac{U_T}{(1-n)^{\frac{1}{2}}} \tag{26}$$

n = gas volume fraction at exit

When considering oil and gas bubbly jets, as opposed to water and gas, the properties for the oil are changed for the water terms. Additional terms may be added for 3 phase jets.

Defining the Reynolds, Weber and Ohnesorge numbers in terms of the continuous phase (water or oil):

$$Re = \frac{\rho U' D}{\mu} \quad (27) \qquad We = \frac{\rho (U')^2 D}{\sigma} \quad (28) \qquad Oh = \frac{\mu}{(\rho \sigma D)^{\frac{1}{2}}} \quad (29)$$

The gas fraction will contribute to the buoyancy of the jet. Most experiments of droplet breakup are designed with jet-like outlet flow, however, deepsea releases with large volume flows and large outlet diameters may behave more plume-like. The buoyancy flux, F_B,

$$F_B = g'Q \tag{30}$$

Q = total exit volume flow

g' = reduced gravity, $g' = \frac{g[\rho_W - \rho_{oil}(1-n)]}{\rho_W}$

g = acceleration of gravity

ρ_W = density of water

$\rho_{oil}(1-n)$ = density of the mixture of oil and gas

A length, $l_M = \frac{M^{\frac{3}{4}}}{F_B^{\frac{1}{2}}}$ is defined as the transition from jet-like to plume-like behavior in buoyant plumes (Papanicolaou and List, 1988). Where M is the momentum flux described above.

Papanicolaou and List (1988) showed that the flow behaves like a jet at downstream distances $z < l_M$ and like a plume at distances $z > 5l_M$. The relative distance $\frac{l_M}{D}$ may indicate whether droplet splitting will take place in the jet-like or plume-like section of the buoyant plume.

The exit Froude number is found by insertion of the expressions for Q, F_B and M into this equation.

$$\frac{l_M}{D} = Fr \tag{31}$$

$$Fr = \frac{U'}{(g'D)^{\frac{1}{2}}} \tag{32}$$

High exit Froude numbers predict jet-like flow breakup while low exit Froude numbers imply buoyant plume flow in the droplet splitting zone (Johansen et al., 2013).

In plume-like flow (low Froude number), a modified velocity is needed to describe the droplet breakup as the velocity is primarily determined by the buoyancy flux (Papanicolaou and List, 1988). The jet-flow velocity will scale with the exit velocity.

The correction for buoyancy in large volume flows is given by:

$$U_e = U'(1 + Fr^{-1}) \tag{33}$$

At the transition to plume-like behaviour, when the Froude number is small, the modified velocity will approach $U_e = Fr^{-1} = (g'D)^{1/2}$

When the Froude number is large, in jet-like flow, $U_e \approx U'$

The corrected velocity U_e is then used in the Weber number:

$$We = \frac{\rho U_e^2 D}{\sigma} \tag{34}$$

2.4.3 Prediction of droplet sizes

Using the equations from the previous sections, Brandvik et al. (2015) found the modified Weber constants of A 24.6 and B 0.08 based on empirical data. These numbers were derived from the near full scale DeepSpill experiment and meso-scale Tower Basin experiments, and are used in the current OSCAR oil modelling software. As discussed above, the droplet breakup is contingent upon the oil properties and exit velocities. There are also differences in droplet breakup related to the buoyancy of the plume found in larger releases. Much of the droplet size distribution data collected focuses on low velocity releases (Faksness et al., 2016; Johansen et al., 2003a; Reddy et al., 2012).

3 Objective and hypothesis

The objective of this study was to characterize a selection of subsea releases possible from a typical aging oilfield along the NCS, focusing on:

1. using experimental data to optimise the existing droplet breakup model in the OSCAR simulation tool.
2. Possible biologic consequences from an oil spill along the NCS.
3. The Njord field as a possible source for previously collected oil pollution samples.

It is hypothesised that if the previously derived values for A and B of the modified Weber scaling predict droplet sizes too small for a given set of release conditions, then the OSCAR modelling system will not accurately predict the fate of the oil droplets in the environment.

4 Materials and Methods

This study is divided in two parts, a droplet breakup experimental study and a modelling study using the SINTEF OSCAR oil spill contingency and response simulation tool. The following sections describe the equipment, materials and methods used in the experimental portion of this project. Afterwards, a description of the variables used in the OSCAR modelling system.

4.1 SINTEF MiniTower

The SINTEF MiniTower was designed as a bench scale method to monitor droplet sizes in an oil plume and to test dispersant effectiveness. It is 0.8 m high and has a 160 L capacity, see figures 4.1-4.3. It allows for the continuous monitoring of an oil plume generated by a turbulent jet (Brandvik et al., 2014). Oil and produced water are injected from a piston pump system and mixed before they are released as a turbulent jet from the nozzle. A gas line is also connected to pressurized air in order to simulate gas releases. LabView systems engineering software is used to control the flow rates in order to simulate different turbulence levels. A continuous flow (up to 100mL/min) of fresh sea water from the Trondheim fjord passes from the bottom of the tank upwards, where it is drained. This allows the continuous washing of oil droplets to prevent oversaturation and buildup. The seawater temperature varied from 7.8 to 9.9°C. A static mode is available for dispersant testing but was not used during this study.

Oil and produced water lines were passed through a water bath heated to 58.9°C before entering the mixing chamber. Through testing, this was determined to be the water bath temperature that resulted in a liquid temperature of approximately 50°C measured just below the exit nozzle. This was to replicate stable reservoir conditions and maintain consistent viscosity conditions for the oil (Skancke et al., 2016). The exit nozzle is easily interchangeable in the system, 0.50mm and 0.25mm nozzles were used in this study to replicate the desired exit velocities while minimizing the plume volume.
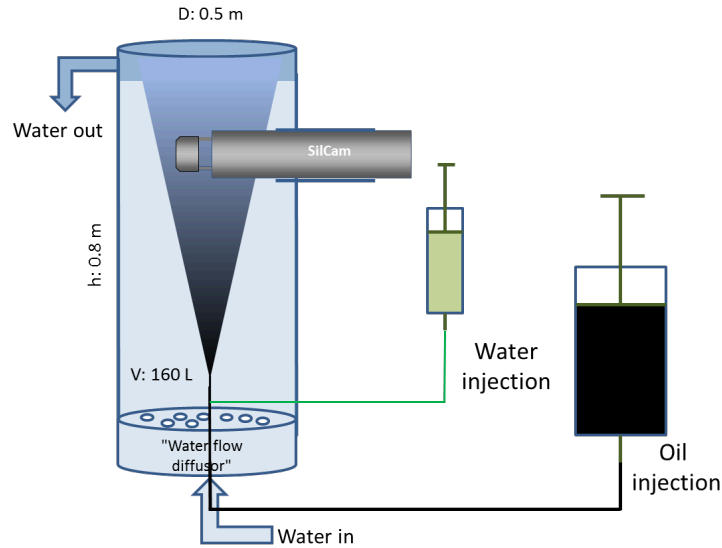
Figure 4-1 Outline of the SINTEF MiniTower. Illustrating the flow through system of seawater (water in and out) and the injection system for produced water and oil. The SINTEF Silhouette Camera system was used to measure droplet sizes in this study. Figure adapted from Brandvik et al. (2014).

In a typical experiment, LabView was opened and controls initiated. The primed oil and water piston pumps were turned on, and the gas pressure was set (if needed). The heater for the water bath containing the oil and water coils was then turned on and set to a temperature of 58.9°C. Fresh seawater was run through the MiniTower system for approximately 10 minutes for the entire system to achieve the seawater temperature. Before an experimental release was begun, the water pump was run to push out any cold water or oil left in the lines from the previous experiments. Folders were created for the SilCam data and LabView data log (produced water, seawater, oil, and gas flow rates, seawater temperatures, and timing), and an appropriate SilCam config file was selected, see Appendix A for the file commands. It is possible to create a LabView log file with preset flow rates and timings, however, with the test SilCam software used, this sometimes resulted in error messages. Therefore, manual control of flow settings was primarily used. SilCam test software was then started, selecting "Acquire images" and "Live view". It is possible to process images in Realtime. However, with the test version used, this seemed to slow the image acquisition and resulted in more error messages, therefore it was not used. Post processing by selecting "process historical data" and the appropriate files was used instead. Due to the high concentrations of oil, frequent fouling of the camera occurred. When droplets were noted to adhere to the image area, experiments were stopped and a cleaning cycle was performed. At some points, errors

resulted in the live view not functioning and the bitmap images had to be inspected after acquisition for inconsistencies using the file player application. Each set of experimental conditions were run and measured for approximately 90 seconds. Data was then selected in 30 second time windows from each experiment following post processing.

A SilCam
B Oil and produced water piston pumps
C Controls for piston pumps
D Seawater in
E Heater
F Water bath
G Seawater out
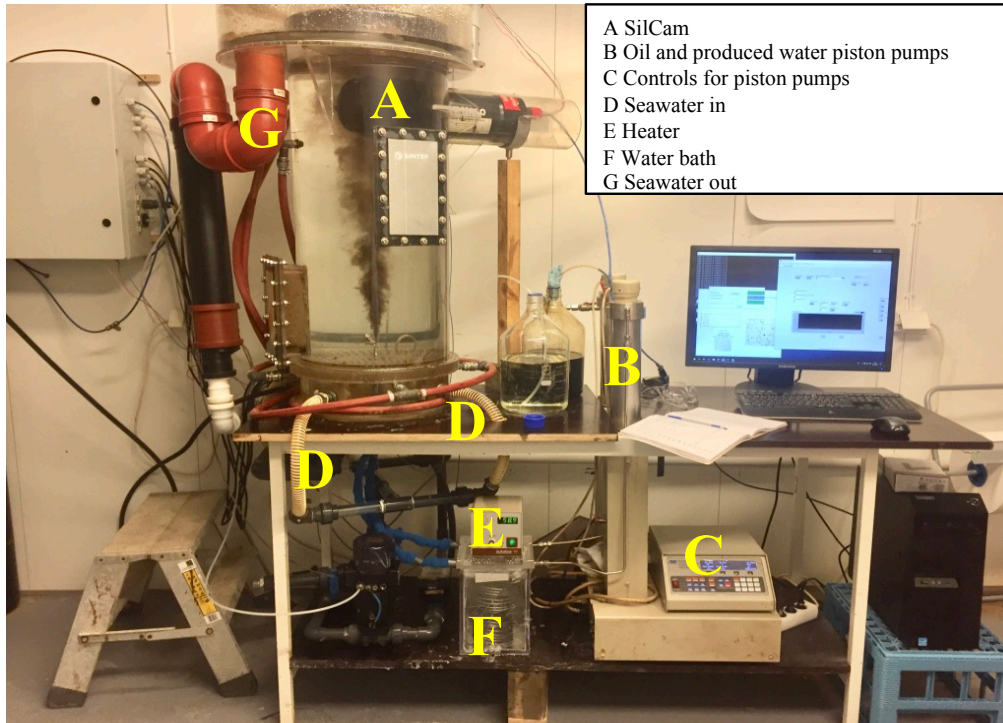
Figure 4-2 Image of the MiniTower setup used in this study. Showing the water/oil piston pumps, water bath and computer system.
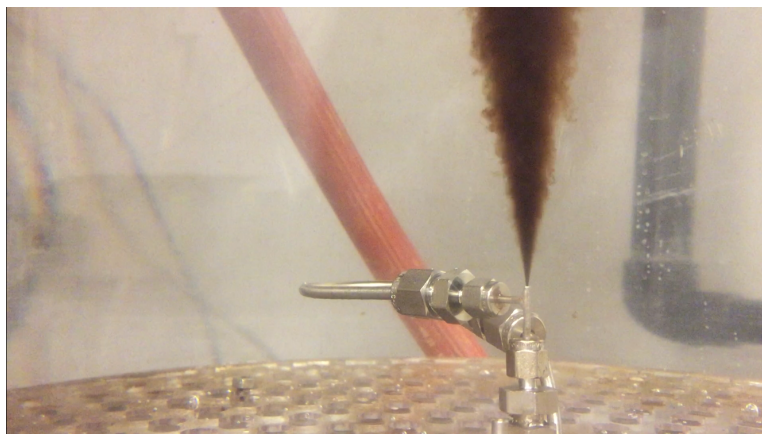
Figure 4-3 Close up image of an oil jet emitted from the nozzle of the SINTEF MiniTower.

A summary of conditions that were manipulated throughout the MiniTower experiments is given in Table 4-1 below.

Table 4-1 Parameters that were manipulated during the MiniTower experiments and the range of conditions used.

Parameter	Conditions
Oil flow	0-200mL/min
Produced water flow	0-200mL/min
Gas flow	0-75mL/min
Nozzle diameter	0.25 or 0.50 mm
Seawater flow	50-100mL/min

4.2   SINTEF Silhouette Camera

The LISST-100 is a laser diffraction camera previously used for the study of droplet sizing in oil plumes with the MiniTower. The size range it is capable of measuring is from 2.5-500μm in diameter (Davies et al., 2012). Under high concentration conditions, oversaturation of droplets in the imaging zone may lead to excess scattering using a laser diffraction camera. During this study, the droplet sizes expected and the ability to distinguish particle types (gas or oil) were beyond the capabilities of LISST-100. SINTEF developed the Silhouette camera, an *in situ* imaging system, to quantify high concentrations of suspended particles from 30-12000μm (Davies et al., 2012). An advantage of the SilCam over the LISST-100 is that it is able to distinguish between oil, gas and oil coated gas bubbles. However, the SilCam is also not be able to take measurements if the concentration is too great or when there is too much overlap of particles.

The exit speeds, droplet concentration and multiphase nature for these experiments were challenging for the SilCam, yet necessary to define a small subsea pipeline leak. Due to the extreme conditions required of the camera in these experiments, a test version of the SilCam software was developed. Emlyn Davies performed software updates as necessary to accommodate camera issues with handling the high concentrations and small droplets. The parameters for the maximum number of particles to count was increased 1000 times and the percent saturation increased to 100% from the standard settings in the config file to better count the small droplets generated, see Appendix A for the config file commands. However, at times the software had some limited functions in terms of live view or particle differentiation.
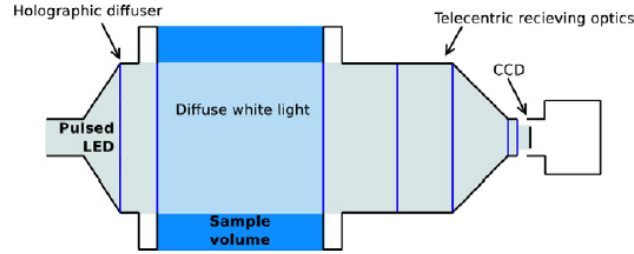
Figure 4-4 Illustration of the optical configuration of the silhouette system. Illustration taken from Davies et al. (2017).

The SilCam imaging system utilizes backlighting to create silhouettes of particles suspended between the light source and the camera, see figure 4-4. Particle dimensions are quantifiable, allowing the size distributions and concentrations to be calculated. Oil droplets and gas bubbles are distinguished by optical properties related to their composition, by passing light of different wavelengths through and recording the signatures of the transmitted light (Davies et al., 2017). The magnification of the camera was 0.5x, yielding a pixel size of 7.2μm and minimum quantifiable diameter of 28μm by equation 35 (Davies et al., 2017; SINTEF, 2018). The pathlength was adjusted to 2.5mm to accommodate the largest particles to pass without disruption, with 7 images taken per second. The entire system is contained within a water-proof, high pressure housing with the ability to adjust the pathlength manually, see figure 4-5.

$$D_{min} = 2\sqrt{\frac{12P^2}{\pi}} \tag{35}$$

P = pixel size

Figure 4-5 Illustration of the silhouette camera system within the high-pressure housing. Illustration taken from Davies et al. (2017).

4.2.1   Data treatment with SilCam

The basic processing steps applied to each image of the SilCam are outlined. The detected particles are binarized (made black and white) to produce a series of zeros and ones to represent the corrected image (Davies et al., 2017). This binary image is used to count the particles and

determine their geometry and type. The particle size distribution is determined by counting Equivalent Circular Diameters (ECD). The particles are separated into the log-spaced size bins used by the LISST-100 system but extending to the much larger size of 12000μm (Davies et al., 2017).

The background image correction is carried out in two ways. By an average of images recorded in clean water and from a moving-average of images from either side of each raw image. The clean water background removes noise and gradients in the background illumination. The moving-average method removes particles or oil droplets that adhere to the housing windows from the analysis. The SilCam removes items that are stationary or touching the edges of the images. If something new arrives, it will be removed after some time. The time it takes to remove an item is controlled by the script in the configuration file: "[Background] num_images = 15". This means that the software uses the 15 previous images to find and remove the background (4-seconds if you are recording at 4Hz). The background correction is continuously updating, so it is always using the 15 previous images while calculating droplets on the current image. This is an advantage during high-concentration measurements where fouling is problematic.

Following processing, a MATLAB script with plots of the ECD versus time, d_{50} versus time and volume concentration versus diameter of a selected time window are obtained, see figure 4-6. The data from a selected time window can be converted to an excel file using the SilCam software. Thirty second time windows were used for this study.

4.2.2 Droplet size distribution functions

Two distribution functions are most commonly used in oil droplet breakup experiments, the lognormal distribution and the Rosin-Rammler distribution. Currently, there is no theoretical reasoning for using one distribution function over another (Johansen et al., 2013). The method used should be the best overall fit to the experimental data. The current study applies experimental conditions that result in very small droplet sizes. The advantage of the Rosin-Rammler distribution is that it accounts for the drop off that occurs when the droplet sizes reach the maximum stable

size. Due to the droplet sizes of this study being well below the maximum stable droplet size, a lognormal distribution is assumed in all experiments. This means that the d_{50} and peak heights should be equivalent and interchangeable, see figure 4-6. Experiments that displayed bimodal or multimodal distributions were either repeated or excluded from the results. For the OSCAR modelling, the Rosin-Rammler relation was used as the larger exit diameters and slower speeds meant the maximum stable droplet size was obtained in the larger releases.
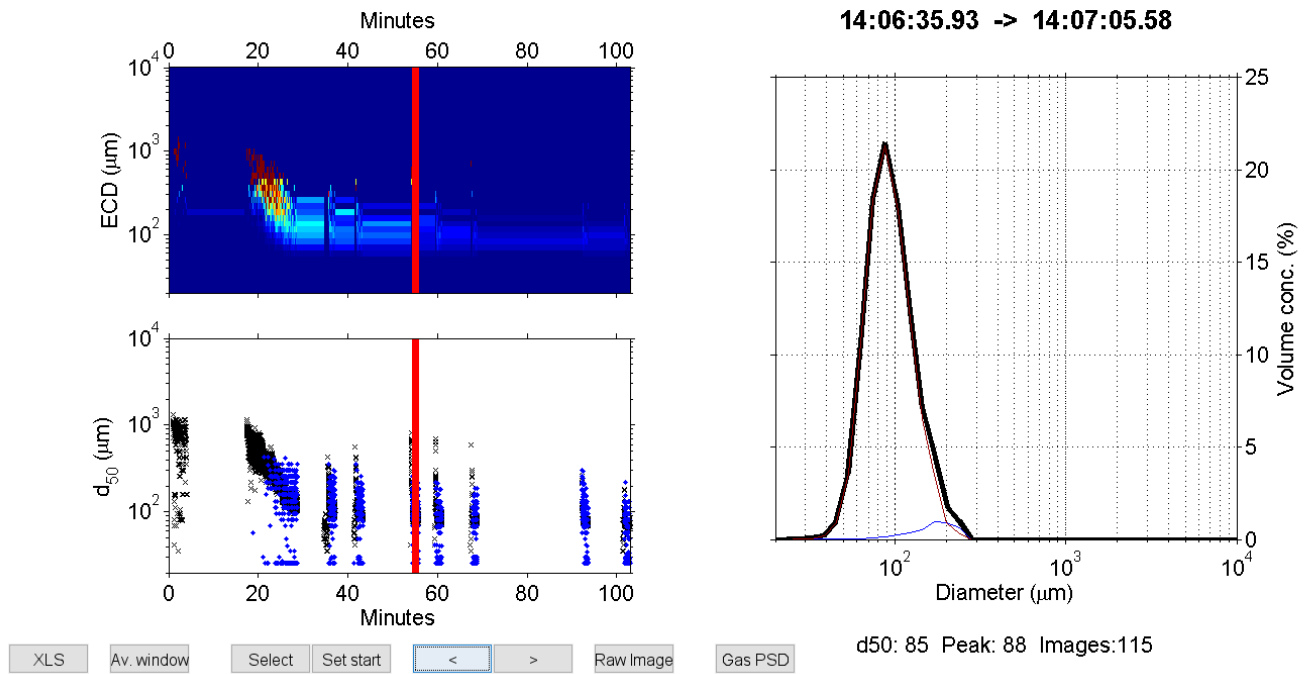
Figure 4-6 MATLAB interpretation of data showing a lognormal distribution. The d_{50} and peak height are nearly equivalent. The left screen can be toggled to view different time snapshots of the experiment progress, by moving the time window (red lines) shows the histogram of the distribution profile in the right window. The pictured peak is from the experiment using Oseberg 2017 oil at a flow of 50mL/min from the 0.25mm nozzle. The program is measuring mainly oil (brown line) with minimal false reporting of gas (blue line). The black line describes the total volume concentration.

4.2.3 Standard Particle Solutions

In order to verify the particle sizing of the SilCam, standard solutions of mono disperse polypropylene particles were allowed to settle through the viewing area of the SilCam prior to taking oil measurements, see figure 4-7. The stock solutions are synthesized at SINTEF to have uniform particle sizes of 80 and 346 μm respectively. Therefore, a steep, narrow peak is expected to be read by the SilCam, representing a single size of particle. The config file used to direct the

SilCam must have the threshold adjusted to 0.98 in order to read these particles, as they are much more translucent than oil. The typical threshold for measuring oil is set to 0.85.
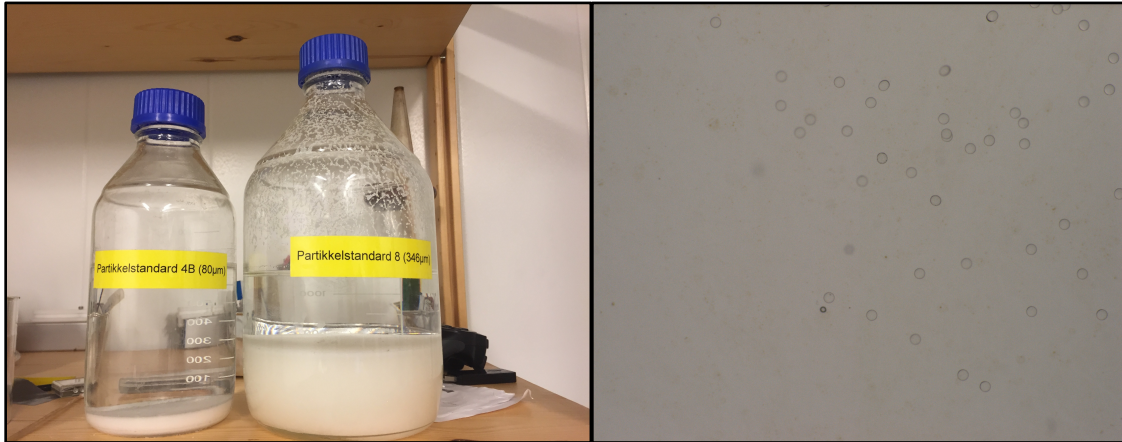
Figure 4-7 Standard solutions prepared at SINTEF. Appearance of the images taken by the SilCam for the 346 um standard particles.

4.3 Oil Type

The oil ultimately used for this study was the Norwegian Oseberg 2017 Blend. This is a light paraffinic blend with low viscosity and high evaporative loss, see Table 4-2. Experiments were attempted with Grane and Njord oils, however, they were not included in the results. This will be discussed further in the results and discussion sections.

Table 4-2 Oil composition and properties. Selected data are from earlier weathering studies at SINTEF (Brandvik et al., 2015b; Resby and Wang, 2004; Strøm, 2013).

Oil	Oseberg Blend	Grane	Njord
Density, Kg/L	0.8261	0.941	0.807
Pour point, °C	-15.0	-24	-15.0
Viscosity, mPas at 13°C	9.6	593	5
Paraffins, vol %	43.9	24.6	40.6
Naphthenes, vol %	30.5	37.3	42.3
Aromatics, vol %	25.6	38.1	17.1
IFT mN/m	20	11	-
150 °C – evaporative loss (vol%)	23	3	24
200 °C – evaporative loss (vol%)	35	5	37
250 °C – evaporative loss (vol%)	46	13	48

4.4 OSCAR modelling

Following the laboratory droplet breakup experiments, the OSCAR simulation tool was used to assess the consequences of potential oil spills from a mature field along the NCS. Droplet data optimized for small diameter releases obtained from the experimental portion was used. The likelihood of oil pollution samples collected near Frøya originating from the Njord field was also assessed.

4.4.1 Choice of model

For this project the SINTEF OSCAR model system with Plume3D and GASTRACK, version MEMW 10.0.1, with a NTNU student licence obtained from May Kristin Ditlevsen was used.

4.4.2 Scenario parameters

The scenarios selected were intended as generalizations of possible leaks in an aging field along the NCS. Many fields at the tail end of production would contain large amounts of produced water in a release, this is reflected by all scenarios having a 20% mass by release of oil with the remainder being water. It was estimated that small and medium pipeline leaks would have a lower percentage of gas than a full blowout. Two different pipeline leaks were modelled, a 0.010m diameter small leak and a 0.080m diameter medium leak. A 0.245m diameter full scale blowout was modelled. Two different months were selected, June and January, to delineate seasonal differences (summer and winter) between scenarios and recovery. The scenario parameters are given in Table 4-3. Two additional scenarios, Scenario 4 summer and winter, were run with all parameters identical to Scenario 1 except that the droplet size data was manually input using the Modified Weber model optimized during the experimental portion of this study.

Table 4-3 Scenario parameters for the different releases, by season.

Parameter	Scenario 1 summer	Scenario 1 winter	Scenario 2 summer	Scenario 2 winter	Scenario 3 summer	Scenario 3 winter
Start time	2000-06-01 8:00 UTC	2000-02-01 8:00 UTC	2000-06-01 8:00 UTC	2000-02-01 8:00 UTC	2000-06-01 8:00 UTC	2000-02-01 8:00 UTC
Duration	30 days	30 days	30 days	30 days	30 days	30 days
Oil profile	Oseberg Blend 2006 20% by mass oil	Oseberg Blend 2006 20% by mass oil	Oseberg Blend 2006 20% by mass oil	Oseberg Blend 2006 20% by mass oil	Oseberg Blend 2006 20% by mass oil	Oseberg Blend 2006 20% by mass oil
Oil density	0.8447 Kg/L	0.8447 Kg/L	0.8447 Kg/L	0.8447 Kg/L	0.8447 Kg/L	0.8447 Kg/L
Release location	Njord field	Njord field	Njord field	Njord field	Njord field	Njord field
Longitude	7°11.9800' E	7°11.9800' E	7°11.9800' E	7°11.9800' E	7°11.9800' E	7°11.9800' E
Latitude	64°16.2400' N	64°16.2400' N	64°16.2400' N	64°16.2400' N	64°16.2400' N	64°16.2400' N
Release rate	3600L/hr	3600L/hr	90000L/hr	90000L/hr	6000m^3/day	6000m^3/day
Release duration	7 days	7 days	7 days	7 days	7 days	7 days
Total oil released	1.411x10^{5}L	1.411x10^{5}L	3.568x10^{6}L	3.568x10^{6}L	9.919x10^{3}m^3	9.919x10^{3}m^3
Salinity of formation water in the release	35	35	35	35	35	35
Temperature of release	50°C	50°C	50°C	50°C	50°C	50°C
Release diameter	0.010m	0.010m	0.080m	0.080m	0.245m	0.245m
GLR	2.5	2.5	2.5	2.5	10	10
Gas density	0.8Kg/Sm^3	0.8Kg/Sm^3	0.8Kg/Sm^3	0.8Kg/Sm^3	0.8Kg/Sm^3	0.8Kg/Sm^3
Air temperature	10°C	-5°C	10°C	-5°C	10°C	-5°C
Depth (above sea floor)	0	0	0	0	0	0
Suspended sediment	0	0	0	0	0	0
Settling velocity	3	3	3	3	3	3
Wind induced current	auto	auto	auto	auto	auto	auto
Surface drift rate	3.5	3.5	3.5	3.5	3.5	3.5

4.4.3 Response parameters

Three response alternatives were used, no response, mechanical response or chemical response. The mechanical response modelled was vessel-based deployment of booms and skimmers and file named Oseberg.pipeline.leak.0.800.june.20190220.rsp. Four vessels were defined, with deployment from the coast near the NOFO facilities at Kristansund and the Norwegian Coastal Administration depots in Ørland. The chemical response involved vessel-based application of the dispersant Dasic NS, from 4 defined vessels and the response file was named chemical_oseberg_njordfield.rsp. Boats were deployed from the coast near the same depots as for the mechanical recovery. A tanker was made available for offloading at the 2000 meter exclusion

zone in the mechanical model. A tanker was also available for dispersant transfer to vessels at the 2000 meter exclusion zone in the chemical model. The response files are summarised in Tables 4-4 and 4-5.

Table 4-4 Mechanical recovery vessels

Parameters	Standard vessel - system	NOFO Passive	Standard vessel - system	NOFO Passive	Standard vessel - system	NOFO Active	Standard vessel - system	NOFO Active
Vessel	NOFO #1		NOFO #2		NOFO #3		NOFO #4	
Response time (hrs)	1		72		72		72	
Operational at night	65%		65%		0%		0%	
Strategy	Newest (excl 1000)		Newest (excl 1000)		Newest (excl 2000)		Newest (excl 2000)	
Swath width (m)	185		185		185		185	
Max operational wave height (m)	3.5		3.5		3.5		3.5	
Max operational speed (knot)	0.7		0.7		0.7		0.7	
Effectiveness %	80		80		80		80	
Skimming capacity (m3/h)	200		200		200		200	
Internal Tank Capacity (m3)	1500		1500		1500		1500	
Cruise speed (OR Vessel), knots	14		14		14		14	
Transfer time to external tanker (h)	6		6		6		6	
Exclusion zone (m)	1000		1000		2000		2000	
Offload	Unlimited		Unlimited		Unlimited		Unlimited	
Threshold /film thickness (mm)	0.1		0.1		0.1		0.1	

Table 4-5 Dispersant application vessels

Parameters	NOFO vessel	NOFO vessel	NOFO vessel	NOFO vessel
System	High dosage system	High dosage system	High dosage system	High dosage system
Vessel	NOFO #1	NOFO #2	NOFO #3	NOFO #4
Strategy	Newest (excl 1000)	Newest (excl 1000)	Newest (excl 2000)	Newest (excl 2000)
Spray width (m)	28	28	28	28
Max application speed (knots)	5	5	5	5
Effectiveness % (OSCAR)	80	80	80	80
Total application rate (L/min)	120	120	120	120
Dispersant treatment/dosage (m3/Km^2 - gal/acre)	27.8	27.8	27.8	27.8
Number of trips	Unlimited	Unlimited	Unlimited	Unlimited
Assumed oil film thickness (mm, water-free)	0.8	0.8	0.8	0.8
Film Thickness /threshold (mm)	0.1	0.1	0.1	0.1
Dispersant	Dasic NS	Dasic NS	Dasic NS	Dasic NS
Dispersant dosage (%)	*3.5 %*	*3.5 %*	*3.5 %*	*3.5 %*
Dispersant ratio	1:25	1:25	1:25	1:25

Internal Tank Capacity (m3)	50	50	50	50
Cruise speed (knots)	14	14	14	14
Response time (hours)	1	72	168	168
Turnaround time (hours)	6	6	6	6
Effectiveness in darkness	65%	65%	0%	0%
Visc. Limit (cP)	Use database	Use database	Use database	Use database
Exclusion zone (m)	1000	1000	2000	2000

4.4.4 Model parameters

The model parameters are given in Table 4-6. These parameters are the same for all scenarios, and are important in order to reproduce OSCAR simulations. The two additional scenarios, Scenario 4 small pipeline releases in summer and winter, were run with the empirically derived d_{50} 501 µm and d_{95} 1130 µm manually input, all other input was the same.

Table 4-6 Model parameters

Parameter	Value
Liquid/solid particles	10000
Dissolved particles	10000
Gas particles	100
Concentration grid resolution (cell size [m])	500x500
Vertical resolution (number of cells)	10
Concentration grid depth	Min:0 Max:300
Lower concentration limit	2
Surface grid resolution	500x500
Refinement	1
Output interval	3 hours
Internal time step	15 minutes
Near field model	Plume3D
Use distance to Nearest Neighbour	OFF
Approx. ext. conc.	ON
Stretch env. Data	ON
Adjust surfacing thickness	ON

4.4.5 Environmental parameters

4.4.5.1 Current and wind

The current and wind files used were obtained from Ragnhild Lundmark Daae with data from the year 2000. The current files used were DNMI_Curr4km_Jun2000.dir and DNMI_Curr4km_Jan2000.dir, for summer and winter scenarios respectively. The wind file used for all scenarios was NHAV65_7.WND. All files were for the Norwegian Sea area (Province parameter in OSCAR input).

4.4.5.2 Salinity and temperature

The salinity and temperature profiles at the nearest available coordinate was Longitude 7.5E and Latitude 64.5N obtained February 24, 2019 from the NVODS database using the World Ocean Atlas 2001 1x1 degree monthly means. These were the closest dates to the model scenario timeline. See temperature and salinity profiles in Figure 4-8.
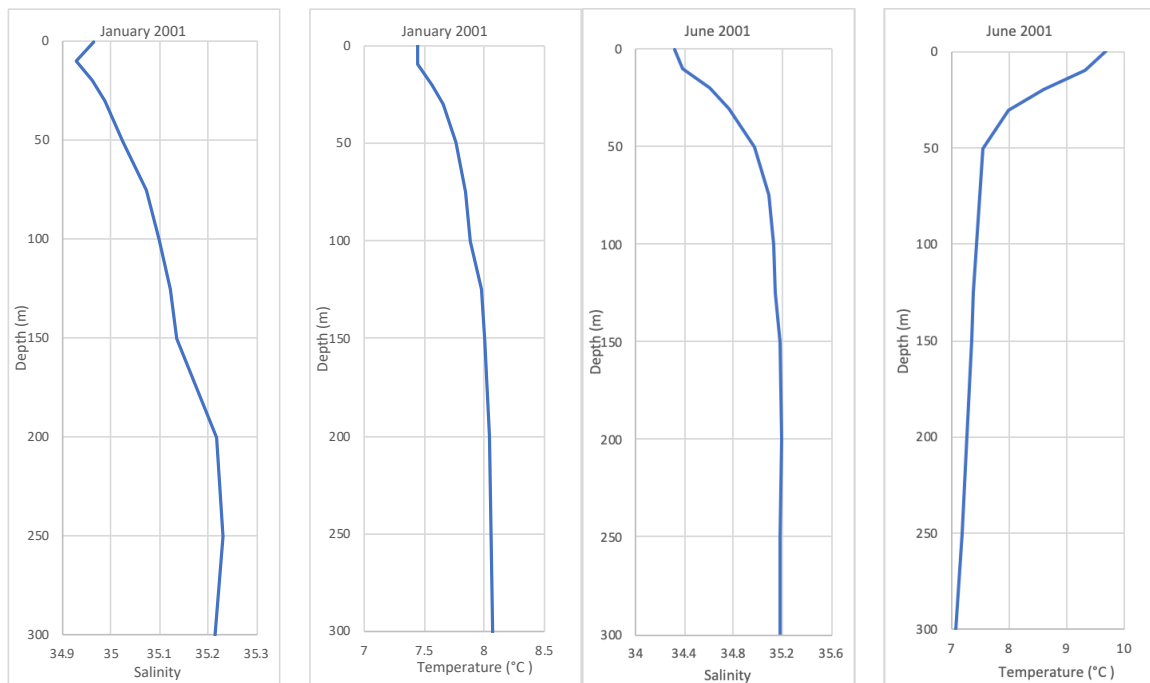

Figure 4-8 Salinity and temperature profiles for January 2001 and June 2001 (National Virtual Ocean Data System (NVODS), 2001).

4.4.6   Biologic component of the Njord field

The Njord field lies in a biologically diverse area near the Froan Protected area. The area is an important habitat for fish, seabirds and seals (Atlas of Marine Protection, 2019). Commercial fish stocks in the Norwegian Sea are generally considered satisfactory, however, certain species are seeing a decline in stocks. The *Clupea harengus* stock is declining as a result of weak recruitment. While *Sebastes mentella* stocks are increasing, the *Sebastes marinus* stock is at a historically low level and no fishing of this species is permitted (The Directorate of Fisheries and the Norwegian Environment Agency, 2018). A table of important fish species for the area are given in Table 4-7, along with the spawning months and IUCN status. The population density for fish by region was not available, however, distribution and spawning grounds are reported for numerous species and overlap with the Njord field and Froan areas (Geodata from the Institute of Marine Research, n.d.; Rantrud, 2016).

Table 4-7 Fish species distributed along the Njord field and their spawning season (S). The species' IUCN status from 2015-2018 publications is reported with the following categories: critically endangered (CR), Highly endangered (EN), Vulnerable (VU), Near threatened (NT), and Least concern (LC). The threatened and near threatened categories are underlined. Adapted from Statoil (2016) and IUCN (2018).

Species	IUCN (year published)	Jan	Feb	Mar	Apr	May	Jun	Jul	Aug	Sept	Oct	Nov	Dec
Nordøstarktisk Sei *Pollachius virens*	LC (2015)	S	S										S
Norsk vårgytende sild *Clupea harengus*	LC (2015)		S	S									
Vanlig Uer *Sebastes marinus*	VU (2015)				S	S							
Snabeluer *Sebastes mentella*	EN (2015)			S	S								
Øyepål *Trisopterus esmarkii*	LC (2014)	S	S	S	S	S							

The fish present provide important resources for fishing, as well as, sustenance for other marine animals, including seals and seabirds. The Froan reserve and nearby coastline are important habitat for Harbour seals (*Phoca vitulina*) and the Grey seal (*Halichoerus grypus*) both listed as IUCN LC species in 2007. The Froan reserve and surrounding area is an important breeding, migrating,

molting and wintering site for numerous seabirds. The predicted density by species of seabird is given in table 4-8.

Table 4-8 Predicted seabird density by species and season in 10 x 10 Km² map grids near the Njord field. Density categories are based on the Seapop.no number of individuals per square grid, summarizing as: low <0.3; medium 0.3-10; high >10; no data - (SEAPOP, 2018). The species' IUCN status from 2015-2018 publications is reported with the following categories: critically endangered (CR), Highly endangered (EN), Vulnerable (VU), Near threatened (NT), and Least concern (LC). The threatened and near threatened categories are underlined. Adapted from Statoil (2016), SEAPOP (2018) and IUCN (2018) webpages.

Species and sensitivity	(year published)	Summer (Apr-June)	Autumn (July-Oct)	Winter (Nov-March)
Alkekonge *Alle alle*	LC (2015)	medium	low	high
Alke *Alca torda*	NT (2015)	low	low	medium
Lunde *Fratercula arctica*	VU (2018)	medium	medium	high
Havhest *Fulmarus glacialis*	LC (2018)	high	high	high
Fiskemåke *Larus canus*	LC (2015)	low	-	-
Polarmåke *Larus hyperboreus*	LC (2015)	low	low	low
Svartbak *Larus marinus*	LC (2015)	medium	medium	high
Gråmåke *Larus argentatus*	NT (2015)	medium	medium	high
Krykkje *Rissa tridactyla*	VU (2015)	high	medium	high
Havsule *Morus bassanus*	LC (2015)	low	medium	low
Polarlomvi *Uria lomvia*	LC (2015)	low	low	low
Lomvi *Uria aalge*	NT (2015)	medium	medium	medium

4.4.6.1 *Species sensitivity to oil*

Most laboratory studies use high concentrations of oil in toxicity studies which are not environmentally relevant concentrations. Due to the complexity and variety in composition of different oil types, along with complex interactions of oil in the environment, it is difficult to assess the toxicity of a particular oil to a specific species. Surface oil is the leading cause of oil spill mortality for birds and sea mammals (Peterson, 2003). Following the literature review findings from French-McCay (2009), a threshold thickness of a lethal dose to an individual marine animal

of 10g/m^2 was used in their risk assessments. However, other authors have reported that an oil thickness of 1g/m^2 is 100% lethal to birds oiled by such a slick, while 0.1g/m^2 is not enough to cause acute mortality (Varoujean et al., 1983). The latter interval of 0.1g/m^2 to 1g/m^2 is selected for assessment during this study as it is a more conservative estimate than the higher value. It must also be noted that in order to become coated in oil, the bird must swim through the slick for some distance to obtain a lethal dose (French-McCay, 2009, 2002). It is not possible to determine the behaviour of an individual animal or total risk exposure with the version of OSCAR used.

Fish are impacted by water column concentrations of oil. Egg and larval stages of fish are particularly at risk as they lack the motility to escape an oil spill. The distribution of fish eggs and larvae will determine if they are impacted by a spill. *Clupea harengus* eggs are demersal and are affected by increased oil in the sediment. *Trisopterus esmarkii*, *Pollachius virens*, *Sebastes mentella* and *Sebastes marinus* eggs are pelagic and are more susceptible to increased water column concentrations of oil (Anderson and Akenhead, 1981; Nash et al., 2012; Olsen et al., 2010).

Following a literature review of 93 studies, Johansen et al. (2003) found the lowest reported LC$_{50}$ to be 90 ppb across multiple species of fish, algae and invertebrates. This was considered to be the threshold at which only the most sensitive organisms face mortality. However, herring eggs exposed to much lower concentrations of 9.1ppb for fresh crude and 0.4ppb for weathered crude, displayed a multitude of effects including malformations, genetic damage, decreased size and inhibited swimming, and mortality (Carls et al., 1999; Incardona et al., 2015). Weathered crude oils tend to be much more toxic due to the loss of more volatile and less toxic components, leaving a higher percentage of PAHs (polycyclic aromatic hydrocarbons) in the mixture. Though low dose, chronic exposure are suspected of population level effects (Peterson, 2003), the value of 90 ppb for acute effects is used as the threshold LC$_{50}$ in this study.

4.4.7 Maps and Locations

During September 2017, as part of the NTNU course KJ3050, marine oil pollution samples were collected around Frøya, an island outside the Trondheim fjord, Sør-Trøndelag, Norway. The first map shows the location of Frøya in relation to Trondheim (figure 4-9).

Only 6 of the 21 samples were analyzed by GC/FID and GC/MS. The chromatograms and spectra showed heavy weathering and half of the oils analyzed were possible crude oils (Bakkerud et al., 2017). Part of this thesis work was to investigate if the Njord field is a possible source of pollution along the coast near the Trondheim fjord and Froan Protected Area. If the Njord field is deemed a possible source for these samples, then further analysis of the remaining oils along with samples of Njord field oils as candidate oils should be carried out using the Nordtest method (Daling et al., 2002).

Figure 4-9 Overview of the exit of Trondheim Fjord into the Norwegian Sea highlighting Frøya, Sør-Trøndelag, Norway (Bakkerud et al., 2017). Image obtained from Google Maps (n.d.).

Samples were collected on September 19, 2017 from Sandholmen (island 1, N 63°48' and 8°23' E) and Humlingsværet (island 2, N 63° 45' and 8°24' E) shown in figures 4-10 to 4-12.
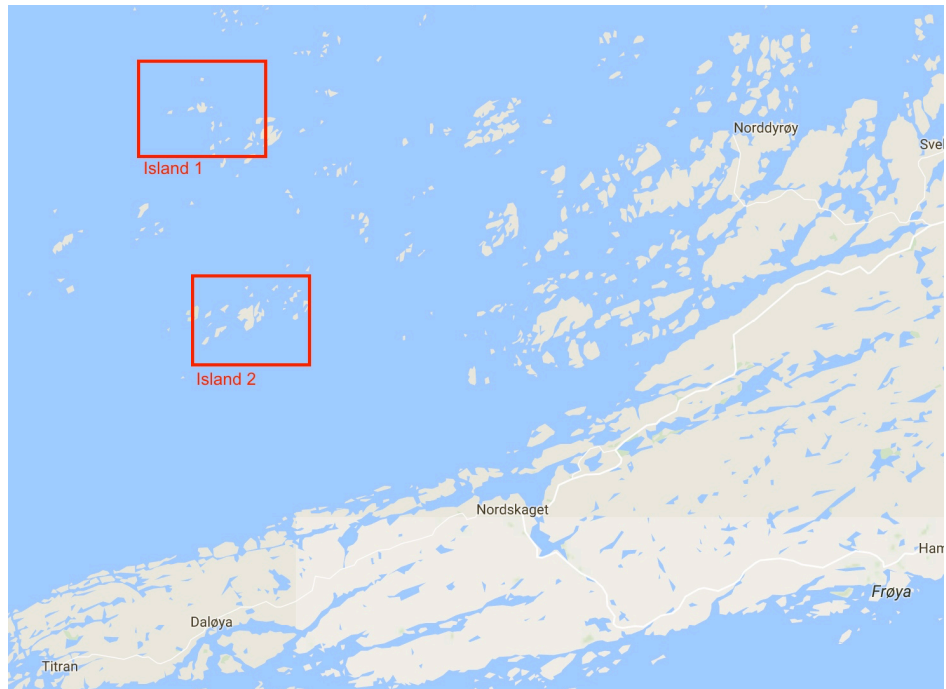
Figure 4-10 Map of Frøya with the islands, Sandholmen and Humlingsværet, highlighted (Bakkerud et al., 2017). Image obtained from Google Maps (n.d.).

Figure 4-11 Sampling island 1 (Sandholmen) with all samples marked with coordinates. The samples include Sintef-ID from 6621-51 to 6632-62 (Bakkerud et al., 2017). Image obtained from Google Maps (n.d.).

Figure 4-12 Sampling island 2 (Humlingsværet) with all samples marked with coordinates. The samples include Sintef-ID from 6633-63 to 6640-70 (Bakkerud et al., 2017). Image obtained from Google Maps (n.d.).

5 Results

The following chapter is a presentation of the results obtained from the SINTEF MiniTower experiments and OSCAR simulations. There will be a brief overview of the experiments and description of the results obtained.

5.1 Minitower

The MiniTower generates a continuous plume of oil droplets resulting from a turbulent jet. The SilCam recorded continuously during the experimental releases and a 30 second time window was then selected from each set of experimental conditions. This time window was expected to be a representative sample of the population, following a lognormal distribution.

In some instances, deviations from the lognormal distribution occurred. These experiments were either not included as results or presented with explanations to their deviations. A summary of all experiments with a brief explanation for inclusion or removal from the analysis can be found in Appendix B. Further commentary is found in the discussion section.

5.1.1 Standard Solutions

SINTEF stock solutions of mono disperse polypropylene particles of 80 and 346 μm were used to assess the accuracy of the SilCam. The SilCam measured the particles at 81 and 360 μm. This provides an absolute error of 1μm and 14 μm respectively, or a relative error of 1.25% and 3.89%. Note the MATLAB script outputs from the SilCam (figures 5-1 and 5-2) show a steep and narrow curve, representing minimal diversion from a single, measured value.
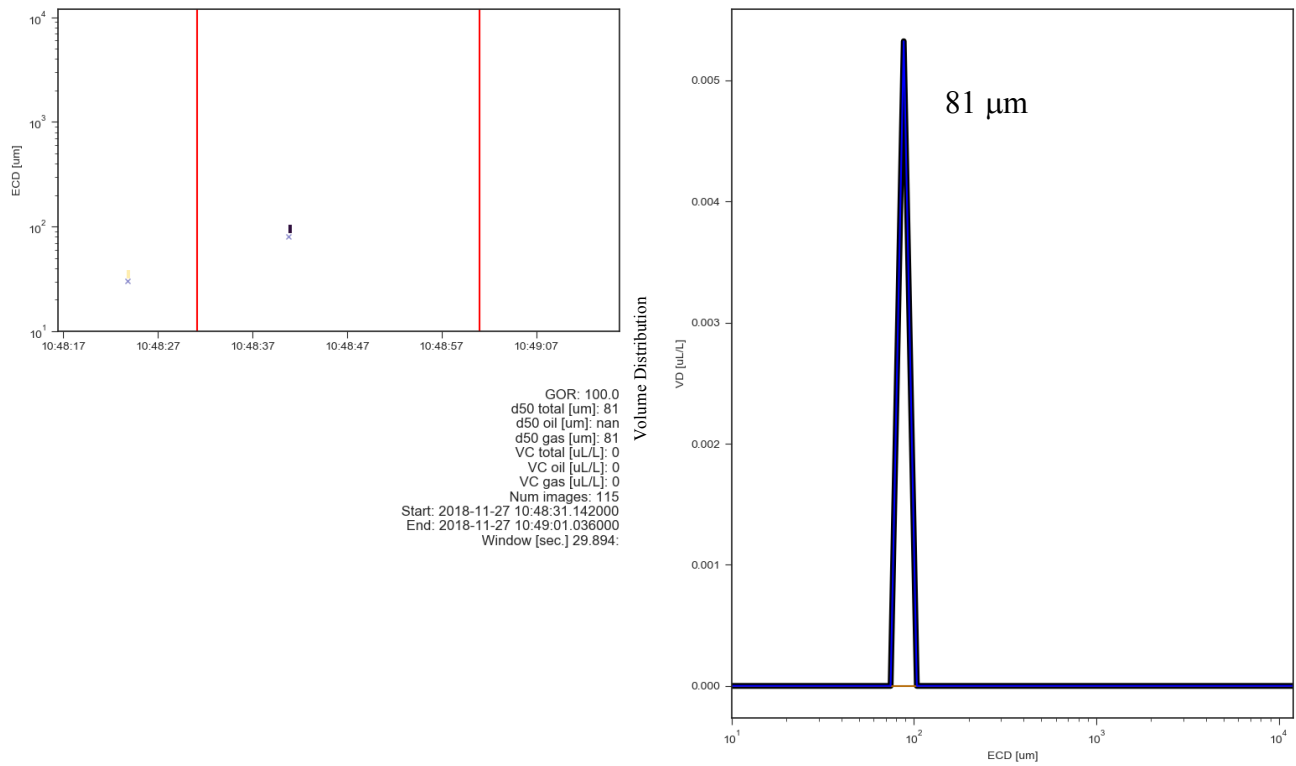
Figure 5-1 SilCam software MATLAB script output showing narrow peak over 81 μm for the 80 μm polypropylene stock solution.
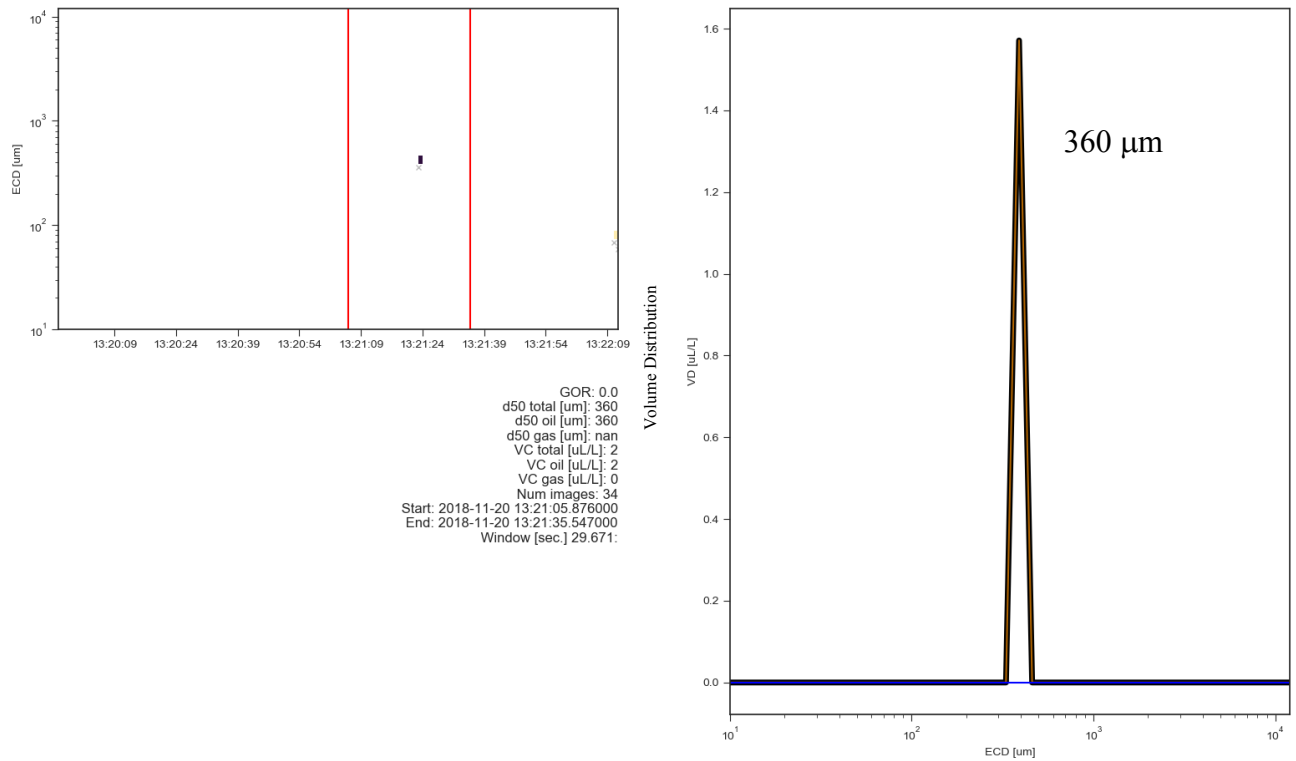

Figure 5-2 SilCam software MATLAB script output showing narrow peak over 360 μm for the 346 μm polypropylene stock solution.

5.1.2 Oil Type

As the field of interest was the Njord field, the intention was to use Njord oil for the experimental portion. Njord is a very light-coloured oil (see figure 5-3) and as such, the SilCam with the configuration used had difficulty quantifying the oil, reporting a large portion of the droplets as gas. Machine learning and a software update are planned to resolve this issue but it was beyond the timeline and budget of this master project. Therefore, Oseberg Blend 2017, a light, paraffinic oil type, used in many SINTEF studies with good results, was used instead. It should be mentioned that Oseberg Blend was then also used as the oil type in the modelling aspect of the project, even though this oil is not found in the Njord field.
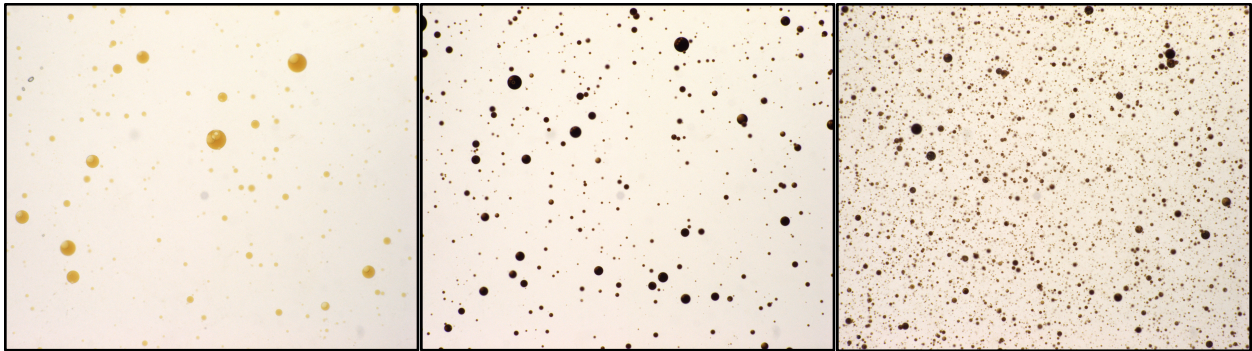

Figure 5-3 SilCam bitmap photos of the droplets produced from Njord and Oseberg oil turbulent jets at different flow rates. Pictured left: Njord oil with flow rate of 75mL/min. Middle: Oseberg blend 2017 with flow rate 75mL/min. Pictured right: Oseberg blend 2017 with flow rates of oil 50mL/min and produced water 75mL/min.

5.1.3 Turbulence Regime

Turbulent break up experiments can be classified in terms of Ohnesorge versus Reynolds number plots (figure 5-4) to describe the release regime. All experiments performed fall in the transitional or atomization zone.
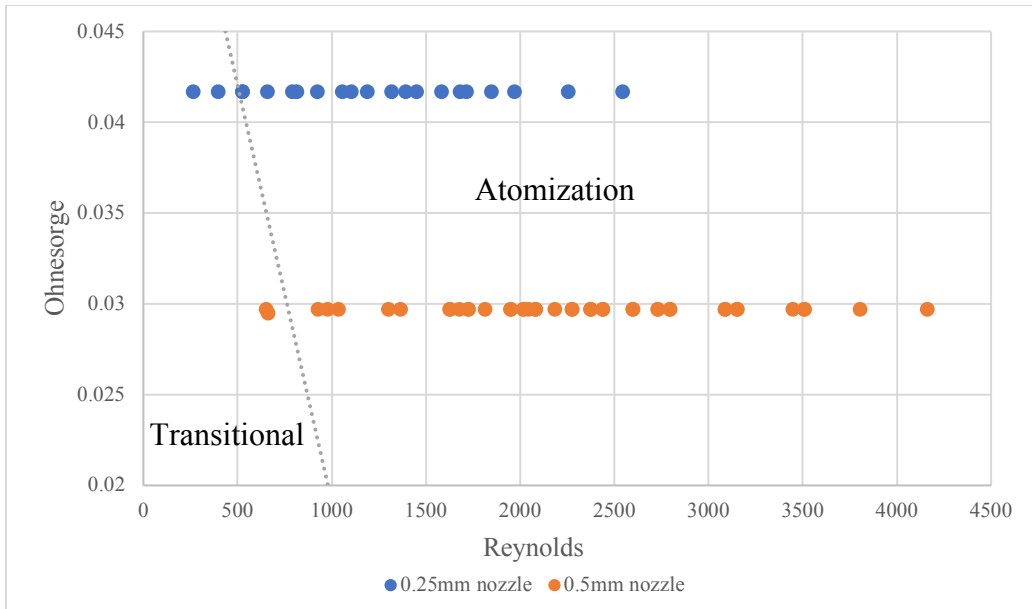
Figure 5-4 Ohnesorge versus Reynolds number plot for all experimental conditions carried out. The dotted line in the diagram shows the boundary between transitional and atomization breakup.

The turbulent conditions produced in the MiniTower during this study were very different from those produced during the DeepSpill experiment (Johansen et al., 2003a). However, the DeepSpill turbulent conditions were similar to the larger releases modelled (figure 5-5). By comparison, the small pipeline leak modelled is more similar in Ohnesorge and Reynolds description to the experimental releases carried out in the MiniTower than to the DeepSpill experiment.
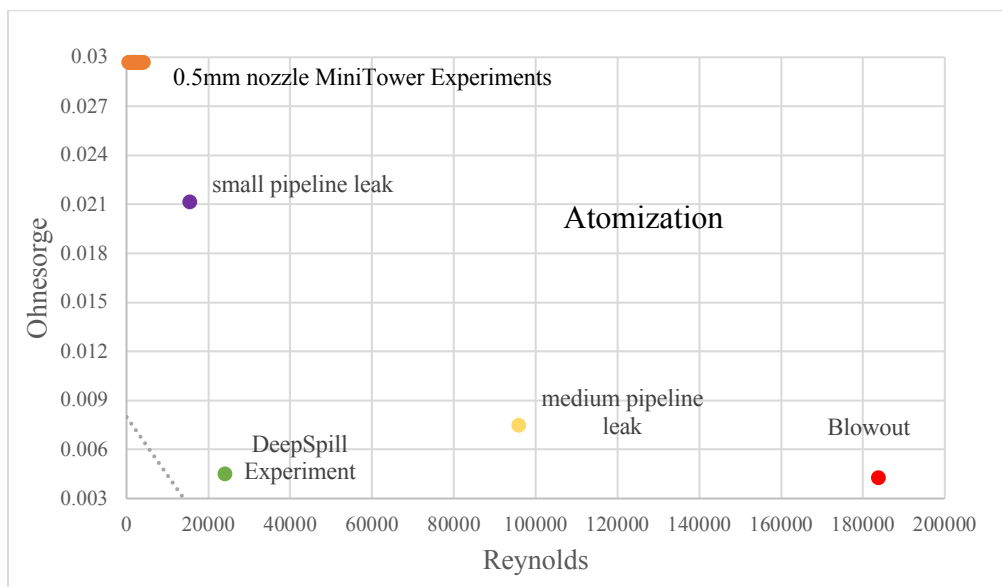

Figure 5-5 Ohnesorge versus Reynolds number plot showing the approximate position of the DeepSpill experimental conditions relative to conditions produced in the experimental and modelling portions of this study. The dotted line in

46

5.1.4   Droplet Distributions

Both a 0.25 mm and 0.50 mm nozzle were used as exit diameters for the releases. Experiments performed included releases containing increasing flow rates of oil alone, releases where the oil flow rate was held constant while increasing the flow rate of produced water, and experiments where oil was held constant with changing flow rates of both produced water and gas. Ultimately, only experiments where the total exit velocity, U_e, reached 10 m/s or more were included in the analysis. With the test version of SilCam software used and high concentrations of oil and oil coated gas or water droplets, there was difficulty in quantifying the experiments performed with gas. These were not included in the results.

The selected experimental conditions were produced for 90 seconds. As much as possible, the 30 second time window from which data was then selected was within the middle to final half of an experiment. Selecting droplet distributions from the very start of the release will contain a greater number of large, fast droplets, whereas near the end of the experiment will have a greater proportion of small, slow droplets.

5.1.4.1   0.25 mm nozzle diameter

Experiments completed with the 0.25 mm nozzle included experiments of oil only and oil with produced water. Experiments with oil only had flow rates from 30 mL/min to 70 mL/min. The distributions are displayed on the following graph (figure 5-6).
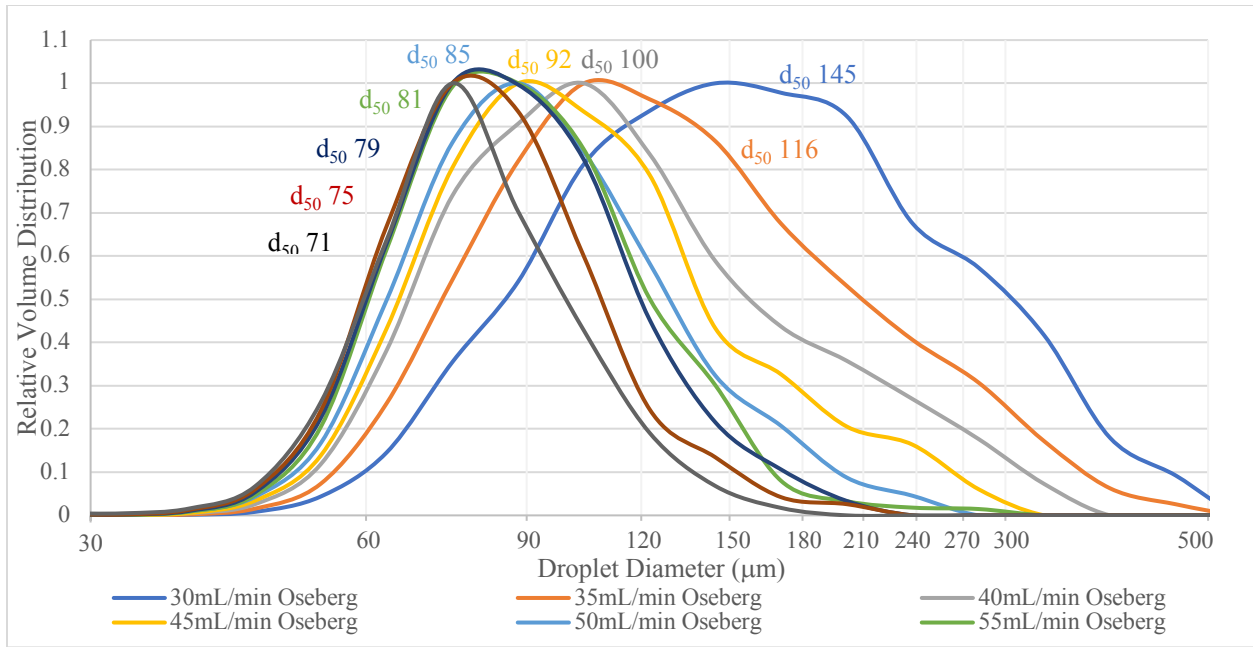
Figure 5-6 Droplet size distribution of experiments using Oseberg 2017, oil only, with flow rates from 30 to 70 mL/min and a 0.25mm nozzle.

The following chart (figure 5-7) describes the experiments using a 0.25 mm exit diameter where the oil flow rate is held constant at 20 mL/min and the produced water flow is changed from 0 to 70 mL/min.
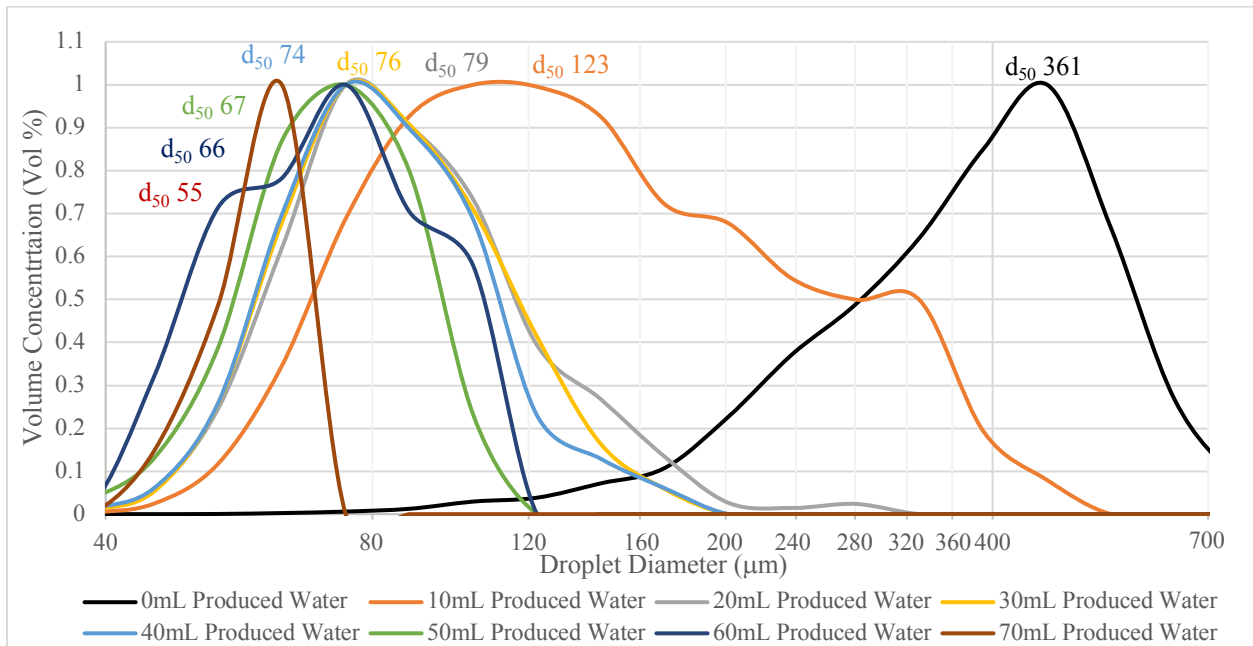

Figure 5-7 Droplet size distribution of experiments using Oseberg 2017, with oil flow rate of 20mL/min and produced water from 0 to 70 mL/min and a 0.25mm nozzle.

As with the 0.25 mm nozzle, experiments were completed with oil alone, and oil with produced water while using a 0.50 mm nozzle. Some experiments were repeated due to bimodal distributions. The following are distributions for Oseberg 2017 oil alone with flow rates of 125 mL/min to 200 mL/min, see figures 5-8 and 5-9. When the experiment was repeated, a bimodality was again observed. Upon inspection of the SilCam photos, large amounts of oil droplets can be seen fouling the lens, with some possibly slowing moving. This will be further addressed in the discussion chapter, sections 6.1.1 and 6.1.2. The greatest peak height, rather than the cumulative d_{50}, was selected to represent the mean diameter value of these distributions.
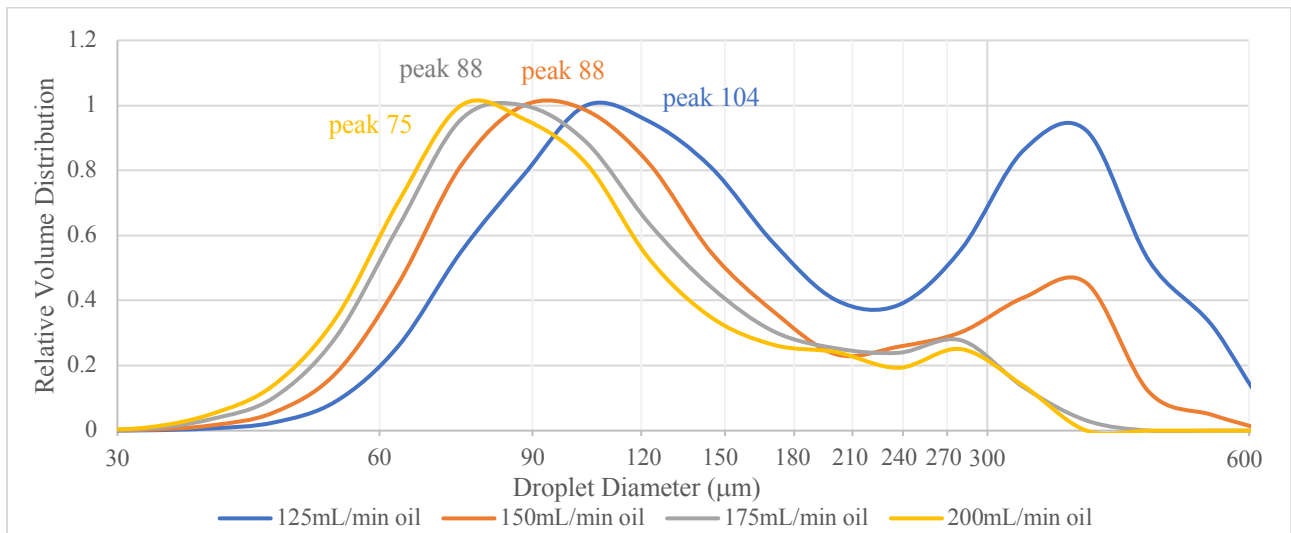

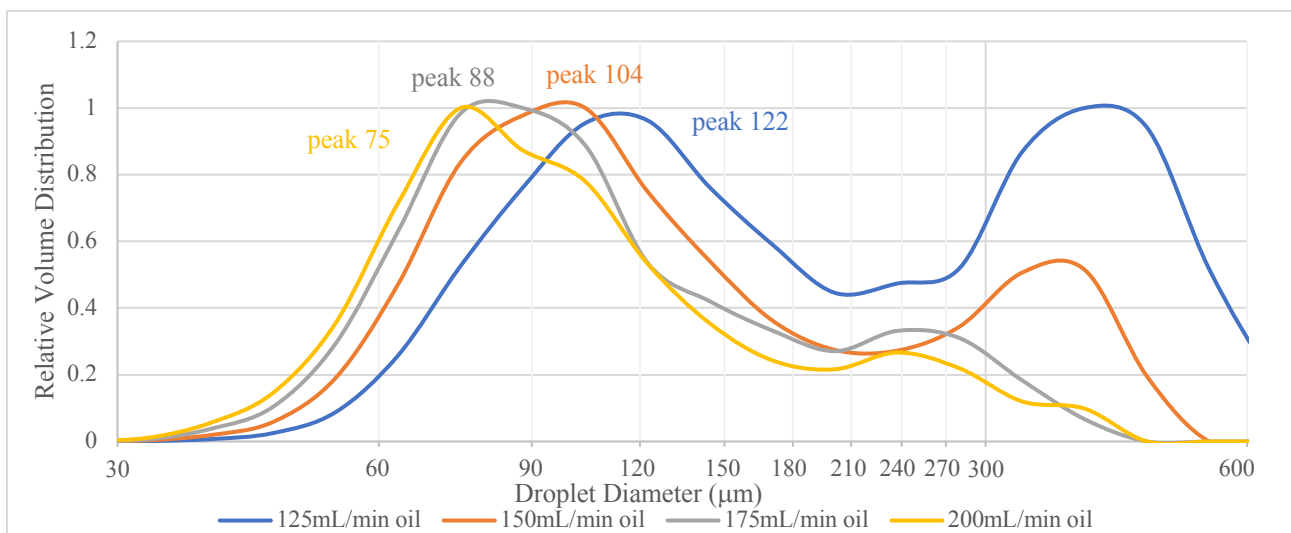*Figure 5-8 Oseberg 2017, oil only, flow rate 125-200mL/min, 0.5mm nozzle*

Figure 5-9 Oseberg 2017, oil only, flow rate 125 - 200 mL/min, 0.5mm nozzle.

Experiments with the oil flow constant and changing produced water flows were carried out for two different flow rates of oil. At an oil flow of 50 mL/min, the produced water was adjusted from 100 to 200 mL/min (figure 5-10). The upper figure shows the same series plotted with oil alone at 50mL/min to show the change in d_{50}. A large droplet, emerging from coalesced oil adhered to the camera, created a second peak in the 175 mL/min produced water series but its presence has not changed the measured d_{50} of the droplets. The measured values are much smaller than predicted from the Modified Weber formula. This experiment was repeated and the smaller droplet sizes were confirmed. This indicates that another process was occurring, this will be discussed further in section 6.1.2. The repeated experimental data is found in Appendix C.
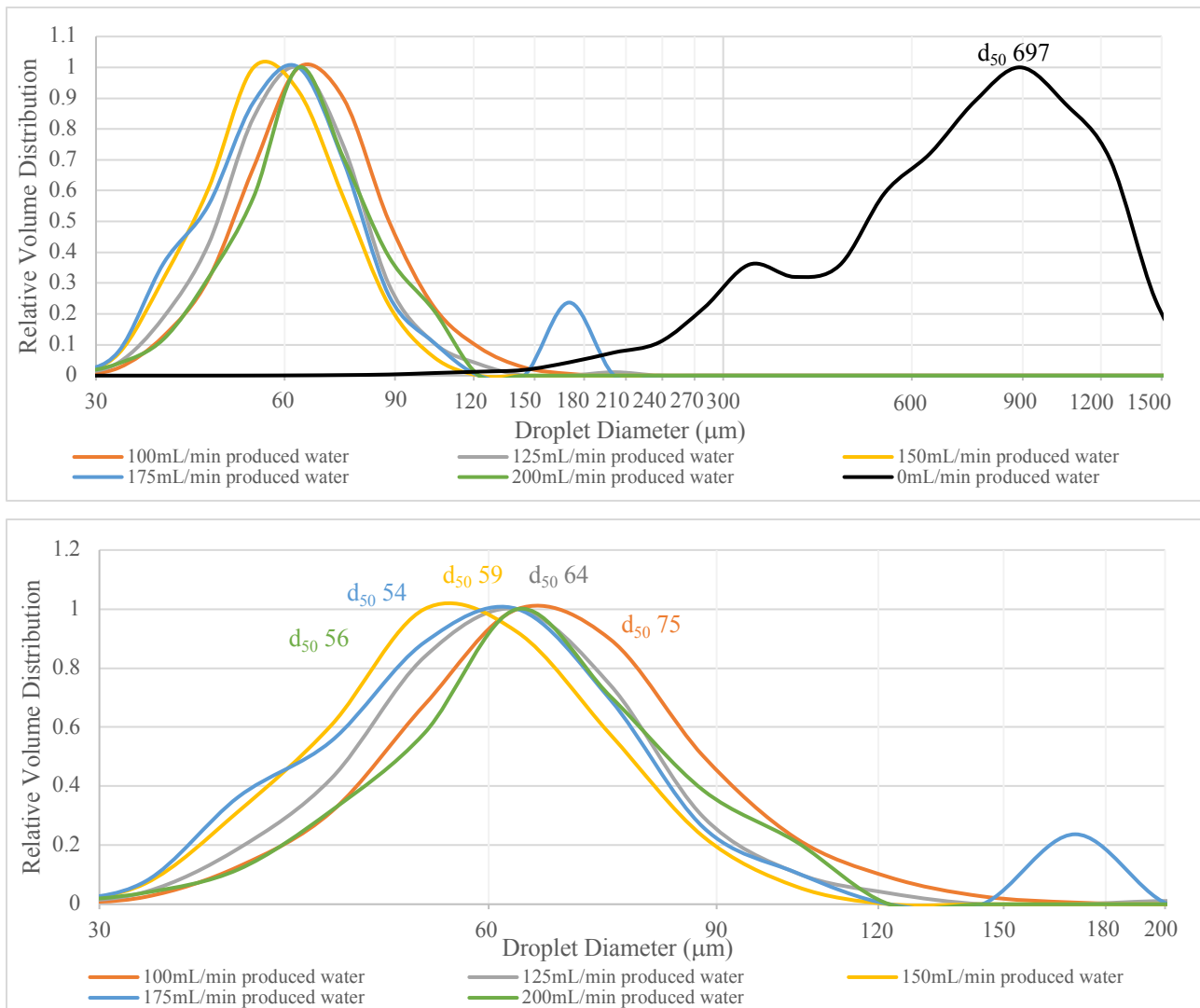

Figure 5-10 Oil flow constant at 50 mL/min with produced water from 100 to 200 mL/min, 0.5mm nozzle. Above, the same figure including the d_{50} of oil alone at 50mL/min.

A second oil flow rate of 100 mL/min was carried out with produced water flow rates from 50 to 125 mL/min. Figure 5-11 shows that the distributions are lognormal, however, the measured values are well below the predicted values from the Modified Weber equation. This experiment had also been repeated in order to confirm the low diameters, indicating that another process was occurring, see section 6.1.2 for a discussion of this process. The data for the repeated experiments may be found in Appendix C.
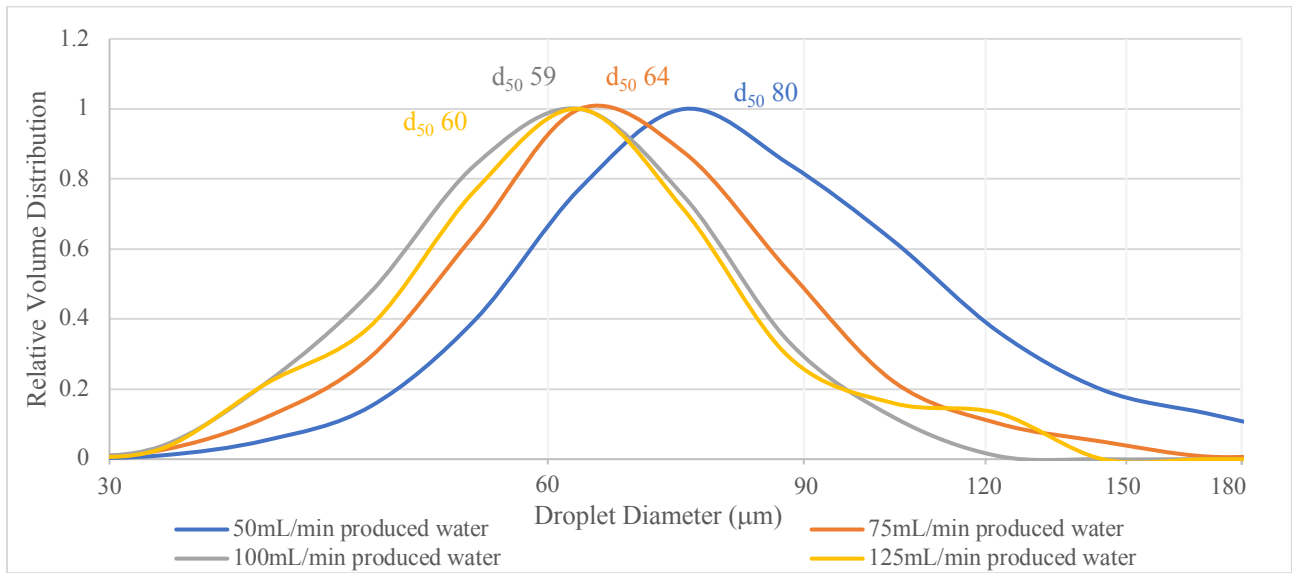
Figure 5-11 Oseberg 2017 at constant flow rate of 100 mL/min with produced water ranging from 50 to 125 mL/min, 0.5mm nozzle.

5.1.5 Correlation of droplet size with discharge conditions

The droplet size decreases with increasing exit velocity; however, the relationship is not linear, see figure 5-12. As the exit velocity continues to increase, the decrease in droplet size begins to plateau. The U_e increased linearly amongst the experiments, figure 5-13.
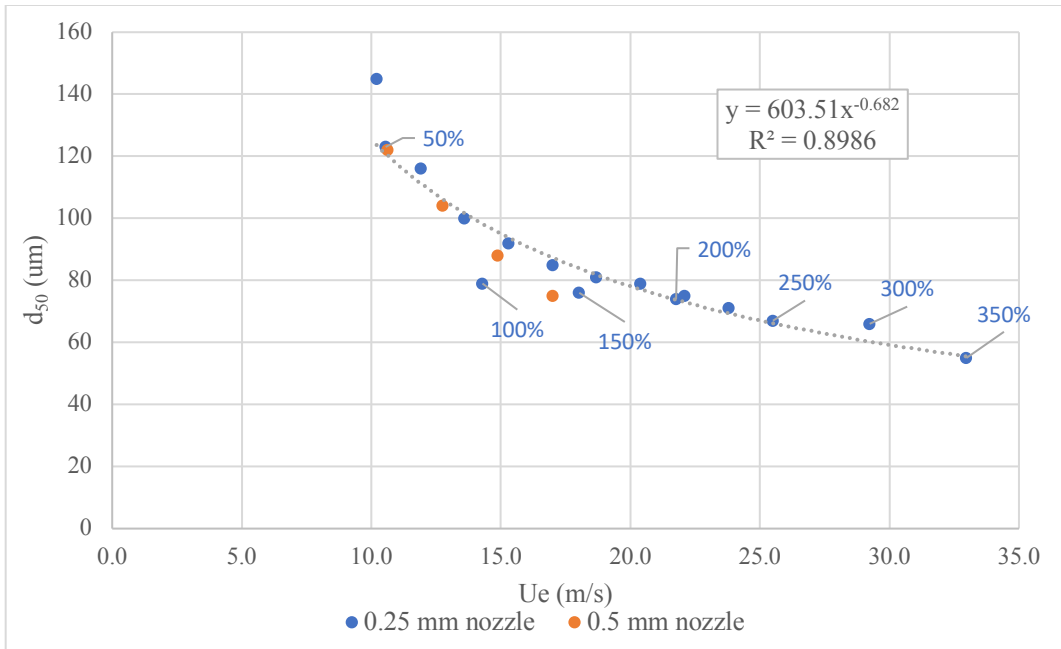
Figure 5-12 d_{50} versus Ue graph. The droplet d_{50} decreases as the exit velocity (Ue) is increased. Releases with produced water are denoted with the percentage of water relative to oil.
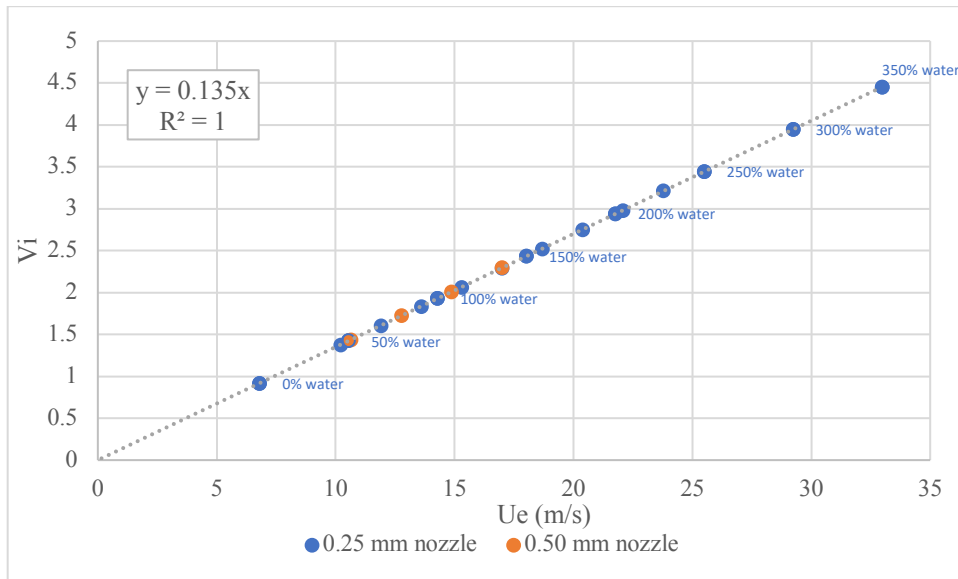
Figure 5-13 Vi versus Ue graph. The linear increase of Vi with increasing Ue among the experiments.

The exit velocity increased steadily with the percentage of produced water, figure 5-14, in the series of experiments with the 0.25 mm nozzle with oil and produced water.
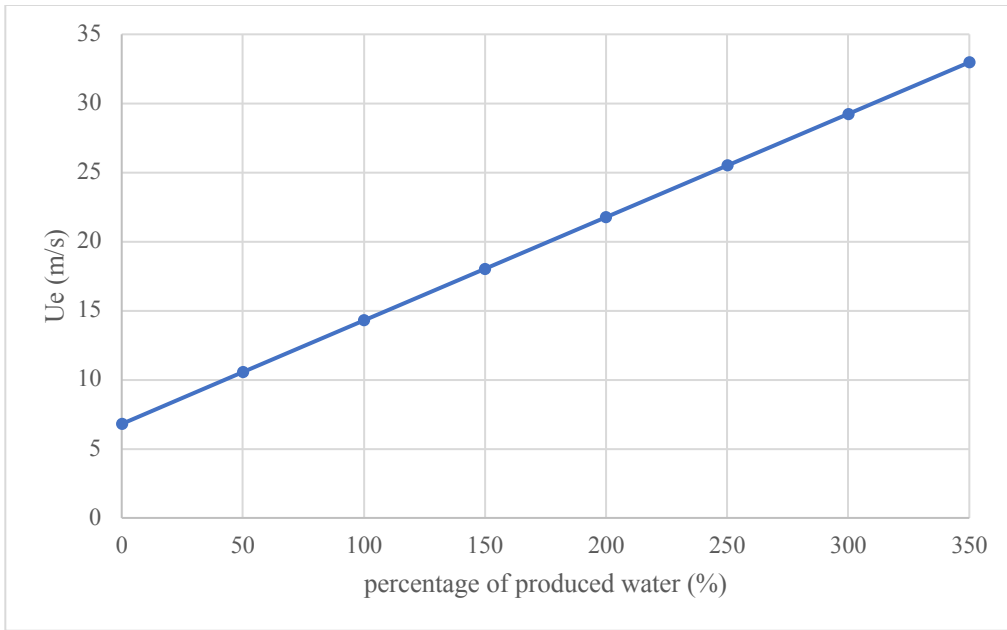
Figure 5-14 Plot of Ue versus the percentage of produced water in the release. The exit velocity increased with increasing percentages of produced water.

The droplet d_{50} decreased rapidly from 0% to 50% produced water. The change in droplet d_{50} then decreased with increasing percentages of produced water, figure 5-15.
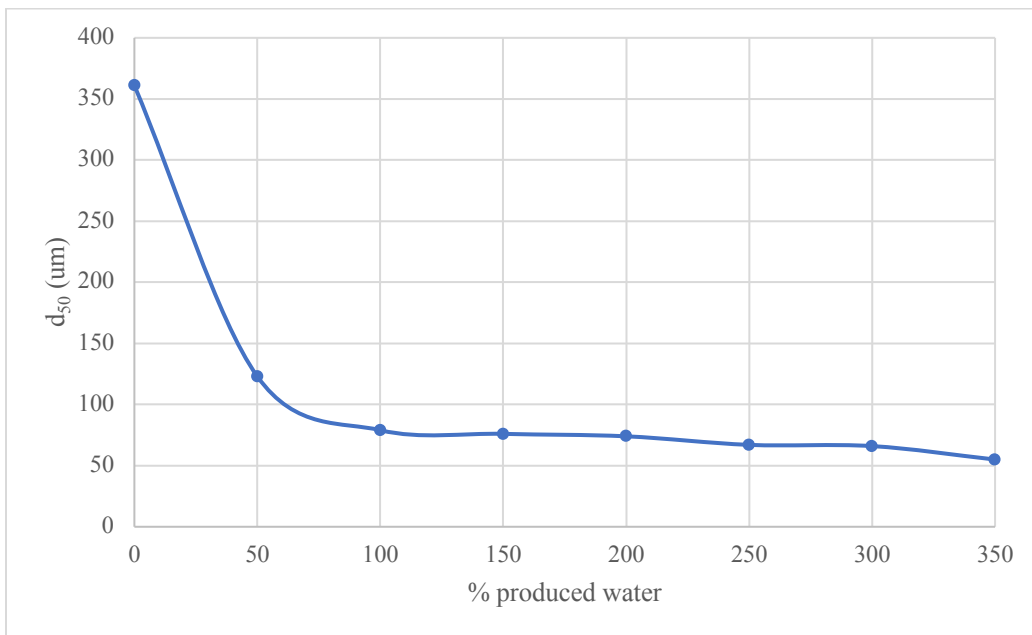
Figure 5-15 d_{50} versus the percentage of produced water plot.

5.1.6 Predicted versus measured values

Plotting the predicted versus measured d_{50} with the line showing a correlation of one, a large deviation is observed for the experiments using the 0.50 mm nozzle along with produced water. The measured values are much smaller than predicted, see figure 5-16. In moderate percentages of produced water, the measured d_{50} was much lower than predicted. As the percentage of water was increased (with an associated increase in turbulence) the values begin to approach the predicted values, see figure 5-17. Removing these experiments, figure 5-18, shows much better agreement between the remaining values. The argument for removing these values is presented in the discussion, section 6.1.2.
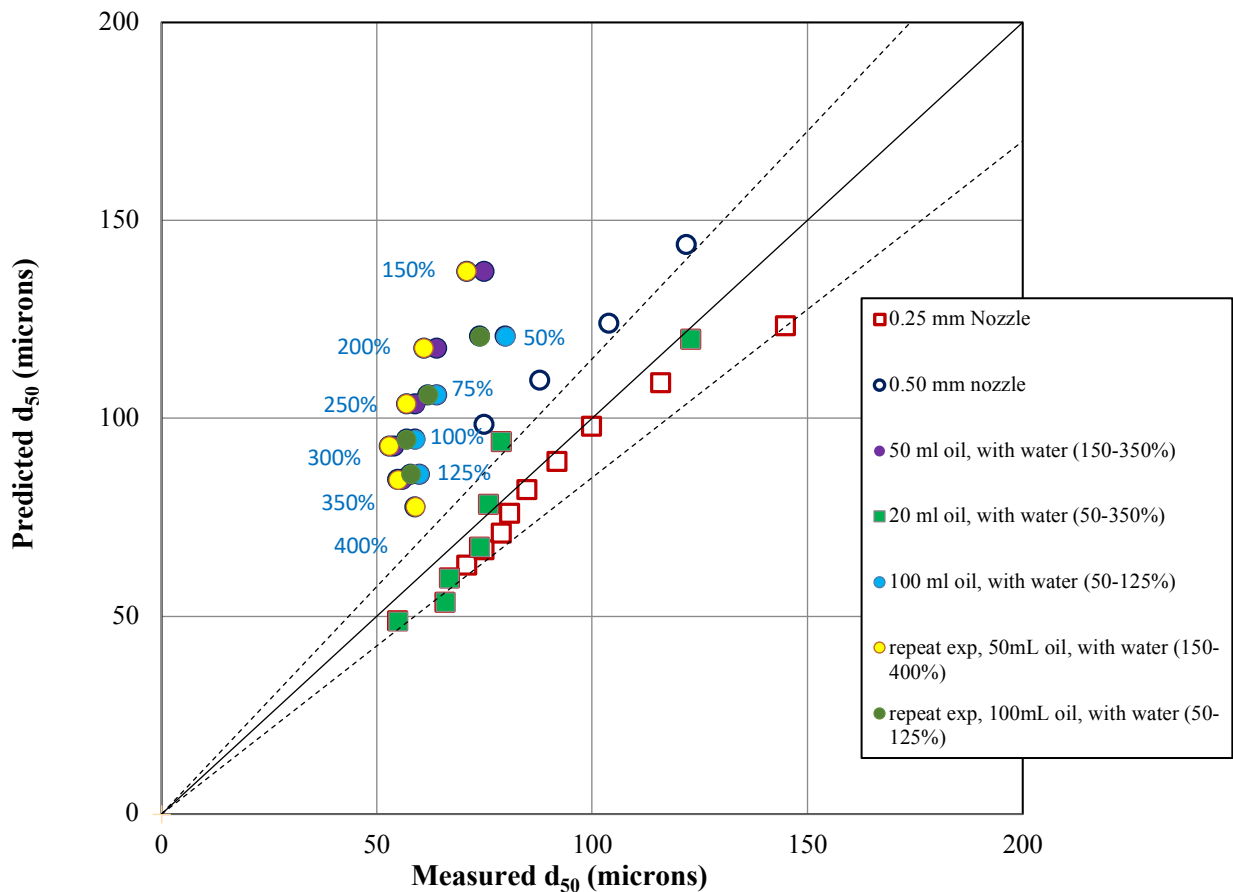
Figure 5-16 Predicted d_{50} versus Measured d_{50}, all values considered. Broken lines show a 10% deviation from the correlation of one line.
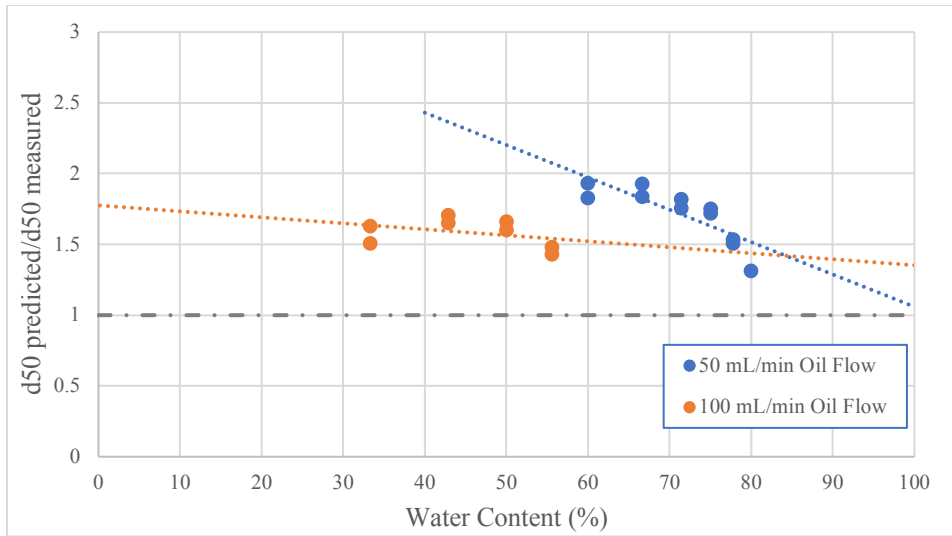
Figure 5-17 Ratio of the predicted d₅₀ to the measured d₅₀ versus the percentage of produced water in the release. In moderate to high percentages of water, the observed d₅₀ was significantly lower than predicted. The negative slope shows that as the percentage of water was increased (with an associated increase in turbulence) the values begin to approach the predicted value.
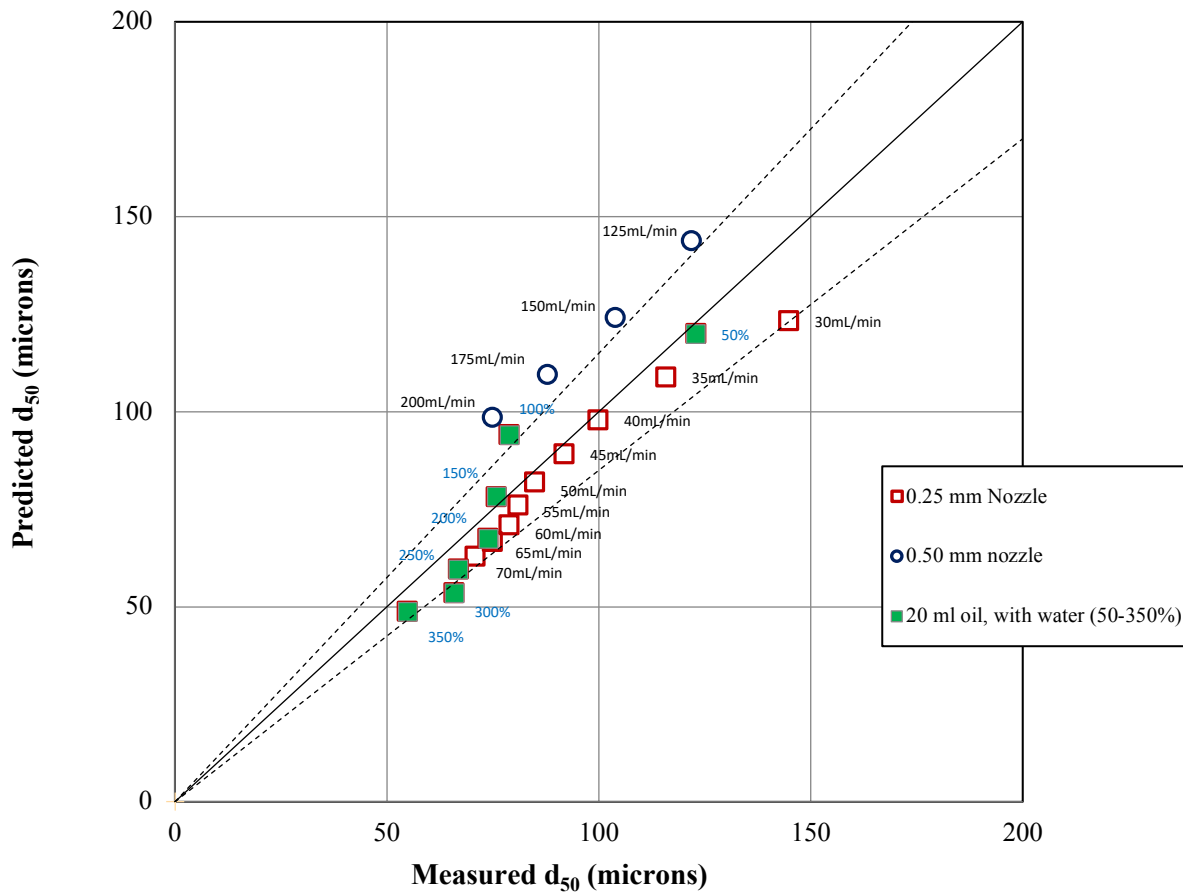
Figure 5-18 Predicted d₅₀ versus Measured d₅₀, with the 0.50 mm nozzle, oil with produced water data removed. Broken lines show a 10% deviation from a correlation of one line.

5.1.7 Modified Weber Constants

The modified Weber constants, A and B, are empirically derived constants. The previous values, 24.6 and 0.08, are optimized from the SINTEF Tower Basin and the DeepSpill experiment (Brandvik et al., 2015b, 2013) and best describe low velocity releases. New empirical values for A and B, 8.5 and 7.68, were optimized by linear best fit for the high velocity data collected from this series of experiments. The same plots as seen above are shown, first with the old values of A and B, figure 5-19. Then with the newly derived values, figure 5-20. As shown, the old values tend to underestimate droplet sizes based on the Modified Weber equation. The new values show better agreement between predicted and measured droplet sizes. There are many combinations of A and B that will result in a linear regression slope of 1 in the following two graphs (predicted d_{50} is equal to observed d_{50}), these are plotted in figure 5-21 left. The values ultimately chosen for A and B are the peak of the R^2 versus A graph, figure 5-21 right, where the variability of the response variable is most highly explained by the linear model.

$$y = 0.7208x$$
$$R^2 = 0.6908$$
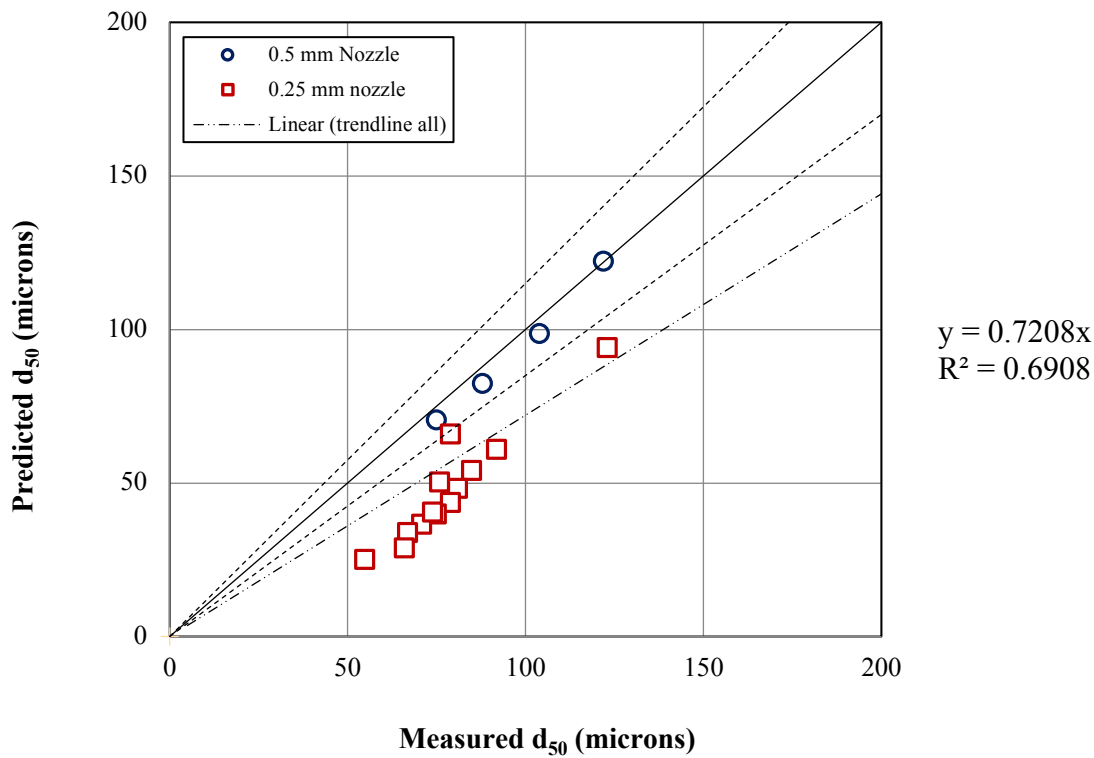
Figure 5-19 Predicted d_{50} versus Measured d_{50}, with values utilizing the Modified Weber of A and B constants, 24.6 and 0.08. The resulting linear regression line, broken line with double dots, is well below the expected correlation of 1 line. Broken lines show a 10% deviation from a correlation of 1.
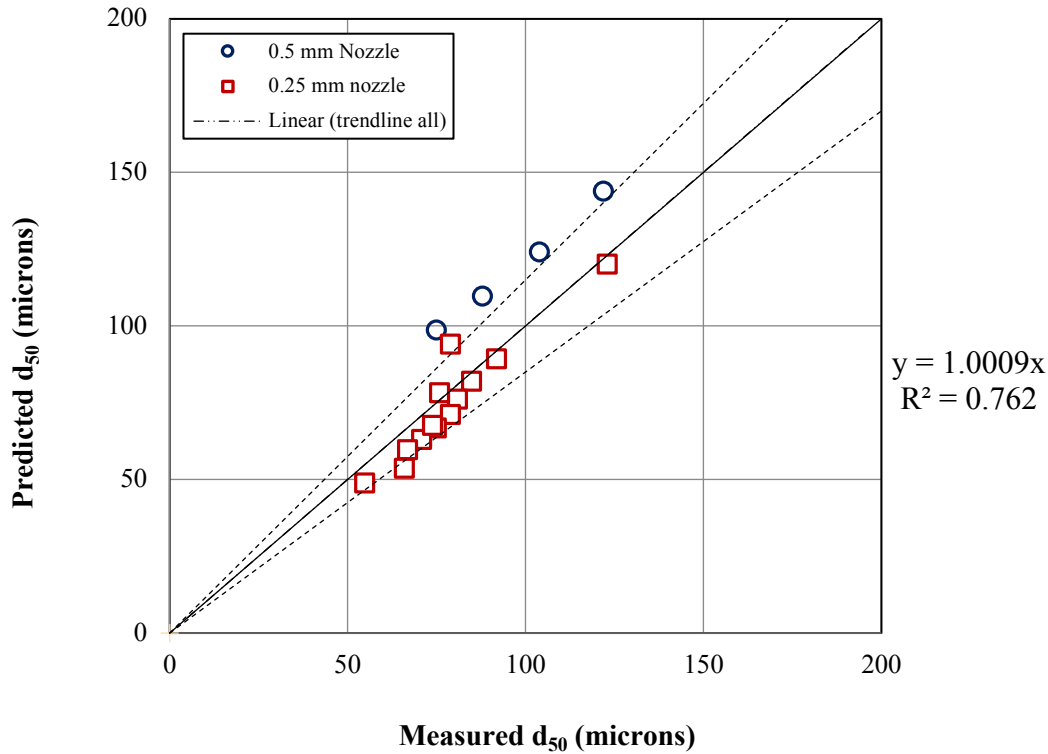
Figure 5-20 Predicted d_{50} versus Measured d_{50}, with predicted values utilizing the newly derived Modified Weber constants, 8.5 and 7.68. The data fits well with the line of correlation of 1. Broken lines show a 10% deviation from a correlation of 1.
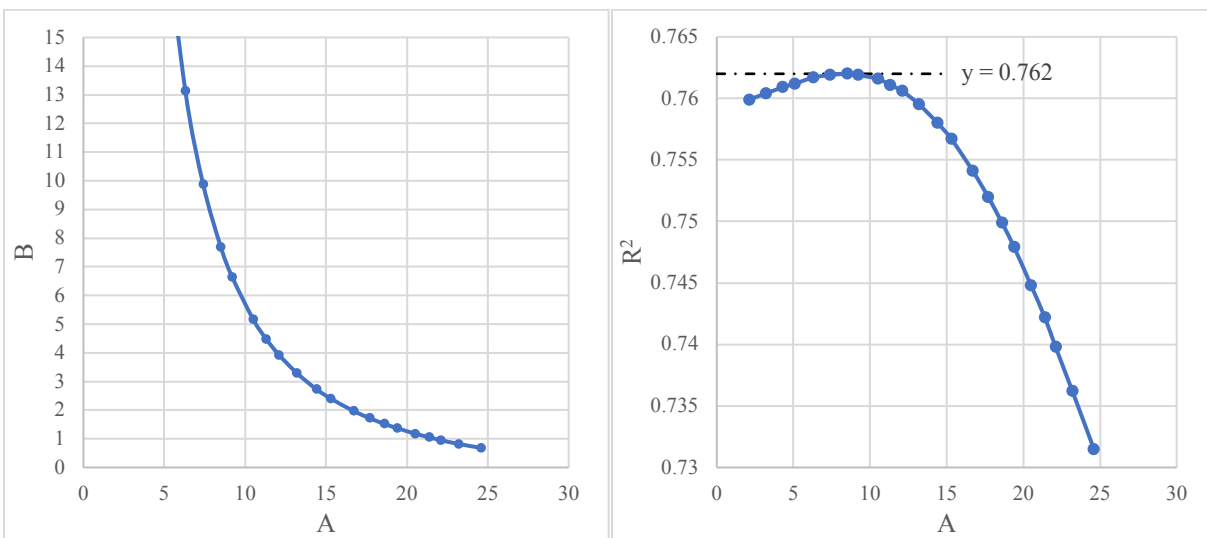
Figure 5-21 Left: Combinations of A and B that provide a correlation of 1 in the predicted d_{50} versus measured d_{50} graph. Right: R^2 as a function of parameter A combined with B graph, selecting the value of A at the peak, or greatest value of R^2, to best describe the response variability in the linear regression.

The Modified Weber scaling can be simplified to $\frac{d_{50}}{D} = AWe^{*-\frac{3}{5}}$, section 2.4.1. Plotting d_{50}/D versus the Modified Weber number yields the following graphs, figure 5-22, using the previously

determined values of A and B (left) and the values of A and B determined experimentally from this study (right). The data is better represented in this model with the new values of A and B.
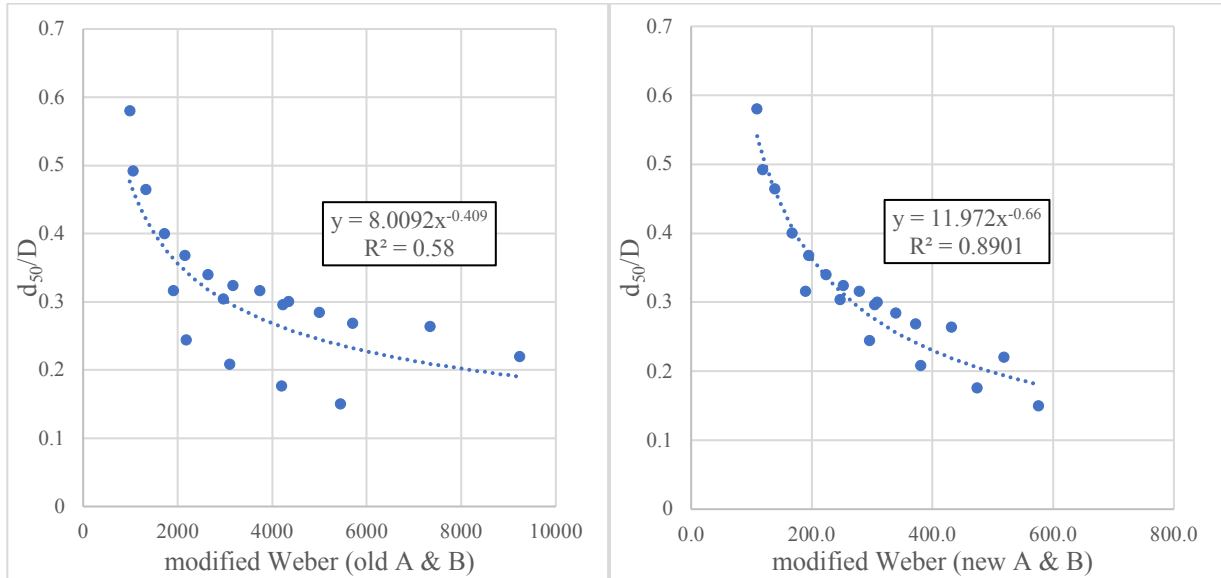
Figure 5-22 plots of d_{50}/D versus the modified Weber number, using the previous values for constants A and B on the left and the new values on the right. The modified Weber number using the new experimentally optimized A and B show a better fit to the regression line.

5.2   OSCAR modelling

In compliment to the MiniTower experimental study, an oil spill modelling exercise was carried out using the SINTEF OSCAR simulation tool to assess the consequences of a selection of different oil spills along the NCS. The Njord field was considered as a possible source for oil pollution samples collected during fieldwork in 2017. The information gained from the droplet breakup experiments was used to explore how droplet size prediction may impact the modelled behavior of an oil spill.

5.2.1   Droplet sizes

Table 5-1 shows the difference in d_{50} and d_{95} droplet sizes calculated in OSCAR, along with the manually adjusted droplet sizes, 501 and 1130 µm, that were derived empirically from the

experimental portion of this study. The same maximum stable droplet sizes calculated in OSCAR were used for all scenarios.

Table 5-1 OSCAR droplet size determination

Scenario	d_{50} (µm)	d_{95} (µm)	d_{max} (mm)
Small pipeline leak, summer	262	591	8.597
Small pipeline leak, winter	262	591	8.575
Small pipeline leak, summer, adjusted droplet sizes	501	1130	8.597
Small pipeline leak, winter, adjusted droplet sizes	501	1130	8.575
Medium pipeline leak, summer	1.696 mm	3.825 mm	8.597
Medium pipeline leak, winter	1.697 mm	3.826 mm	8.575
Blowout, summer	3.812 mm	8.597 mm	8.597
Blowout, winter	3.803 mm	8.576 mm	8.576

5.2.2 Surface thickness time series

The surface thickness (g/m^2) may be plotted versus time (in days), with the polluted area on a secondary axis. This allows assessment of the extent and severity of the impacted area. Thresholds for mortality are included, with the most conservative literature values found. A non-lethal surface thickness of 0.1 g/m^2 is considered the threshold for where only the most sensitive individuals will be at risk for mortality, whereas 1 g/m^2 is considered completely lethal (French-McCay, 2002; Varoujean et al., 1983). Figures 5-23 to 5-26 show the surface thickness time series for the summer small and medium pipeline leaks and the full blowout, without any response methods. The summer blowout with chemical response figure is also shown, it is the only scenario that showed a large decrease of surface oil with any response method. The remaining charts may be found in Appendix D.

Figure 5-23 Mass of oil by polluted area (g/m²) for the summer small pipeline release, no response methods used.
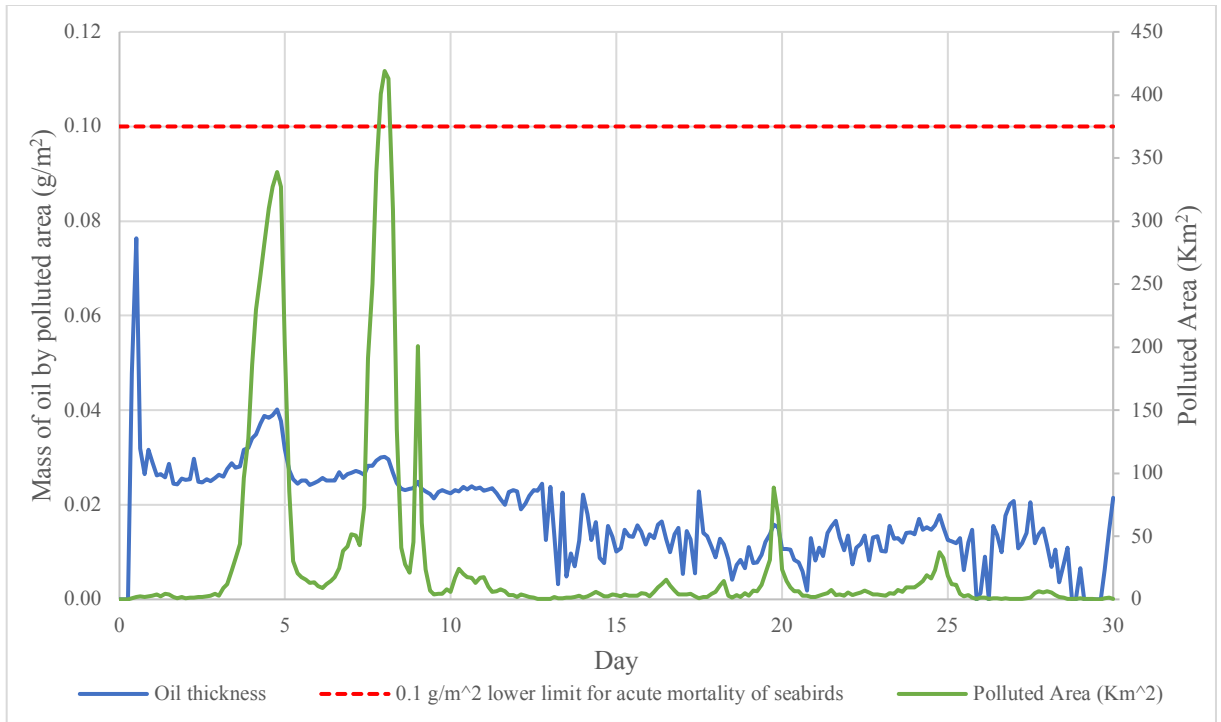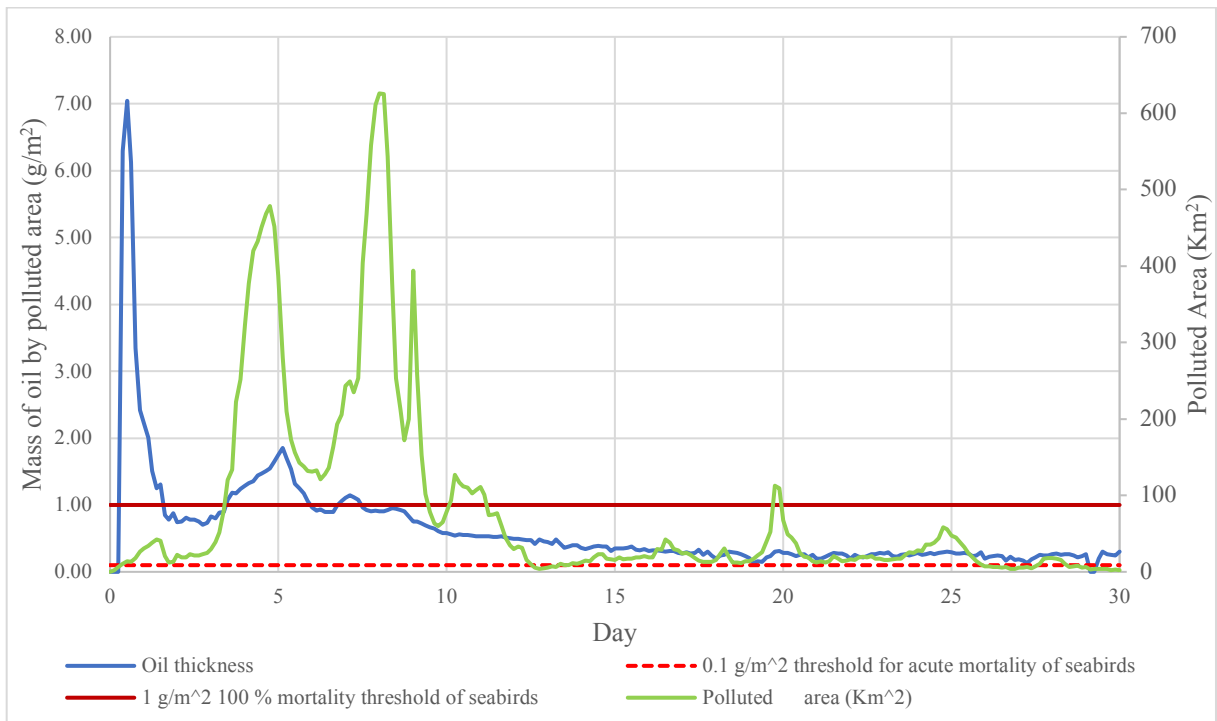

Figure 5-24 Mass of oil by polluted area (g/m²) for the summer medium pipeline release, no response methods used.
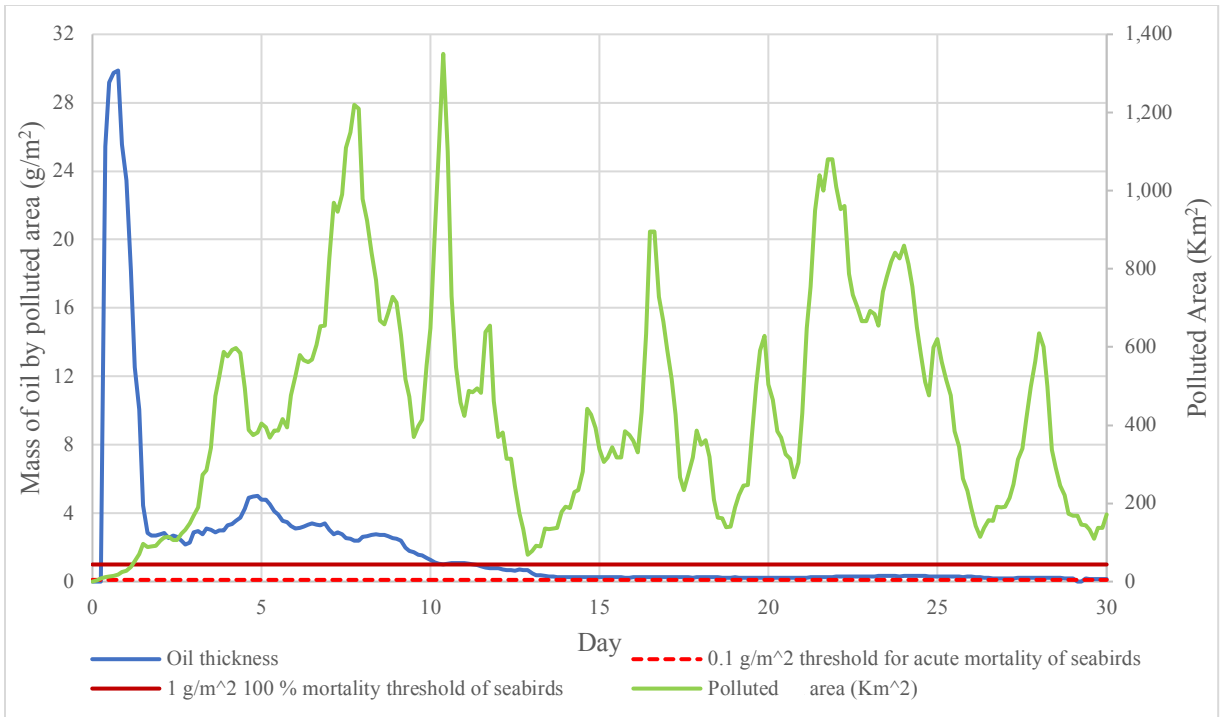
60

Figure 5-25 Mass of oil by polluted area (g/m²) for the summer blowout, no response methods used.
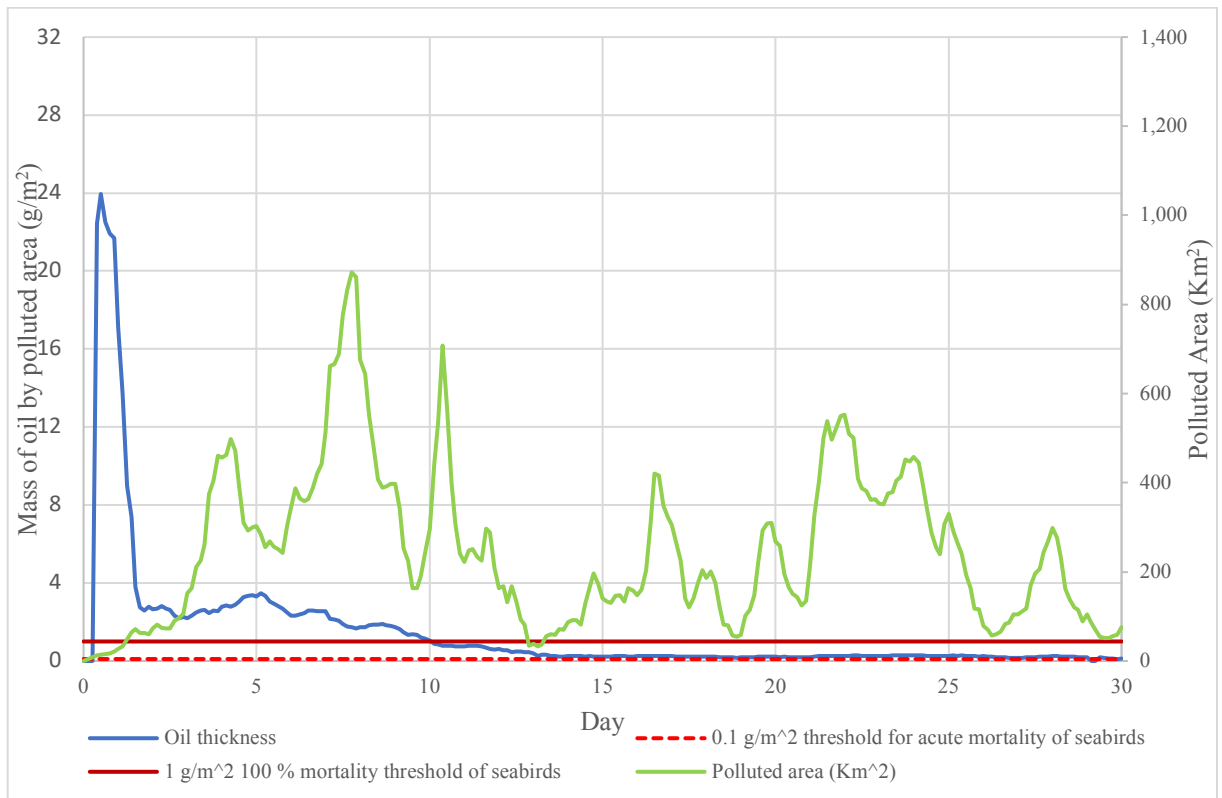
Figure 5-26 Mass of oil by polluted area (g/m²) for the summer blowout, chemical dispersants applied.

The following paragraphs describe the surface thickness (g/m^2) time series.

The surface thickness of oil did not reach the limiting value for effects on seabirds in the small pipeline leak scenarios, figure 5-23. The surface thickness was also below the threshold for response methods.

In the medium pipeline leak scenarios, the thickness surpassed the 100% mortality threshold in the first 4-5 days, figure 5-24. For the remaining days, the thickness remained above the minimum threshold but below the higher limit. Limited effectiveness of response was seen.

In the blowout scenarios, the thickness surpassed the 100% mortality threshold in the first 7-10 days, figures 5-25 and 5-26. Mechanical response did not greatly reduce the impacted area, while chemical response decreased the impacted area, especially in the summer. The thickness remained above the minimum threshold but below the higher limit to the end of the scenario.

The following table 5-2 summarizes the polluted area maximum (greatest peak height) where the surface thickness surpassed the 100% mortality threshold, as a means of comparing the severity of consequences to the biologic resources amongst the different scenarios. This shows the maximum area impacted at any time during the scenario.

Table 5-2 Summary of the surface thickness time series

Scenario	Area peak maximum over 1g/m^2 (Km^2)	Decrease in area affected due to response (Km^2)	Total amount oil treated with dispersants (tonnes)	Total amount oil recovered by skimmers (tonnes)	Total oil released (tonnes)
Small pipeline leak, summer and winter	0	-	0	0	119
Medium pipeline leak, winter	70		0	0	3014
Medium pipeline leak, winter, mechanical	70	0	0	21	3014
Medium pipeline leak, winter, chemical	40	30	171	0	3014
Medium pipeline leak, summer	620		0	0	3014
Medium pipeline leak, summer, mechanical	610	10	0	95	3014
Medium pipeline leak, summer, chemical	500	120	308	0	3014
Blowout, winter	450		0	0	8378
Blowout, winter, mechanical	450	0	0	58	8378

Blowout, winter, chemical	350	100	2112	0	8378
Blowout, summer	1350		0	0	8378
Blowout, summer, mechanical	1200	150	0	576	8378
Blowout, summer, chemical	860	490	2844	0	8378

5.2.3   Water column concentration time series

The water column concentration (ppb) may be plotted versus time (in days), with the polluted volume on a secondary axis. This allows assessment of the extent and severity of the impacted volume. Thresholds for mortality are included, with the most conservative literature value found. A lowest reported value of LC_{50} of 90ppb (Johansen et al., 2003b) is used as a concentration threshold where it is assumed only the most sensitive organisms will be impacted with 50% mortality of the population. Figures 5-27 to 5-30 show the water column concentration time series for the summer small and medium pipeline releases and the summer blowout without any response methods. The summer blowout with chemical response figure is also shown, to show the effect to the water column with dispersant use. The remaining figures may be found in Appendix E.
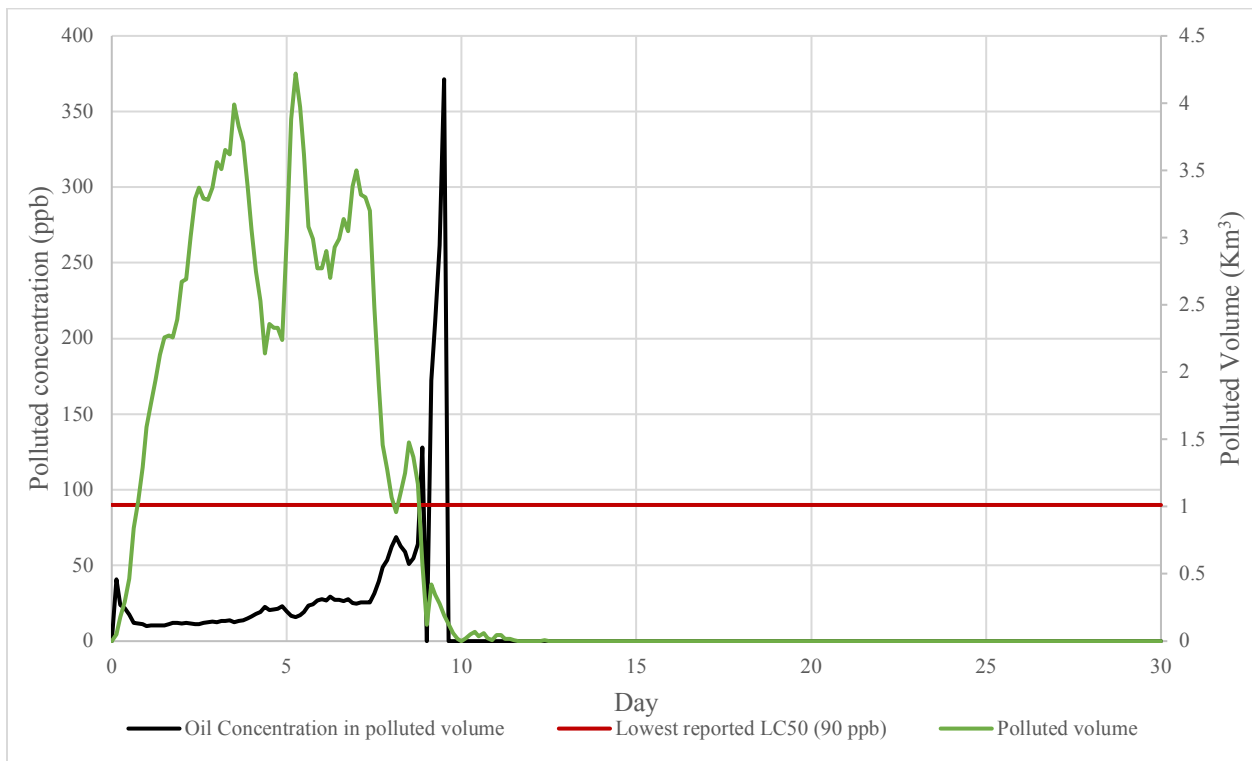
Figure 5-27 Polluted concentration (ppb) of the summer small pipeline release, with no response method.
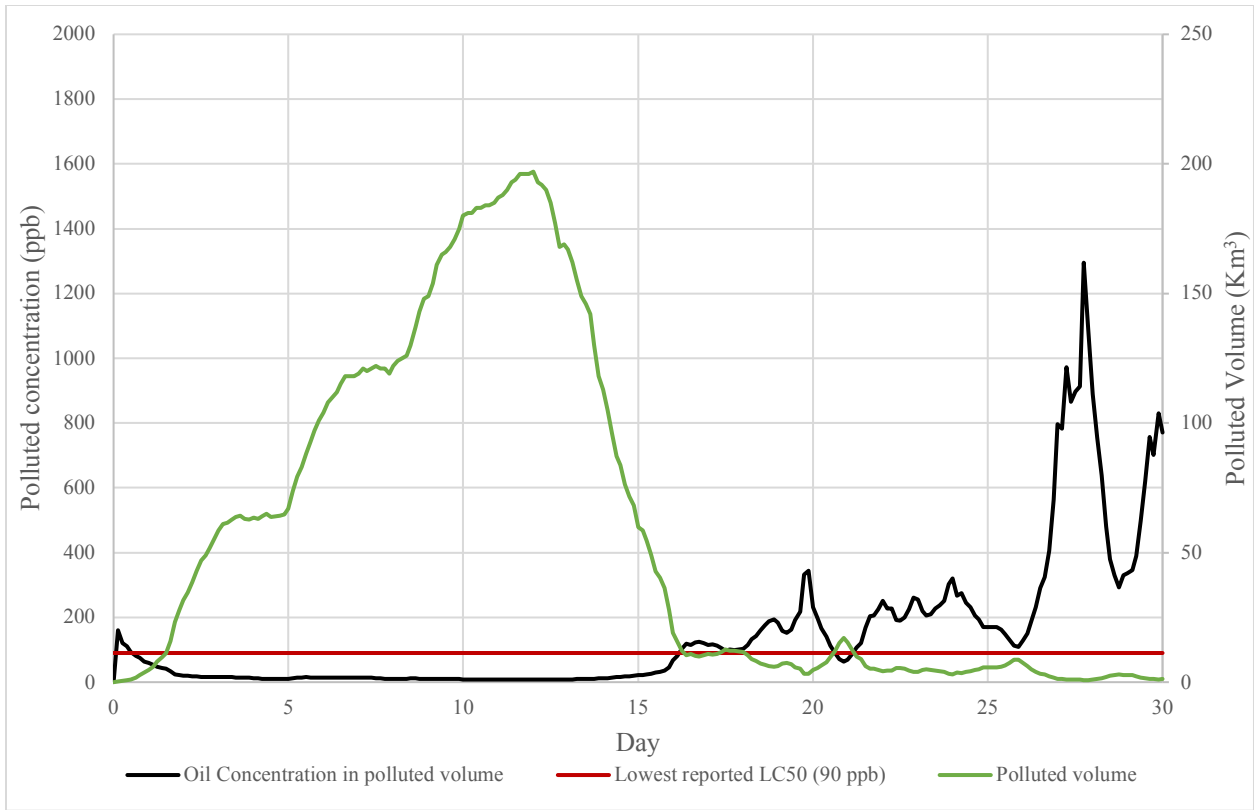
Figure 5-28 Polluted concentration (ppb) of the summer medium pipeline release, with no response method.
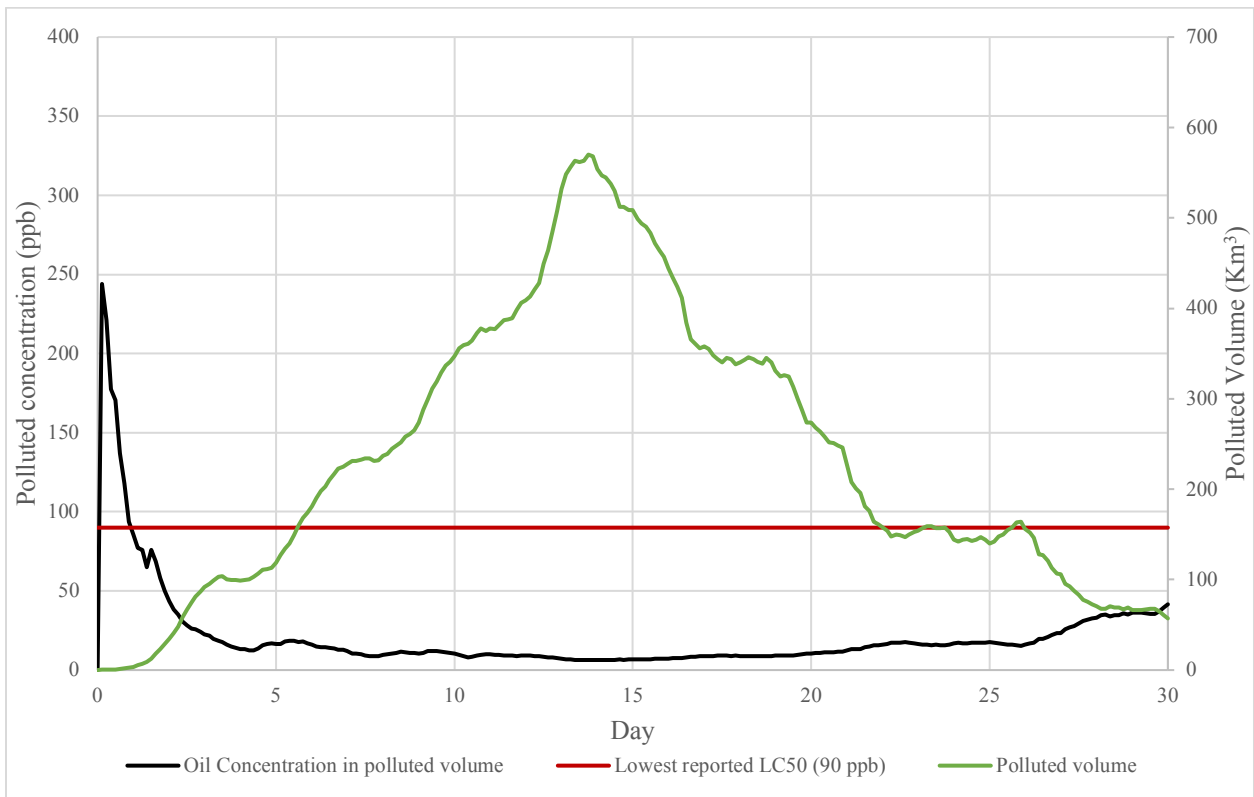
Figure 5-29 Polluted concentration (ppb) of the summer blowout, with no response method.
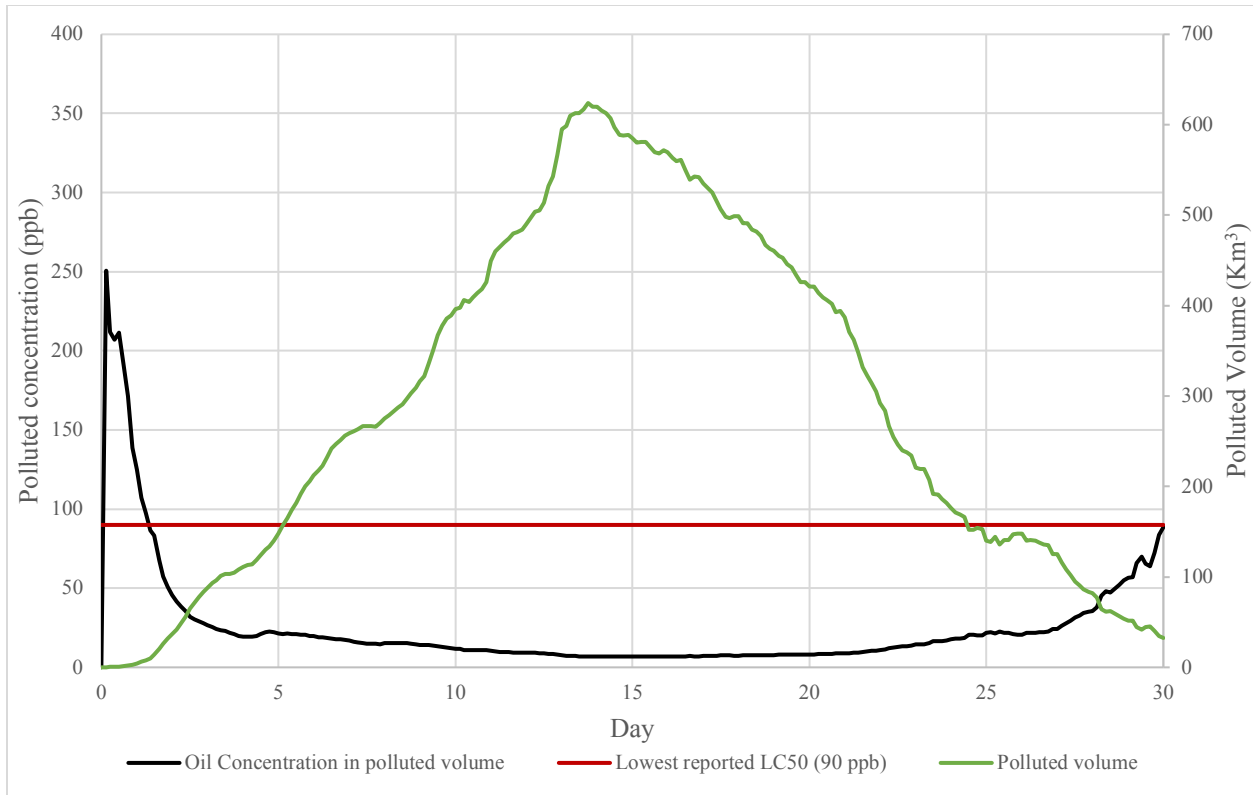
Figure 5-30 Polluted concentration (ppb) of the summer blowout, with chemical dispersants applied.

The following paragraphs describe the water column concentration time series.

In both the summer and winter small pipeline leak scenarios, large peaks were seen in the 9-11 day range. These peaks were very large (up to 10ppm) and over very small volumes (less than 0.0075Km³). This was due to the OSCAR impacted volume output approaching zero quickly but the reported oil mass was not decreasing at the same rate, resulting in unrealistically high concentration values. Upon review of the overall maximum concentration and mean concentration animations in OSCAR, no concentration value over 0.5ppm was seen. Therefore, any values over 0.5ppm were removed from these graphs. In both scenarios, the water column concentration was below the 90 ppb threshold throughout the timeseries with the exception of a peak over this threshold at day 9, seen in a very small volume, less than 0.6Km³ in each.

In both the summer and winter medium pipeline leaks, the concentration spiked over the 90ppb threshold in the first day before dropping. The concentration remained low but spread over a large volume until day 15-16, when the impacted area started to decrease but the concentrations rose

over the 90ppb threshold. The concentration remained more or less over the threshold limit until the end of timeseries, with the chemical response showing the greatest water column concentrations.

In summer and winter blowout scenarios, the concentration spiked in the first 1-2 days to 200-250 ppb before dropping below the 90ppb threshold. The concentrations remained low but spread over a large volume until the end of the simulations in the summer, with dispersant use increasing the concentration to 90 ppb in the final day. In the winter, the concentrations remained low but spread over large volumes until day 21, when the impacted area started to decrease but the concentrations rose over the 90ppb threshold.

The following table 5-3 summarizes the polluted volume maximum (greatest peak height) where the water column concentration surpassed the LC_{50} threshold as a means of comparing the severity of consequences to biological resources amongst the different scenarios. This shows the maximum volume impacted during in the scenario.

Table 5-3 Summary of the water column concentration time series

Scenario	Volume peak maximum over 90ppb (Km^3)	Change in volume affected due to response (Km^3)	Total amount oil treated with dispersants (tonnes)	Total amount oil recovered by skimmers	Total oil released (tonnes)
Small pipeline leak, winter	0.6	-	0	0	119
Small pipeline leak, summer	0.25	-	0	0	119
Medium pipeline leak, winter	9.5		0	0	3014
Medium pipeline leak, winter, mechanical	6	-3.5	0	21	3014
Medium pipeline leak, winter, chemical	11	+1.5	171	0	3014
Medium pipeline leak, summer	11		0	0	3014
Medium pipeline leak, summer, mechanical	9.5	-1.5	0	95	3014
Medium pipeline leak, summer, chemical	10	-1	308	0	3014
Blowout, winter	30		0	0	8378
Blowout, winter, mechanical	27	-3	0	58	8378
Blowout, winter, chemical	38	+8	2112	0	8378
Blowout, summer	4		0	0	8378
Blowout, summer, mechanical	3.8	-0.2	0	576	8378
Blowout, summer, chemical	30	+26	2844	0	8378

5.2.4 Mass balance for all scenarios

OSCAR estimates the fate of oil in the environment and how it is partitioned with different processes. The oil is distributed amongst the atmosphere (evaporation), water surface, water column, sediments, shoreline, biodegradation and amount recovered (if mechanical response methods were used). Dispersant use increases oil in the water column. The following is a description of the partitioning of oil in the environment during each scenario.

In the small pipeline releases, very little oil reached the surface. Any oil that did, evaporated rapidly, a very thin surface sheen is expected. Slightly more oil reached the surface days 4 to 10 in the summer.

The winter medium pipeline releases showed a thin surface slick, too thin for mechanical or chemical responses to be effective. The summer medium pipeline releases also showed a thin surface slick, with a small amount being thick enough for mechanical or chemical response measures.

The winter blowout scenarios showed no decrease in surface oil with response methods. Greater amounts of oil were at the surface in the first days before spreading out.

The summer blowout scenarios showed large amounts of oil at the surface in the first 10 days. Limited effectiveness was seen with mechanical recovery of oil. Chemical response did substantially decrease the presence of surface oil.

The full duration mass balance for each scenario is presented in Figures 5-31 to 5-33.

Figure 5-31 Mass balance for the small pipeline releases, summer (left) and winter (right).
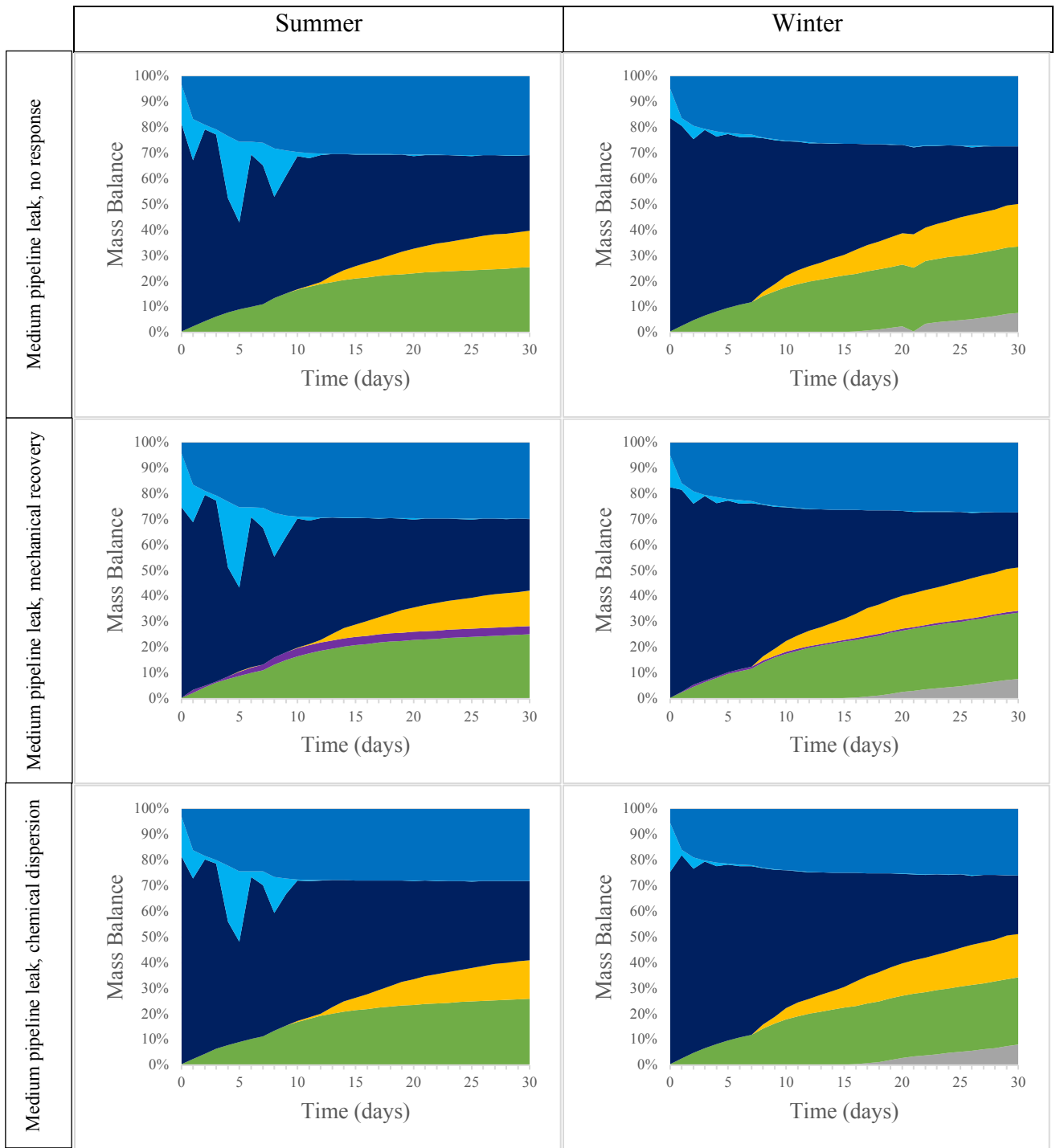
Figure 5-32 Mass Balance for the medium pipeline leaks, summer and winter, with no response, mechanical recovery and dispersant application.
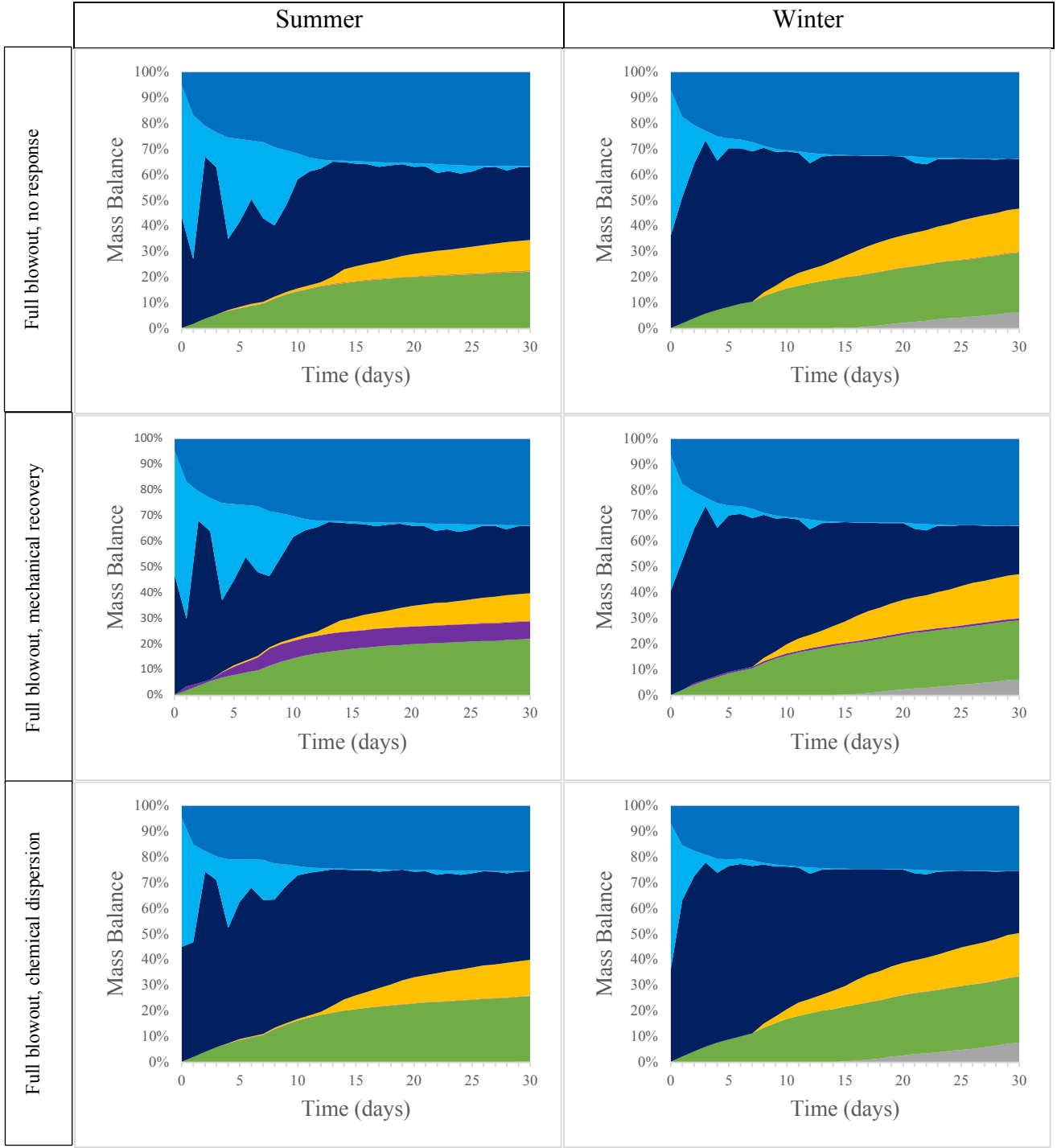
Figure 5-33 Mass balance for the full blowout scenarios, summer and winter, with no response, mechanical recovery and dispersant application.

5.2.5 Shoreline oiling

The anticipated shoreline oiling is low, with low concentrations of oil ($<0.001 \text{Kg/m}^2$) reaching the shore in any given scenario. The summer blowout scenarios were the only ones to display small areas of higher concentrations of $0.001 - 1.0 \text{ Kg/m}^2$, see example in figure 5-34 and the summary of mass percent of oil reaching the shoreline, table 5-4. This amount was not large enough in the small or medium pipeline leaks to account for any percentage of the mass balance. Larger releases saw greater incidence of shoreline hits, and response methods decreased the percentage of oil ashore by 20-67% in these cases. The trend for the location of the shoreline hits was along the Norwegian coast north of the opening of the Trondheim Fjord, see images in Appendix F. The Frøya area received shoreline pollution during the summer blowout scenarios only.

Table 5-4 Mass percent of oil reaching the shore by scenario.

Scenario	Mass percent of oil reaching the shore (%)
Small pipeline leaks	0
Medium pipeline leaks	0
Winter blowout, no response	0.3
Winter blowout, mechanical recovery	0.2
Winter blowout, chemical dispersion	0.1
Summer blowout, no response	0.5
Summer blowout, mechanical response	0.4
Summer blowout, chemical dispersion	0.2
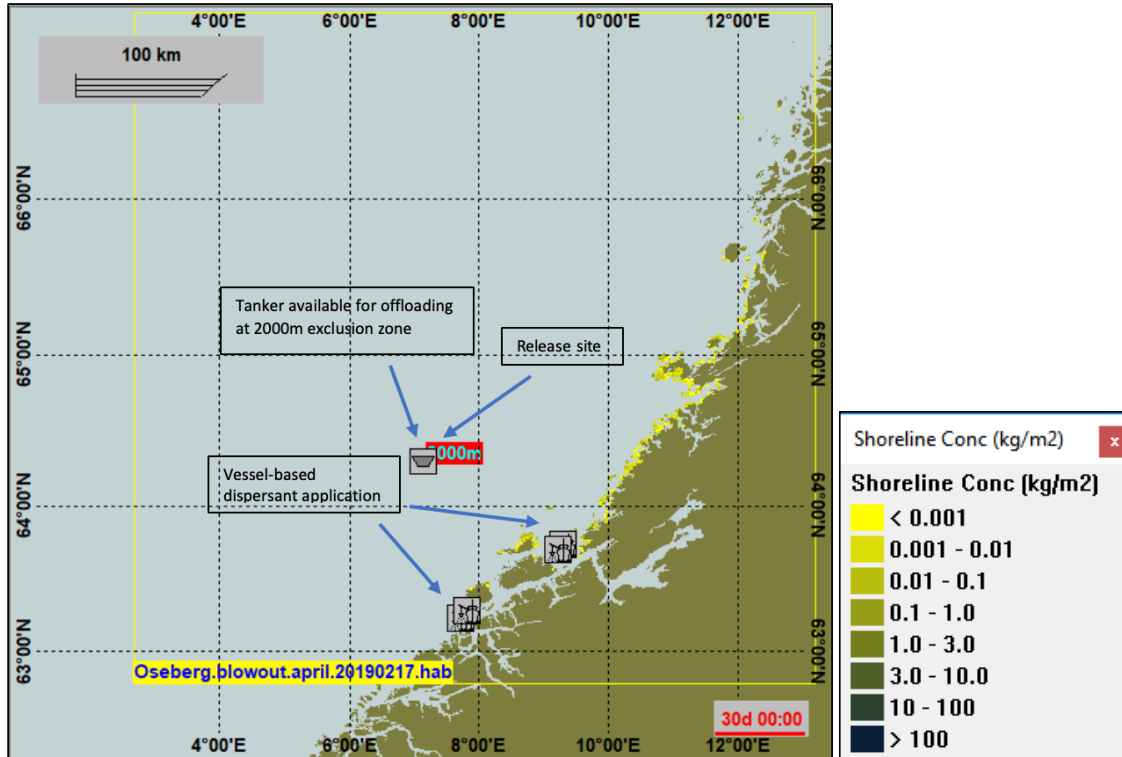
Figure 5-34 OSCAR image illustrating shoreline hits during the summer blowout scenario with chemical dispersion. Response vessels and the release site are indicated. The legend for the shoreline concentration gradient is seen on the right.

5.3   Comparison of newly derived Weber constants to the constants used in OSCAR

New Modified Weber constants of A 8.5 and B 7.68 were derived from the experimental portion of this thesis. These values were used to calculate the d_{50} of 501 μm and d_{95} of 1130 μm for the small pipeline release that were subsequently used as input into OSCAR. This was done to explore if the oil droplet size would impact the behavior of the oil spill and result in deviations from the default settings in OSCAR, which uses the previous values of A 24.6 and B 0.08.

The mass balance for the full scenarios are seen below, figure 5-35. In the winter, little oil remains at the surface due to high winds and currents.

In the summer, more oil is seen at the surface within the first 4 to 10 days. Looking more closely at these days, there is increased oil at the surface, with greater evaporation, at day 4 and 8 with these new constants, figure 5-36.
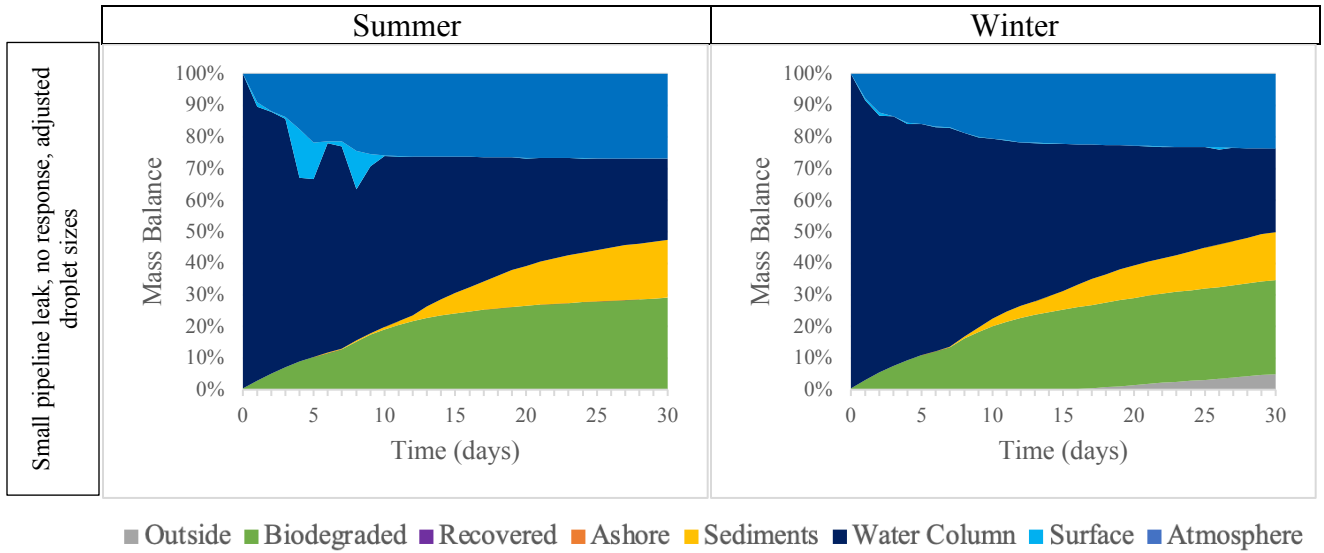
	Summer	Winter

Figure 5-35 Mass balance graphs for the small pipeline leaks in the summer (left) and winter (right) using the new modified Weber constants.

▪ Outside ▪ Biodegraded ▪ Recovered ▪ Ashore ▪ Sediments ▪ Water Column ▪ Surface ▪ Atmosphere
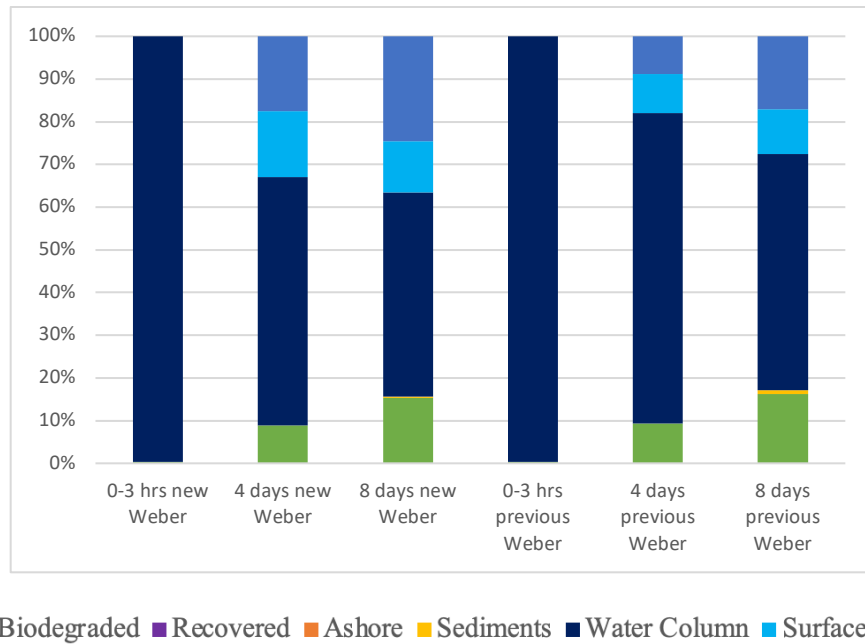
Figure 5-36 Comparing Weber constants. Mass balance graphs for 0-3 hours, and 4 and 8 days after the beginning of the release for the summer small pipeline leaks. The results obtained with the new Modified Weber constants are on the left and the previous values on the right.

During the summer, the larger droplet sizes rise quickly to the surface in the first day, resulting in a small slick that surpassed the 0.1 g/m2 limit for toxicity to seabirds (figure 5-37). This slick quickly spreads and thins. However, a greater impacted area is expected relative to what the

previous constants predicted. Due to increased oil reaching the surface, a corresponding decrease to the impacted volume is seen (figure 5-38). Charts for the winter are found in Appendix G.
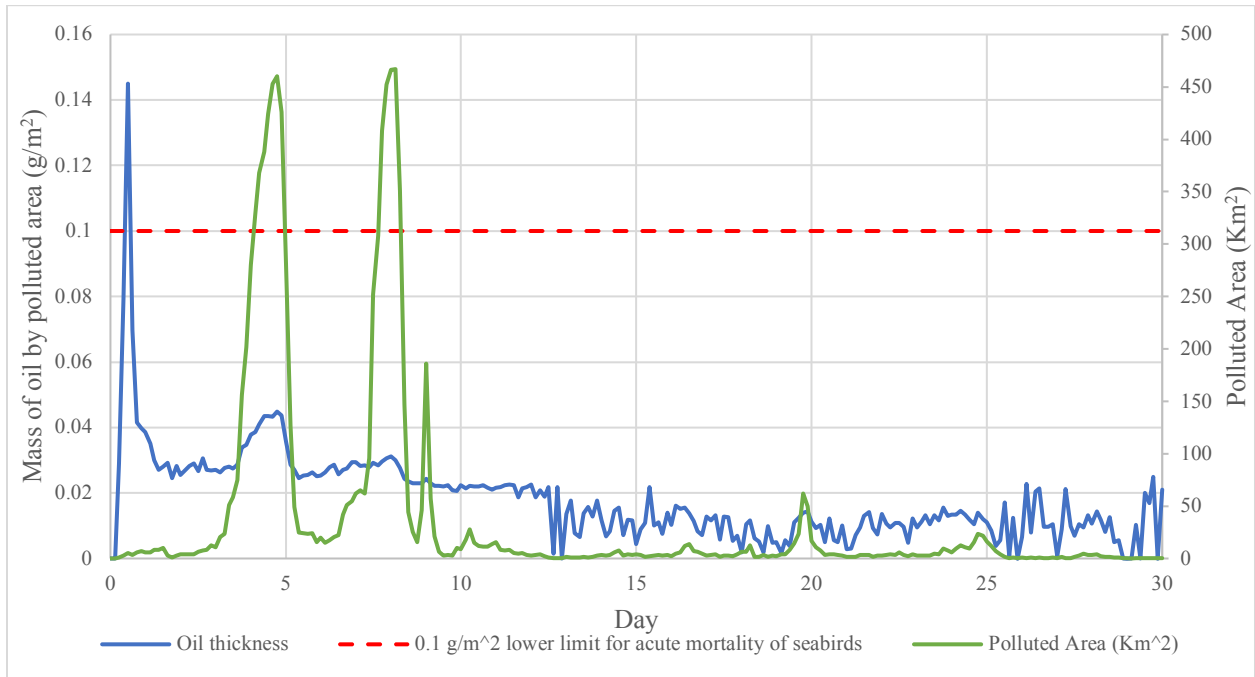
Figure 5-37 Surface thickness for small pipeline releases in the summer using the new Modified Weber values obtained in the experimental portion of this thesis.
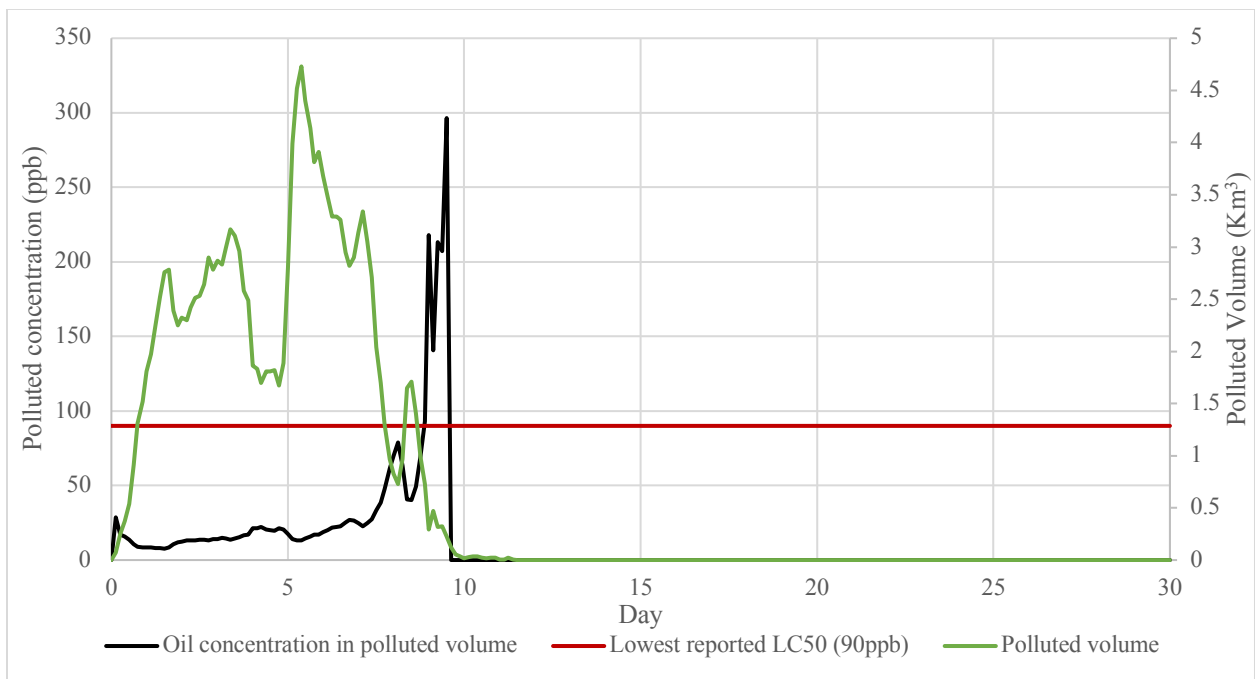
Figure 5-38 Polluted volume for small pipeline releases in the summer using the new Modified Weber values obtained in the experimental portion of this thesis.

6 Discussion

The following is a discussion of the results presented in the previous chapter. This includes commentary on important aspects of the procedure and explanation of the results obtained. Along with ideas and suggestions for future work.

6.1 MiniTower and the Silhouette Camera

Turbulent jet experiments were used to quantify the droplet distributions obtained from high velocity, low diameter oil releases. The following is a discussion of the droplet data obtained from the MiniTower experiments.

6.1.1 Challenges

The conditions produced during the experiments generated high concentrations of droplets. Effective management of oversaturation was an important consideration. The MiniTower has a fixed position for the camera, therefore it is not possible to increase the distance of the camera above the plume to reduce the concentration of droplets, as is done in larger test facilities. The measures taken to reduce saturation were reducing the exit nozzle size, increasing the seawater flow and decreasing the sample volume. The sample volume was decreased by making the gap to the camera quite narrow, a 2.5mm opening with a 3.5mm gap between the recessed portion of the camera and backlight housing. This allowed only a small portion of the plume to enter in to the imaging zone. While this did help to decrease problems with high droplet concentrations, it did cause other issues.

The narrow gap resulted in coalescence of oil on the rim, sometimes partially blocking the gap to the camera lens. This meant that a lower portion of droplets were entering the camera at this time, possibly affecting the distribution. Sometimes part or all of this coalesced oil would dislodge and enter the imaging area. This could then skew the data, making a large particle with correspondingly high volume. The gap may also prevent some larger particles from entering, even if they are

smaller than the gap itself. This occurs as they may be more likely to deflect off the rim and not enter the sample volume of the camera.

The narrowness of the sample volume made it likely that some droplets would stick to and coat the lens, with additional droplets then coalescing together to previously adhered droplets. Occasionally, these droplets would move slowly across the lens. If there was a droplet slowly creeping up the window, it may have resulted in a bi-modal distribution. This is because the background correction will remove only part of the droplet, as it is not completely stationary. While this should not normally produce large effects in the data, when the droplet sizes are very small and resulting volumes are small, the presence of a large droplet (with resulting high volume) has the capacity to alter the results. In these instances of bimodality, the greatest peak height was selected instead of the d_{50} to represent the droplet distribution. As a lognormal distribution is expected, this is an acceptable representation of the d_{50} while removing the effect of large, coallesced droplets.

The small opening gap also made it difficult to clean the imaging area. In the MiniTower, a water jet is positioned on the lid above the camera. Water is released approximately 15 centimeters above the camera and must enter to gap to remove any oil. This does not always generate sufficient pressure to rinse the oil off. A small jet positioned directly into the camera gap may prove more effective at removing fouled oil.

If fouling of the camera was excessive around the opening or visible on the SilCam live view, the experiments were stopped and a rinse cycle was performed to remove the excess oil before continuing. However, for several experiments, the live view was not available in order to have stable processing with the test version of the software used. Unfortunately, there was some incidence of droplets adhered to the camera during these runs that were not noted until the images could be reviewed at the completion of the experiment.

Experiments were attempted with oil, produced water and gas. The gas coated the camera lens and created noise, resulting in some level of uncertainty in the SilCam distinguishing oil coated gas or water droplets from oil alone. Due to the occurrence of multimodal peaks, these experiments were

dropped and not repeated, as machine learning along with an update to the SilCam software was planned. This was beyond the budget and timeframe of this master project. Therefore, only experiments with oil alone at different flow rates, and oil and produced water at different flow rates were included.

6.1.2 Data Selection

In some instances, deviations occurred to the lognormal distribution or expected droplet size. The following is a discussion on some of these deviations with suggested explanations and what could be done in the future to prevent them.

The SilCam underestimates the size of transparent droplets (Brandvik et al., 2015a). It was intended to use Njord oil for this study but further machine learning is required for the SilCam to appropriately size and determine the GOR for this light-colored oil type. Grane was also used for a few experiments, however, it clogged the 0.25mm nozzle and it was only possible to use the 0.5 mm nozzle with this oil. At mixed releases with oil and water, Grane displayed an inconsistent, slug flow until high flow rates of produced water were used. Because of the challenges of working with this oil, additional litres were not obtained from the SINTEF storage facilities. Therefore, only experiments using Oseberg blend 2017 were used for analysis.

Only experiments where the Ohnesorge versus Reynolds number plot were within the atomization zone were included for analysis. A cut-off at the exit velocity, U_e, of 10 m/s or higher was used to ensure that the experiments included were well within the atomization zone. As the exit velocity is increased, the conditions produced shift further to the right in the plot (higher Reynolds number), see figure 5-4. Lower velocities near the transition zone produced a polydispersion of large and small droplets, as opposed to atomization which produced a lognormal distribution.

The minimum quantifiable limit of the SilCam is 28μm (Davies et al., 2017). It is unlikely that inability to measure smaller droplets was a problem for measuring accurate d_{50} with the release conditions for this study; the droplet distributions obtained showed symmetrical lognormal

distributions in all experiments. However, this limit should be considered, especially if future experiments require even higher exit velocities. In such cases, it may be necessary to use the LISST-100 which has a lower quantifiable limit.

Data sets showing a single peak in the histogram were selected for analysis. This is due to the anticipated data being a representative sample of the population, in a lognormal distribution. Instances where multiple peaks were seen may be attributed to scenarios where the concentration was too high, when the turbulence generated a particle distribution that was too small for the SilCam to read or when fouling of the lens occurred. The experiments of the 0.50mm nozzle with oil only flow from 125 to 200 mL/min displayed large, secondary peaks in the 350 to 400 μm range, figures 5-8 and 5-9. These did shift the accumulated d_{50} to the right. The experiments were repeated, unfortunately, with the test version of SilCam used, there were oil droplets fouling the lens which could not be observed during the experiment and a bimodal peak was again observed. Rather than repeat the experiments a third time, resulting in additional water pollution, these results are included in the analysis using the maximum peak height instead of the accumulated d_{50}.

Additionally, some of the results obtained consistently showed much smaller droplets than predicted. These were the experiments with 0.5mm nozzle and oil mixed with produced water, figures 5-10 and 5-11. The initial experiments showed bimodal peaks, so were repeated. The second set produced the same small droplets, this time with the expected lognormal distribution. This demonstrates a secondary process occurring in the mixing of the oil and water. Ideally there should be laminar flow in the pipe leading to the exit nozzle. However, the water is mixed in to the oil approximately 20 cm before the exit nozzle, this may generate turbulence. When this turbulence is greater than the turbulence generated at the exit nozzle, smaller droplets result (figure 6-1). This is due to small droplets being generated at the mixing point that are smaller than what is generated at the exit. These small droplets will not break down further due to the lower exit turbulence. Also, when the percentage of water is high, water is the continuous phase and oil will not coalescence back to larger droplets that would be broken down by the exit turbulence. Because the break up regime observed was not produced by the exit conditions, the results for the 0.50mm nozzle of oil with produced water were not included in the results. The mixing turbulence is a factor to consider for future experiments. Changing the diameter of the water and/or oil inlet pipes,

or increasing the distance to the exit nozzle from the point of mixing may help to decrease this effect.
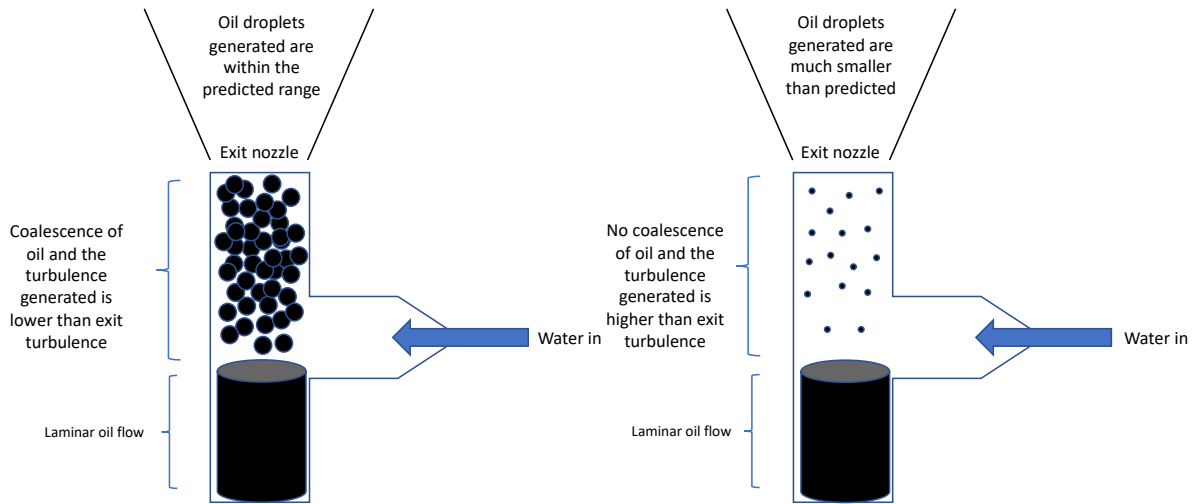
Figure 6-1 Turbulence during oil and produced water mixing. The addition of produced water in the inlet tube generated a turbulence greater than the exit turbulence when moderate to high water flows were used. This higher turbulence generated smaller droplets than predicted. When there is no or little produced water added, turbulence generated in the inlet tube is low and coalescence of any oil droplets formed can occur. The oil is the continuous phase in the inlet tube and the turbulence generated at the exit nozzle determines the droplet diameter (left). When the percentage of produced water is moderate to high, the droplet diameters are determined by the turbulence in the water inlet tube not the exit nozzle (right).

6.1.3 Droplet size and release conditions

One method to decrease the incidence of oversaturation at the camera was use small exit nozzle sizes, 0.25mm and 0.50mm, which effectively reduced the volume of the plume while simulating the desired exit velocities. Brandvik et al. (2013) collected droplet size and exit velocity data in a meso-scale facility using exit nozzle diameters from 0.5 to 3.0 mm. The values obtained are in good agreement with the values obtained using this study's bench-scale method, see figure 6-2. This suggests that the results obtained in this bench-scale study can be scaled up when controlled for desired exit conditions, such as the exit velocity. However, this study provides a small data set. It is necessary to perform additional tests, including field studies (Faksness et al., 2016), in order to assess the validity and applicability to real life scenarios.
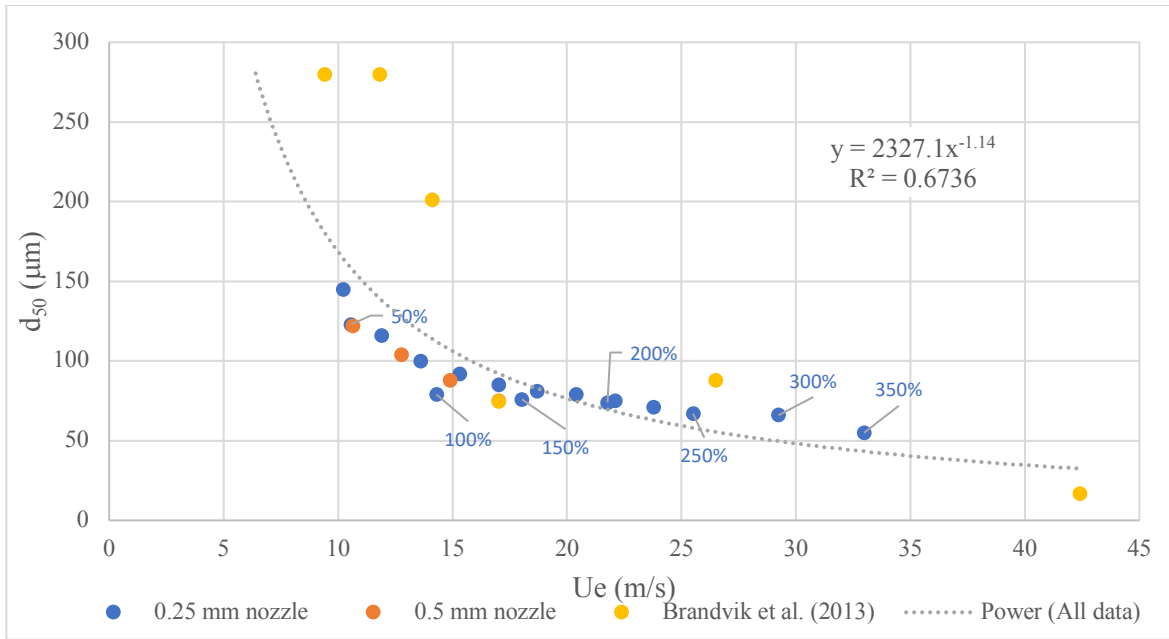
Figure 6-2 Plot of d$_{50}$ versus Ue for the current study and past SINTEF studies. Data adapted from Brandvik et al. (2013).

Release conditions impact droplet sizes, see Theory section 2.4 for a description of the dimensionless numbers used to describe droplet breakup. As the exit velocity increases, the droplet size decreases. However, the relationship is not linear (figures 5-12 and 6-2). The same is seen as increasing flow rates of water are added (figure 5-15). The Modified Weber scaling has been shown to account for both the viscosity and interfacial tension (Brandvik et al., 2013; Johansen et al., 2013). Two breakup regimes, one limited by interfacial tension and the other by viscosity, result in the curved line when plotting the d$_{50}$ versus U$_e$. On the left side of the curve, low V$_i$ is controlled by the interfacial tension but as the U$_e$ is increased, the slope flattens as viscosity forces take over. The experiments performed have V$_i$ values from 1-4, so the values are intermediate with both viscosity and interfacial tension stress effects, with the viscosity stresses seemingly playing a greater role. Johansen et al. (2013) also found that the viscosity term can have a large impact in laboratory scale experiments with untreated oil. This is observed in figure 6-2, where the viscosity limited portion of the curve shows an even distribution of data around the trendline, whereas the interfacial tension limited data only follows the general trend. The data from Brandvik et al. (2013) shows good agreement with the data obtained during this study.

Many real-life variables were not represented by the conditions created in this study. For instance, the addition of dispersants will decrease the interfacial tension, possibly by several orders of magnitude. Additionally, the viscosity will be impacted by deep sea conditions, with high pressures and low temperatures. It is also important to consider that gas void fraction and buoyancy effects may be more prevalent with full scale blowouts.

6.1.4 Droplet measurement

In order to confirm the accurate sizing of the SilCam, measurements were taken from known, mono-disperse suspended particles. These standards were injected above the opening of the SilCam and allowed to settle through the imaging area. The resulting measured droplet sizes showed good agreement with the known sizes.

Previous studies using the LISST-100 are directly comparable to experimental conditions generated in this study. A 0.5mm nozzle using 0.2 L/min oil, with the resulting exit velocity (U_e) of 17.0m/s generated a peak diameter of 74.5 μm (Brandvik et al., 2013). The result obtained for this thesis was 85 μm. These show good agreement as the predicted value is 98 μm. The SilCam obtained a distribution closer to the predicted value. Furthermore, these represent adjacent log sized bins of 74.5 and 87.9 of the LISST data collection as seen in figure 6-3. The use of the SilCam appears valid for the conditions produced during this droplet study.
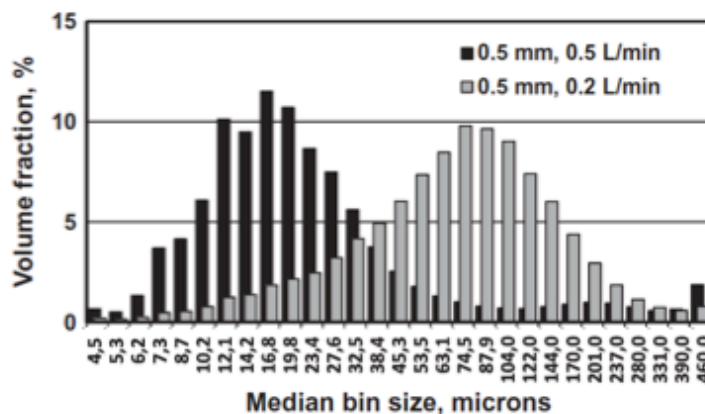

Figure 6-3 Results from the LISST instrument showing the droplet distribution of experiments that were replicated during this study (Brandvik et al., 2013).

6.1.5 Modified Weber Constants

The previous constants of A and B for the Modified Weber equation were empirically derived from larger scale releases such as the DeepSpill experiment (Brandvik et al., 2015b). The lower exit velocities create significantly different release conditions than what is expected from a small, high velocity pipeline leak and the predicted droplet sizes are too small, see figure 5-19. The need for new Modified Weber Constants for small, high velocity leaks is recognized. Therefore, new Modified Weber Constants, A 8.5 and B 7.68, were optimised with linear regression from the experimental data. The predicted versus measured d_{50} plot shows good agreement with these new constants, with a trendline showing the relationship between the predicted value of d_{50} to be 1.0009 times that of the measured value (figure 5-20). The previous values of A and B, 24.6 and 0.08 (Brandvik et al., 2015), predict the droplets to be much smaller than measured, with the predicted value of d_{50} to be 0.7208 times that of the measured value (figure 5-19).

The R^2 value obtained from the linear regression of the predicted versus observed values for d_{50} appears low at 0.762. However, this may be an effect due to the small data set, particularly since few experiments with the 0.5mm nozzle size were suitable for use in the analysis. Inspection of the residual plots (Appendix H) show that the balance of points above or below the 0 line to be fairly balanced and comparable from graph to graph for different values of A and B. Therefore, the values of A and B that provided the highest R^2, the best explanation of response variable variation, were chosen. However, there was not a large difference between the obtained R^2 values, ranging from about 0.700 to 0.762. The result of A 8.5 and B 7.68 should be considered preliminary. The value for B is nearly two orders of magnitude greater than the previously reported value (Brandvik et al., 2015) and an order of magnitude greater than the largest suggested value (Johansen et al., 2013). It is not clear why the B term is so much larger, it would be beneficial to carry out more experiments to increase the reliability of these values.

Nonetheless, the values of A and B determined result in good predictions of droplet sizes, at least for the given parameters. The modified Weber scaling may be simplified to $\frac{d_{50}}{D} = AWe^{*-\frac{3}{5}}$. Plotting d_{50}/D versus the modified Weber number yields a good fit to the regression line when the

new values of A and B are used, figure 5-22. The obtained regression line is y = 11.972x$^{-0.66}$ with R² = 0.8901. The exponent -0.66 is close to the model value of -0.6 or $\frac{-3}{5}$. Again, these results should be considered preliminary, as the Modified Weber values resulting from these constants are 10 times lower than the previously predicted values and from the values obtained from the Weber formula.

6.2   OSCAR modelling

In compliment to the experimental portion of this thesis, a modelling study of the Njord field area was carried out using the SINTEF OSCAR modelling system. A discussion of the results is provided below, including environmental consequences, suggestions for oil spill response and the possible origins of oil pollution samples collected in 2017. The newly derived values for the Modified Weber scaling are also considered.

6.2.1 Distribution of oil

In order to assess the appropriateness of responses to a potential oil spill, the location and characteristics of the spill must first be estimated.

The OSCAR simulations described the winter small pipeline releases as small areas of thin surface films, with low water column concentrations. In the summer, the films were also thin but spread over a greater area, with low water column concentrations. Recovery methods were not possible with these thin films.

The medium pipeline releases also consisted of thin surface slicks, with summer slicks spreading over a greater surface area. This was likely due to increased wind and wave action continuously removing oil from the water surface during the winter months. Recovery methods were not effective because much of the surface oil was below the 100μm threshold for mechanical recovery or dispersant application. Chemical dispersants did reduce the impacted area by about 120Km² during the summer. The impacted volumes were 200-250 Km³, however, the concentrations were

below the reported LC_{50}. Only small volumes towards the end of the scenario showed concentrations above this value.

Winter blowouts showed thick surface oil during the release phase, before the slicks thinned. Mechanical recovery was not effective, whereas dispersants decreased the area slightly (by about 100 Km^2). Little oil reached the surface, therefore large volumes of polluted water below the LC_{50} were observed. The use of dispersants showed a slight increase in the total volume impacted albeit at low concentrations; where the concentrations were high, an increase in volume was not seen. The summer blowouts generated the thickest slicks covering the greatest area. Because so much of the oil reached the surface, there was less oil in the water column and there was increased evaporation relative to the winter. Mechanical recovery was only slightly effective, where dispersants removed a large area of oil from the surface. The concentrations were below the LC_{50} with exception of the first days (all summer scenarios) and then reaching the LC_{50} during the last days when chemical dispersants were used.

6.2.2 Response considerations

Sea birds are typically most at risk to surface oil, whereas increased water column concentrations will impact fish, particularly at early life stages (eggs and larvae) as they lack the motility to move away from the spill area. Deciding on a response strategy will be a balance between actions that remove oil from the surface (mechanical recovery) and actions that transfer the surface oil to the water column (chemical dispersants). Sea birds are present year-round, with the highest numbers in the winter and nesting in the summer. Different species of fish spawn from December to May.

Response methods are not expected to be beneficial for small to medium sized leaks. This makes detection and stopping the release of the utmost concern to prevent continued damage. If surface oil is present in a summer spill and moving towards a protected area or area of known high density of seabirds, it may be beneficial to apply dispersants to break up the oil. There is little benefit to applying response methods in winter scenarios as increased wind and wave action result in

increased natural dispersion. Also, limited daylight hours and poor weather prevent response actions.

The small pipeline releases do not show surface thicknesses or water column concentrations above the threshold (with exception of small volume at day 9) where animals are expected to be impacted. One concern is that long term exposure of fish eggs and larvae to sublethal doses of oil lead to structural and functional deformities that can impact stock numbers in the future (Peterson, 2003). This leads to the need to ensure that oil companies are able to locate and stop small pipeline leaks.

Chemical dispersion is effective in blowouts in the summer months. Consideration is required should a spill occur in the spring or early summer, as fish eggs and larvae may be present in the region. However, risk of contact with breeding seabirds and the shoreline are at a greater risk at this time as well. The anticipated water concentrations should be below the LC_{50} for the majority of the volume with small volumes above this limit. It will likely be advisable to use the dispersants.

Shoreline impacts are anticipated to be low from the Njord field. Little oil concentration appears along the shoreline for small to moderated leaks, which is encouraging for the important populations of breeding seabirds and seals. Should a large spill occur, it may be advisable to use a targeted boom placement or dispersant use on oil found drifting towards the shoreline. While generalized response methods did decrease the overall shoreline hits during the blowouts, the quantities of oil that reached the shoreline were generally very low.

Oil spill studies provide important information for the type and allocation of response equipment necessary. This allows governments and companies to design effective strategies in the event of a spill. The number and location of response facilities and their mobilisation times are important considerations. Studies also provide information to the oil operator of the variety of spills that may be expected, allowing them to determine appropriate monitoring strategies or identify the need for improvements or to develop new techniques.

6.2.3 Oil pollution samples collected for KJ3050

The trend of the oil to drift in a north eastern direction makes the likelihood low that the oil pollution samples collected for KJ3050 were a result of discharges from the Njord field. Shoreline hits in the areas where samples were collected only occurred at the highest release rates and there has not been a large spill reported from the Njord field. In order for a leak to go on without notice, it would have to be small. Such a leak would then lack the surface extent and quantity to spread, emulsify, then weather in to the form of the tarballs collected. The heavily weathered nature of the samples indicate that the oil was at sea for long periods of time, weeks or months, before reaching the shore. See figure 6-4 for an example of the heavily weathered nature of the tarballs collected, no hydrocarbons smaller than 34 carbons are seen in the GC/FID. Oil from the Njord field would reach Frøya in days to weeks. It is more likely that the samples collected originated from ship traffic or possibly a more southern oilfield. Oil spill fingerprinting analysis of all collected samples and Njord field oils are the only way to conclusively determine if the Njord field was the source. However, the simulation data indicates that this is not an efficient use of time as the Njord field is an unlikely source.

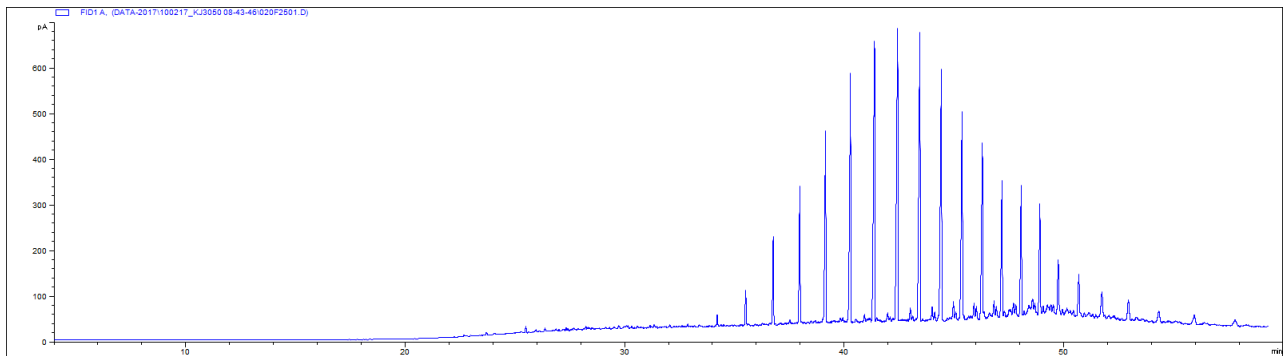*Figure 6-4 GC/FID of sample W1-12 showing heavy weathering (Bakkerud et al., 2017).*

6.2.4 Predicted versus measured values

Accurate prediction of oil droplet sizes is important as it affects where the droplets are anticipated to travel in the environment. Larger droplets will rise to the surface, while smaller droplets may remain submerged for long periods of time. As shown in this study, the former Modified Weber

Constants underestimated the size of oil droplets in scenarios of high velocity leakages. In instances where the oil release conditions anticipate small exit diameters and high exit velocities, it is recommended to use the new Modified Weber constants for prediction of the oil droplet d_{50}. This will allow for more accurate prediction of the distribution of oil throughout the water column and surface during calculations and modelling. This information is necessary for contingency planning, monitoring and allocation of resources during recovery missions.

The predicted droplet sizes using the new modified Weber constants are nearly double those previously predicted. This changes the expected mass balance of the oil and will generate larger surface slicks, especially in the summer.

The surface thickness was below 0.010mm in all small pipeline leak scenarios (OSCAR does not specify how much below 0.010mm). Concentrations of fresh crude oil of 9.1ppb have been found to have negative effects on fish eggs (Carls et al., 1999; Incardona et al., 2015). The effects of chronic, low dose exposure are serious, the ability to identify very thin surface films associated with small pipeline leaks is a priority for subsea oil production and transport.

7 Conclusions

This study demonstrated that the SilCam is a valuable instrument for use in droplet breakup studies in the MiniTower. The planned machine learning and software update will only improve its performance for distinguishing gas and different oil types at high concentrations. It is recommended that a small jet be installed in order to improve cleaning of the camera lens in the sample volume.

The breakup of an oil jet into droplets is governed by the exit velocity and both the interfacial tension and viscosity. Depending on the release conditions, the interfacial tension or viscosity may limit the droplet breakup. This means that as the exit velocity increases, the droplet sizes decrease in a nonlinear fashion. The Modified-Weber model has been developed to estimate the droplet size with the constants A and B optimized from experimental results. Preliminary values of A 8.5 and B 7.68 are presented under recommendation that further experiments are conducted to confirm these values. The use of different oil types would be beneficial to explore how the oil properties will impact these constants. Verifying the values of the Modified Weber constants will be important to predict small diameter, high velocity releases. Whether the values presented are near the actual values or not, they show that the previous empirically derived constants are not optimized to describe small, high velocity releases.

The down scaled experiments carried out are in good agreement with previous studies. They seem to provide valid estimations of real conditions; however, more data is needed. Further experiments in the MiniTower using gas in the release are recommended. Tests in larger scale facilities or even field data would help to confirm the results obtained. For instance, the impact of viscosity on small lab experiments is high and different effects may be seen if deep sea conditions (high pressure and low temperature) are involved.

Aging oilfield leaks are expected to be thin and spread out as they contain high volumes of produced water or gas. This makes response methods relatively ineffective, prevention and early detection are then paramount. The location of many oilfields near the Norwegian coast means that important ecological areas are at risk in the event of an accident. Dispersants show some

effectiveness in oil spill response but consideration to the increased water column concentrations must be taken in to account before use. While shoreline oiling along Frøya occurs from large releases from the Njord field, the surface oil lacks the extent and thickness expected to form the type of tarballs collected along the coast. It is not anticipated that the samples collected in 2017 originated from the Njord field.

8 Bibliography

American Society for Testing and Materials International (ASTM), 2000. Oil Spill Identification by Gas Chromatography and Positive Ion Electron Impact Low Resolution Mass Spectrometry. ASTM D-5739-00. Philadelphia, PA.

American Society for Testing and Materials International (ASTM), 1990. Standard Test Methods for Comparison of Waterborne Petroleum Oils by Gas Chromatography. ASTM D-3328-90. W. Conshohocken, PA.

Anderson, J.T., Akenhead, S.A., 1981. Distibution and Abundance of Redfish and Cod Larvae on Flemish Cap in 1978 and 1979. NAFO Sci. Coun. Stud. 1, 57–63.

Atlas of Marine Protection, 2019. Froan Nature Reserve (Naturreservat) [WWW Document]. URL http://www.mpatlas.org/mpa/sites/770/ (accessed 2.20.19).

Bakkerud, O., McKay, R., Solheim, S., Sveen, E., Vinnes, M., 2017. KJ3050: Marine Organic Pollution Fieldwork. Unpublished report for the course Marine Organic Environmental Chemistry KJ3050, NTNU. Trondheim, Norway.

Bayona, J.M., Domínguez, C., Albaigés, J., 2015. Analytical developments for oil spill fingerprinting. Trends Environ. Anal. Chem. 5, 26–34. https://doi.org/https://doi.org/10.1016/j.teac.2015.01.004

Brandvik, P.J., Daling, P.S., 2015. Crude oils composition and properties: importance for oil spill response operations. Lecture compendium for the course Marine Organic Environmental Chemistry KJ3050, NTNU. Trondheim, Norway.

Brandvik, P.J., Daling, P.S., 1998. Optimising oil spill dispersants as a function of oil type and weathering degree: A multivariate approach using partial least squares (PLS). Chemom. Intell. Lab. Syst. 42(1-2), 73–91. https://doi.org/10.1016/S0169-7439(98)00006-9

Brandvik, P.J., Daling, P.S., Leirvik, F., Johansen, Ø., Davies, E., Krause, D.F., 2014a. Subsea Dispersant Effectiveness Bench-Scale Test Protocol Development and Documentation. SINTEF report no: A26541. Trondheim, Norway. https://doi.org/ISBN: 9788214057539

Brandvik, P.J., Farooq, U., Angell, G., Leirvik, F., 2014b. Sub-surface oil releases - Experimental study of droplet distributions and different dispersant injection techniques - version 2. A scaled experimental approach using the SINTEF Tower basin. SINTEF report no: A26122. Trondheim, Norway.

Brandvik, P.J., Johansen, Ø., Davies, E., Leirvik, F., Belore, R., 2015a. Subsea Dispersant Injection - large-scale experiments to verify algorithms for initial droplet formation (modified Weber scaling). An approach using the Ohmsett facility, NJ, USA and SINTEF Tower Basin in Norway. SINTEF report no: OC2017 A-087. Trondheim, Norway.

Brandvik, P.J., Johansen, Ø., Farooq, U., Davies, E., Leirvik, F., Krause, D., 2015b. Subsurface oil releases - Experimental study of droplet size distributions Phase-II. A scaled experimental approach using the SINTEF Tower basin. SINTEF report no: A26866. Trondheim, Norway.

Brandvik, P.J., Johansen, Ø., Leirvik, F., Farooq, U., Daling, P.S., 2013. Droplet breakup in subsurface oil releases - Part 1: Experimental study of droplet breakup and effectiveness of dispersant injection. Mar. Pollut. Bull. 73(1), 319–326. https://doi.org/10.1016/j.marpolbul.2013.05.020

Brekke, C., Solberg, A.H.S., 2005. Oil spill detection by satellite remote sensing. Remote Sens. Environ. 95(1), 1–13. https://doi.org/https://doi.org/10.1016/j.rse.2004.11.015

Carls, M.G., Rice, S.D., Hose, J.E., 1999. Sensitivity of fish embryos to weathered crude oil: Part I. Low-level exposure during incubation causes malformations, genetic damage, and mortality in larval pacific herring (Clupea pallasi). Environ. Toxicol. Chem. 18(3), 481–493. https://doi.org/10.1897/1551-5028(1999)018<0481:SOFETW>2.3.CO;2

Chen, F., Yapa, P.D., 2007. Estimating the Oil Droplet Size Distributions in Deepwater Oil Spills. J. Hydraul. Eng. 133(2), 197–207. https://doi.org/10.1061/(ASCE)0733-9429(2007)133:2(197)

Daling, P.S., Faksness, L.G., Hansen, A.B., Stout, S.A., 2002. Improved and Standardized Methodology for Oil Spill Fingerprinting. Environ. Forensics 3(3-4), 263–278. https://doi.org/https://doi.org/10.1006/enfo.2002.0099

Davies, E.J., Brandvik, P.J., Leirvik, F., Nepstad, R., 2017. The use of wide-band transmittance imaging to size and classify suspended particulate matter in seawater. Mar. Pollut. Bull. 115(1-2), 105–114. https://doi.org/10.1016/j.marpolbul.2016.11.063

Davies, E.J., Nimmo-Smith, W.A.M., Agrawal, Y.C., Souza, A.J., 2012. LISST-100 response to large particles. Mar. Geol. 307–310, 117–122. https://doi.org/https://doi.org/10.1016/j.margeo.2012.03.006

Faksness, L.G., Brandvik, P.J., Daling, P.S., Singsaas, I., Sørstrøm, S.E., 2016. The value of

offshore field experiments in oil spill technology development for Norwegian waters. Mar. Pollut. Bull. 111(1-2), 402–410. https://doi.org/10.1016/j.marpolbul.2016.07.035

French-McCay, D.P., 2009. State-of-the-Art and Research Needs for Oil Spill Impact Assessment Modeling. Proceedings of the 32nd AMOP Technical Seminar on Environmental Contamination and Response, Emergencies Science Division, Environment Canada, June 2009. Ottawa, Canada, pp. 601–653.

French-McCay, D.P., 2002. Development and application of an oil toxicity and exposure model, OILTOXEX. Environ. Toxicol. Chem. 21(10), 2080–2094.

Gajbhiye, R.N., Kam, S.I., 2008. Leak Detection in Subsea Pipeline : A Mechanistic Modeling Approach With Fixed Pressure Boundaries. Proceedings of the Offshore Technology Conference, May 2008. Houston, Texas. https://doi.org/10.2118/123130-PA

Geodata from the Institute of Marine Research, n.d. Species distribution of fish [WWW Document]. URL http://www.imr.no/geodata/geodataHI.html (accessed 3.16.18).

Hinze, J.O., 1955. Fundamentals of the hydrodynamic mechanism of splitting in dispersion processes. AIChE J. 1(3), 289–295. https://doi.org/10.1002/aic.690010303

Höök, M., Aleklett, K., 2008. A decline rate study of Norwegian oil production. Energy Policy 36(11), 4262–4271. https://doi.org/https://doi.org/10.1016/j.enpol.2008.07.039

Incardona, J.P., Carls, M.G., Holland, L., Linbo, T.L., Baldwin, D.H., Myers, M.S., Peck, K.A., Tagal, M., Rice, S.D., Scholz, N.L., 2015. Very low embryonic crude oil exposures cause lasting cardiac defects in salmon and herring. Sci. Rep. 5, 1–13. https://doi.org/10.1038/srep13499

IUCN, 2018. The IUCN Red List of Threatened Species [WWW Document]. URL https://www.iucnredlist.org (accessed 2.25.19).

Jernelöv, A., 2010. The threats from oil spills: now, then, and in the future. Ambio 39(5-6), 353–366. https://doi.org/10.1007/s13280-010-0085-5

Johansen, Ø., 2003. Development and verification of deep-water blowout models. Mar. Pollut. Bull. 47(9-12), 360–368. https://doi.org/10.1016/S0025-326X(03)00202-9

Johansen, Ø., Brandvik, P.J., Farooq, U., 2013. Droplet breakup in subsea oil releases - Part 2: Predictions of droplet size distributions with and without injection of chemical dispersants. Mar. Pollut. Bull. 73(1), 327–335. https://doi.org/10.1016/j.marpolbul.2013.04.012

Johansen, Ø., Reed, M., Bodsberg, N.R., 2015. Natural dispersion revisited. Mar. Pollut. Bull.

93(1-2), 20–26. https://doi.org/https://doi.org/10.1016/j.marpolbul.2015.02.026

Johansen, Ø., Rye, H., Cooper, C., 2003a. DeepSpill-Field study of a simulated oil and gas blowout in deep water. Spill Sci. Technol. Bull. 8(5-6), 433–443. https://doi.org/10.1016/S1353-2561(02)00123-8

Johansen, Ø., Skognes, K., Aspholm, O.Ø., Østby, C., Moe, K.A., Fossum, P., 2003b. Utredning av helårs oljevirksomhet i området Lofoten – Barentshavet, uhellsutslipp av olje – konsekvenser i vannsøylen (ULB 7-c). SINTEF report no: STF66 F03028. Trondheim, Norway.

Kishawy, H.A., Gabbar, H.A., 2010. Review of pipeline integrity management practices. Int. J. Press. Vessel. Pip. 87(7), 373–380. https://doi.org/https://doi.org/10.1016/j.ijpvp.2010.04.003

Leifer, I., Lehr, W.J., Simecek-Beatty, D., Bradley, E., Clark, R., Dennison, P., Hu, Y., Matheson, S., Jones, C.E., Holt, B., Reif, M., Roberts, D.A., Svejkovsky, J., Swayze, G., Wozencraft, J., 2012. State of the art satellite and airborne marine oil spill remote sensing: Application to the BP Deepwater Horizon oil spill. Remote Sens. Environ. 124, 185–209. https://doi.org/10.1016/j.rse.2012.03.024

Lima Neto, I.E., Zhu, D.Z., Rajaratnam, N., 2008. Bubbly jets in stagnant water. Int. J. Multiph. Flow 34(12), 1130–1141. https://doi.org/10.1016/j.ijmultiphaseflow.2008.06.005

Loh, A., Shim, W.J., Ha, S.Y., Yim, U.H., 2014. Oil-suspended particulate matter aggregates: Formation mechanism and fate in the marine environment. Ocean Sci. J. 49(4), 329–341. https://doi.org/10.1007/s12601-014-0031-8

Makatounis, P.E., Skancke, J., Florou, E., Stamou, A., Brandvik, P.J., 2017. Management of oil spill contamination in the Gulf of Patras caused by an accidental subsea blowout. Environ. Pollut. 231(1), 578–588. https://doi.org/10.1016/j.envpol.2017.08.076

Martínez-Bazán, C., Montañés, J.L., Lasheras, J.C., 2002. Statistical description of the bubble cloud resulting from the injection of air into a turbulent water jet. Int. J. Multiph. Flow 28(4), 597–615. https://doi.org/https://doi.org/10.1016/S0301-9322(01)00078-7

Masutani, S.M., Adams, E.E., 2000. Experimental study of multiphase plumes and application to deep ocean oil spills. Final Report to the U.S. Department of Interior, Minerals Management Service, Contract No: 1435-01-98-CT-30946. Honolulu, Hawaii.

McNutt, M., Camilli, R., Guthrie, G., Hsieh, P., Labson, V., Lehr, B., Maclay, D., Ratzel, A.,

Sogge, M., 2011. Assessment of Flow Rate Estimates for the Deepwater Horizon / Macondo Well Oil Spill. Flow Rate Technical Group report to the National Incident Command, Interagency Solutions Group, U.S. Department of the Interior.

Nash, R., Wright, P., Matejusova, I., Dimitrov, S., O'Sullivan, , Augley, J., Höffle, H., 2012. Spawning location of Norway pout (Trisopterus esmarkii Nilsson) in the North Sea. ICES J. Mar. Sci. 69(8), 1338–1346. https://doi.org/10.1093/icesjms/fss130

National Research Council Transportation Research Board, 2003. Chapter 3, Input of Oil to the Sea. Oil in the Sea III: Inputs, Fates, and Effects. The National Academies Press, Washington, DC. https://doi.org/10.17226/10388

National Virtual Ocean Data System (NVODS), 2001. World Ocean Atlas 2001 1x1 degree monthly means [WWW Document]. URL https://ferret.pmel.noaa.gov/nvods/las/UI.vm#panelHeaderHidden=false;differences=false;a utoContour=false;xCATID=WOA_05_CAT;xDSID=woa05_annual;varid=t00an1;imageSiz e=auto;over=xy;compute=Nonetoken;zlo=0;zhi=0;catid=WOA_05_CAT;dsid=woa05_annu al;varid=t00an1;avarcount=0;xlo=0.5;xhi=359.5;ylo=- 89.5;yhi=89.5;operation_id=Plot_2D_XY_zoom;view=xy (accessed 2.24.19).

Norsk Petroleum, 2019. Resource management in mature areas [WWW Document]. URL https://www.norskpetroleum.no/en/developments-and-operations/resource-management-in- mature-areas/ (accessed 4.8.19).

North, E.W., Adams, E.E., Thessen, A.E., Schlag, Z., He, R., Socolofsky, S.A., Masutani, S.M., Peckham, S.D., 2015. The influence of droplet size and biodegradation on the transport of subsurface oil droplets during the Deepwater Horizon spill: a model sensitivity study. Environ. Res. Lett. 10, 24016. https://doi.org/10.1088/1748-9326/10/2/024016

Norwegian Petroleum Directorate, 2019. Norwegian Petroleum Directorate Factpages [WWW Document]. URL http://factpages.npd.no/factpages/Default.aspx?culture=en (accessed 4.8.19).

Offshore Technology, n.d. Njord Future Project, Norwegian Sea [WWW Document]. URL https://www.offshore-technology.com/projects/njord-future-project-norwegian-sea/ (accessed 1.16.19).

Olsen, E., Aanes, S., Mehl, S., Holst, J.C., Aglen, A., Gjøsæter, H., 2010. Cod, haddock, saithe, herring, and capelin in the Barents Sea and adjacent waters: A review of the biological

value of the area. ICES J. Mar. Sci. 67(1), 87–101. https://doi.org/10.1093/icesjms/fsp229

Palkar, S., Markeset, T., 2012. Extending the Service Life Span of Ageing Oil and Gas Offshore Production Facilities. In: Frick J., Laugen B.T. (eds) Advances in Production Management Systems. Value Networks: Innovation, Technologies, and Management. Proceedings of the International Conference on Advances in Production Management Systems (APMS) 2011. IFIP Advances in Information and Communication Technology, Springer. Berlin, Germany. 384, 213–221. https:doi.org/10.1007/978-3-642-33980-6_25

Papanicolaou, P., List, E., 1988. Investigations of round vertical turbulent buoyant jets. J. Fluid Mech. 195, 341–391.

Peterson, C.H., 2003. Long-Term Ecosystem Response to the Exxon Valdez Oil Spill. Science 302(5653), 2082–2086. https://doi.org/10.1126/science.1084282

Prince, R.C., Owens, E.H., Sergy, G.A., 2002. Weathering of an Arctic oil spill over 20 years: The BIOS experiment revisited. Mar. Pollut. Bull. 44(11), 1236–1242. https://doi.org/10.1016/S0025-326X(02)00214-X

Rantrud, Ø., 2016. Miljørisiko- og beredskapsanalyse for letebrønn 6407/7-9 Njord NF2. Statoil Report.

Reddy, C.M., Arey, J.S., Seewald, J.S., Sylva, S.P., Lemkau, K.L., Nelson, R.K., Carmichael, C.A., McIntyre, C.P., Fenwick, J., Ventura, G.T., Mooy, B.A.S. Van, Camilli, R., 2012. Composition and fate of gas and oil released to the water column during the Deepwater Horizon oil spill. Proc. Natl. Acad. Sci. U.S.A. 109(50), 20229–20234. https://doi.org/10.1073/pnas.1101242108

Reed, M., Johansen, Ø., Brandvik, P.J., Daling, P., Lewis, A., Fiocco, R., Mackay, D., Prentki, R., 1999. Oil Spill Modeling towards the Close of the 20th Century: Overview of the State of the Art. Spill Sci. Technol. Bull. 5(1), 3–16. https://doi.org/https://doi.org/10.1016/S1353-2561(98)00029-2

Resby, J.L.M., Wang, U.M., 2004. Update of weathering properties of Oseberg Blend. SINTEF Technical Report: STF80 F04015. Trondheim, Norway.

SEAPOP, 2018. Breeding populations - selected species [WWW Document]. URL http://www.seapop.no/en/distribution-status/distribution/breeding-populations/index.html (accessed 1.15.19).

SINTEF, 2018. SilCam User Manual. 2018 Version for Experimental and ROV Mounted

Monitoring. Trondheim, Norway.

Skancke, J., Johansen, Ø., Brandvik, P.J., Brakstad, O.G., 2016. Implementing New Features in OSCAR; Oil Temperature and Viscosity During Droplet Formation and Area Specific Biodegradation. SINTEF report no: A27807. Trondheim Norway.

Socolofsky, S.A., Adams, E.E., Boufadel, M.C., Aman, Z.M., Johansen, Ø., Konkel, W.J., Lindo, D., Madsen, M.N., North, E.W., Paris, C.B., Rasmussen, D., Reed, M., Rønningen, P., Sim, L.H., Uhrenholdt, T., Anderson, K.G., Cooper, C., Nedwed, T.J., 2015. Intercomparison of oil spill prediction models for accidental blowout scenarios with and without subsea chemical dispersant injection. Mar. Pollut. Bull. 96(1-2), 110–126. https://doi.org/10.1016/j.marpolbul.2015.05.039

Spaulding, M.L., 2017. State of the art review and future directions in oil spill modeling. Mar. Pollut. Bull. 115(1-2), 7–19. https://doi.org/https://doi.org/10.1016/j.marpolbul.2017.01.001

Stout, S.A., Douglas, G.S., Uhler, A.D., McCarthy, K.J., Emsbo-Mattingly, S.D., 2005. Identifying the Source of Mystery Waterborne Oil Spills—A Case for Quantitative Chemical Fingerprinting. Environ. Claims J. 17(1), 71–88. https://doi.org/10.1080/10406020590952971

Strøm, T., 2013. Re-check weathering properties for Njord and Hyme crude oils. SINTEF report no: A25227. Trondheim Norway.

The Directorate of Fisheries and the Norwegian Environment Agency, 2018. Fisheries [WWW Document]. URL https://www.environment.no/topics/marine-and-coastal-waters/fisheries/ (accessed 2.20.19).

Tinmannsvik, R.K., Albrechtsen, E., Bråtveit, M., Carlsen, I.M., Fylling, I., Hauge, S., Haugen, S., Hynne, H., Lundteigen, M.A., Moen, B.E., Okstad, E., Onshus, T., Sandvik, P.C., Øien, K., 2011. The Deepwater Horizon accident: Causes, lessons learned and improvement measures for the Norwegian Continental Shelf. SINTEF Report: A19148. Trondheim Norway.

Varoujean, D.H., Baltz, D.M., Allen, B., Power, D., Schroeder, D., Kempner, K.M., 1983. Seabird-Oil Spill Behavior Study, Volume 2: Technical Report. Final Report to U.S. Dept. of the Interior Minerals Management Service, Reston, VA, by Nero and Associates, Inc.MMS-QN-TE-83-007, NTIS #PB84- 179. Portland, OR.

Vinnem, J.E., 2014. Offshore Risk Assessment Vol 1: Principles, Modelling and Applications of

QRA Studies, Third. ed. Springer Publishing Company, Incorporated.
https://doi.org/10.1007/978-1-4471-5207-1

Wang, B., Socolofsky, S.A., Lai, C.C.K., Adams, E.E., Boufadel, M.C., 2018. Behavior and dynamics of bubble breakup in gas pipeline leaks and accidental subsea oil well blowouts. Mar. Pollut. Bull. 131(A), 72–86.

Wang, C.Y., Calabrese, R. V., 1986. Drop breakup in turbulent stirred-tank contactors. Part II: Relative influence of viscosity and interfacial tension. AIChE J. 32(4), 667–676.
https://doi.org/10.1002/aic.690320417

9 Appendices

Appendix A

Example SilCam Configuration file

```
[General]
version = 3
loglevel = INFO
logfile = proc/log.log
datafile = proc

[Background]
num_images = 5

[Process]
threshold = 0.85
minimum_area = 12.0
max_particles = 50000000
min_deformation = 0
max_coverage = 100
max_length = 11000
bad_lighting_limit = None
real_time_stats = True

[PostProcess]
pix_size = 6.81
path_length = 2.5

com_port = COM4
window_size = 30
```

```
[ExportParticles]
export_images = True
outputpath = export
min_length = 0

[NNClassify]
model_path = 'C:/model/particle-
classifier.tfl'

[Camera]
configversion = 1
acquisitionframerateabs = 10
triggersource = 'FixedRate'
acquisitionmode = 'Continuous
exposuretimeabs = 100
pixelformat = 'RGB8Packed'
strobeduration = 300
strobedelay = 0
strobedurationmode = 'Controlled'
strobesource = 'FrameTriggerReady'
syncoutpolarity = 'Normal'
syncoutselector = 'SyncOut1'
syncoutsource = 'Strobe1'
gvsppacketsize = 1500
```

Appendix B

The following pages contain an overview of all experiments carried out and the reasoning for inclusion or exclusion from the final analysis.

OIL	DATE OF EXPERIMENT	NOZZLE DIAMETER (M)	OIL FLOW RATE (L/MIN)	WATER FLOW (L/MIN)	GAS FLOW RATE (L/MIN)	USED FOR RESULTS	COMMENTS
OSEBERG	04.12.2018	0.00025	0.010	0.000	0.000	no	Below 10m/s exit velocity (U)
OSEBERG	04.12.2018	0.00025	0.015	0.000	0.000	no	Below 10m/s exit velocity (U)
OSEBERG	04.12.2018	0.00025	0.020	0.000	0.000	no	Below 10m/s exit velocity (U)
OSEBERG	04.12.2018	0.00025	0.025	0.000	0.000	no	Below 10m/s exit velocity (U)
OSEBERG	04.12.2018	0.00025	0.030	0.000	0.000	yes	Lognormal distribution
OSEBERG	04.12.2018	0.00025	0.035	0.000	0.000	yes	Lognormal distribution
OSEBERG	04.12.2018	0.00025	0.040	0.000	0.000	yes	Lognormal distribution
OSEBERG	04.12.2018	0.00025	0.045	0.000	0.000	yes	Lognormal distribution
OSEBERG	04.12.2018	0.00025	0.050	0.000	0.000	yes	Lognormal distribution
OSEBERG	04.12.2018	0.00025	0.055	0.000	0.000	yes	Lognormal distribution
OSEBERG	04.12.2018	0.00025	0.060	0.000	0.000	yes	Lognormal distribution
OSEBERG	04.12.2018	0.00025	0.065	0.000	0.000	yes	Lognormal distribution
OSEBERG	04.12.2018	0.00025	0.070	0.000	0.000	yes	Lognormal distribution
OSEBERG	05.12.2018	0.00025	0.020	0.000	0.000	no	Below 10m/s exit velocity (U)
OSEBERG	05.12.2018	0.00025	0.020	0.010	0.000	yes	Lognormal, skewness to the right
OSEBERG	05.12.2018	0.00025	0.020	0.020	0.000	yes	Lognormal distribution
OSEBERG	05.12.2018	0.00025	0.020	0.030	0.000	yes	Lognormal distribution
OSEBERG	05.12.2018	0.00025	0.020	0.040	0.000	yes	Lognormal distribution
OSEBERG	05.12.2018	0.00025	0.020	0.050	0.000	yes	Lognormal distribution
OSEBERG	05.12.2018	0.00025	0.020	0.060	0.000	yes	Lognormal, skewness to the left

OIL	DATE OF EXPERIMENT	NOZZLE DIAMETER (M)	OIL FLOW RATE (L/MIN)	WATER FLOW (L/MIN)	GAS FLOW RATE (L/MIN)	USED FOR RESULTS	COMMENTS
OSEBERG	05.12.2018	0.00025	0.020	0.070	0.000	yes	Lognormal distribution
OSEBERG	04.02.2019	0.00050	0.050	0.000	0.000	no	Below 10m/s exit velocity (U)
OSEBERG	04.02.2019	0.00050	0.075	0.000	0.000	no	Below 10m/s exit velocity (U)
OSEBERG	04.02.2019	0.00050	0.100	0.000	0.000	no	Below 10m/s exit velocity (U)
OSEBERG	04.02.2019	0.00050	0.125	0.000	0.000	no	Bimodal peaks
OSEBERG	04.02.2019	0.00050	0.150	0.000	0.000	no	Bimodal peaks
OSEBERG	04.02.2019	0.00050	0.175	0.000	0.000	no	Bimodal peaks
OSEBERG	04.02.2019	0.00050	0.200	0.000	0.000	no	Bimodal peaks
OSEBERG	05.02.2019	0.00050	0.050	0.000	0.000	no	Below 10m/s exit velocity (U)
OSEBERG	05.02.2019	0.00050	0.050	0.050	0.000	no	Below 10m/s exit velocity (U)
OSEBERG	04.02.2019	0.00050	0.050	0.075	0.000	no	Lognormal distribution. Droplets smaller than predicted due to turbulence in pipe, explanation in discussion
OSEBERG	04.02.2019	0.00050	0.050	0.100	0.000	no	Lognormal distribution. Droplets smaller than predicted due to turbulence in pipe, explanation in discussion.
OSEBERG	04.02.2019	0.00050	0.050	0.125	0.000	no	Lognormal distribution. Droplets smaller than predicted due to turbulence in pipe, explanation in discussion.
OSEBERG	04.02.2019	0.00050	0.050	0.150	0.000	no	Lognormal distribution. Droplets smaller than predicted due to turbulence in pipe, explanation in discussion.
OSEBERG	04.02.2019	0.00050	0.050	0.175	0.000	no	Lognormal distribution. Droplets smaller than predicted due to turbulence in pipe, explanation in discussion.
OSEBERG	04.02.2019	0.00050	0.050	0.200	0.000	no	Bimodal peak.Droplets smaller than predicted due to turbulence in pipe, explanantion to follow
OSEBERG	05.02.2019	0.00050	0.050	0.000	0.050	no	Multimodal peak
OSEBERG	05.02.2019	0.00050	0.050	0.050	0.050	no	Multimodal peak
OSEBERG	05.02.2019	0.00050	0.050	0.075	0.050	no	Multimodal peak
OSEBERG	05.02.2019	0.00050	0.050	0.000	0.075	no	Multimodal peak
OSEBERG	05.02.2019	0.00050	0.050	0.050	0.075	no	Multimodal peak
OSEBERG	05.02.2019	0.00050	0.050	0.075	0.075	no	Multimodal peak
OSEBERG	13.02.2019	0.00050	0.100	0.050	0.000	yes	Small peak to right of normal distribution. Large droplet visible upon image review.
OSEBERG	13.02.2019	0.00050	0.100	0.075	0.000	yes	Lognormal distribution.
OSEBERG	13.02.2019	0.00050	0.100	0.100	0.000	yes	Lognormal distribution.
OSEBERG	13.02.2019	0.00050	0.100	0.125	0.000	yes	Small peak to right of normal distribution. Large droplet visible upon review.

OIL	DATE OF EXPERIMENT	NOZZLE DIAMETER (M)	OIL FLOW RATE (L/MIN)	WATER FLOW (L/MIN)	GAS FLOW RATE (L/MIN)	USED FOR RESULTS	COMMENTS
OSEBERG	13.02.2019	0.00050	0.100	0.150	0.000	no	Bimodal. Droplets too small, insufficient number of particles counted
OSEBERG	13.02.2019	0.00050	0.100	0.175	0.000	no	Droplets too small, insufficient number of particles counted
OSEBERG	13.02.2019	0.00050	0.100	0.200	0.000	no	Droplets too small, insufficient number of particles counted
OSEBERG	13.02.2019	0.00050	0.125	0.000	0.000	yes	Repeated in order to obtain better peak distribution - still bimodal - slow moving droplets stuck to lens visible on images.
OSEBERG	13.02.2019	0.00050	0.150	0.000	0.000	yes	Repeated in order to obtain better peak distribution - still bimodal - slow moving droplets stuck to lens visible on images.
OSEBERG	13.02.2019	0.00050	0.175	0.000	0.000	yes	Repeated in order to obtain better peak distribution - skewed right
OSEBERG	13.02.2019	0.00050	0.200	0.000	0.000	yes	Repeated in order to obtain better peak distribution - skewed right
OSEBERG	21.02.2019	0.00050	0.050	0.075	0.000	no	Droplets smaller than predicted due to turbulence in pipe, explanation in discussion.
OSEBERG	21.02.2019	0.00050	0.050	0.100	0.000	no	Droplets smaller than predicted due to turbulence in pipe, explanation in discussion.
OSEBERG	21.02.2019	0.00050	0.050	0.125	0.000	no	Droplets smaller than predicted due to turbulence in pipe, explanation in discussion.
OSEBERG	21.02.2019	0.00050	0.050	0.150	0.000	no	Droplets smaller than predicted due to turbulence in pipe, explanation in discussion.
OSEBERG	21.02.2019	0.00050	0.050	0.175	0.000	no	Droplets smaller than predicted due to turbulence in pipe, explanation in discussion.
OSEBERG	21.02.2019	0.00050	0.050	0.200	0.000	no	Droplets smaller than predicted due to turbulence in pipe, explanation in discussion.
OSEBERG	21.02.2019	0.00050	0.100	0.050	0.000	no	Droplets smaller than predicted due to turbulence in pipe, explanation in discussion.
OSEBERG	21.02.2019	0.00050	0.100	0.075	0.000	no	Droplets smaller than predicted due to turbulence in pipe, explanation in discussion.
OSEBERG	21.02.2019	0.00050	0.100	0.100	0.000	no	Droplets smaller than predicted due to turbulence in pipe, explanation in discussion.
OSEBERG	21.02.2019	0.00050	0.100	0.125	0.000	no	Droplets smaller than predicted due to turbulence in pipe, explanation in discussion.
GRANE	06.12.2018	0.00050	0.050	0.000	0.000	no	Grane oil immediately clogged the 0.00025m nozzle and flow was inconsistent with 0.00050m nozzle until flow rates of 100mL/min achieved. Results not included and no further experiments performed with Grane.
GRANE	6.12.2018	0.00050	0.075	0.000	0.000	no	Grane oil immediately clogged the 0.00025m nozzle and flow was inconsistent with 0.00050m nozzle until flow rates of 100mL/min achieved. Results not included and no further experiments performed with Grane.
GRANE	06.12.2018	0.00050	0.100	0.000	0.000	no	Grane oil immediately clogged the 0.00025m nozzle and flow was inconsistent with 0.00050m nozzle until flow rates of 100mL/min achieved. Results not included and no further experiments performed with Grane.

OIL	DATE OF EXPERIMENT	NOZZLE DIAMETER (M)	OIL FLOW RATE (L/MIN)	WATER FLOW (L/MIN)	GAS FLOW RATE (L/MIN)	USED FOR RESULTS	COMMENTS
GRANE	06.12.2018	0.00050	0.125	0.000	0.000	no	Grane oil immediately clogged the 0.00025m nozzle and flow was inconsistent with 0.00050m nozzle until flow rates of 100mL/min achieved. Results not included and no further experiments performed with Grane.
GRANE	06.12.2018	0.00050	0.150	0.000	0.000	no	Grane oil immediately clogged the 0.00025m nozzle and flow was inconsistent with 0.00050m nozzle until flow rates of 100mL/min achieved. Results not included and no further experiments performed with Grane.
NJORD	30.01.2019	0.00050	0.050	0.000	0.000	no	Difficulty for SilCam to distinguish oil droplets due to light color. See discussion.
NJORD	30.01.2019	0.00050	0.075	0.000	0.000	no	Difficulty for SilCam to distinguish oil droplets due to light color. See discussion.
NJORD	30.01.2019	0.00050	0.100	0.000	0.000	no	Difficulty for SilCam to distinguish oil droplets due to light color. See discussion.
NJORD	30.01.2019	0.00050	0.125	0.000	0.000	no	Difficulty for SilCam to distinguish oil droplets due to light color. See discussion.
NJORD	30.01.2019	0.00050	0.150	0.000	0.000	no	Difficulty for SilCam to distinguish oil droplets due to light color. See discussion.
NJORD	30.01.2019	0.00050	0.050	0.025	0.000	no	Difficulty for SilCam to distinguish oil droplets due to light color. See discussion.
NJORD	30.01.2019	0.00050	0.050	0.050	0.000	no	Difficulty for SilCam to distinguish oil droplets due to light color. See discussion.
NJORD	30.01.2019	0.00050	0.050	0.075	0.000	no	Difficulty for SilCam to distinguish oil droplets due to light color. See discussion.
NJORD	30.01.2019	0.00050	0.050	0.100	0.000	no	Difficulty for SilCam to distinguish oil droplets due to light color. See discussion.
NJORD	30.01.2019	0.00050	0.050	0.125	0.000	no	Difficulty for SilCam to distinguish oil droplets due to light color. See discussion.
NJORD	30.01.2019	0.00050	0.050	0.150	0.000	no	Difficulty for SilCam to distinguish oil droplets due to light color. See discussion.
NJORD	30.01.2019	0.00050	0.050	0.175	0.000	no	Difficulty for SilCam to distinguish oil droplets due to light color. See discussion.
NJORD	30.01.2019	0.00050	0.050	0.200	0.000	no	Difficulty for SilCam to distinguish oil droplets due to light color. See discussion.

Appendix C

MiniTower oil droplet experiments
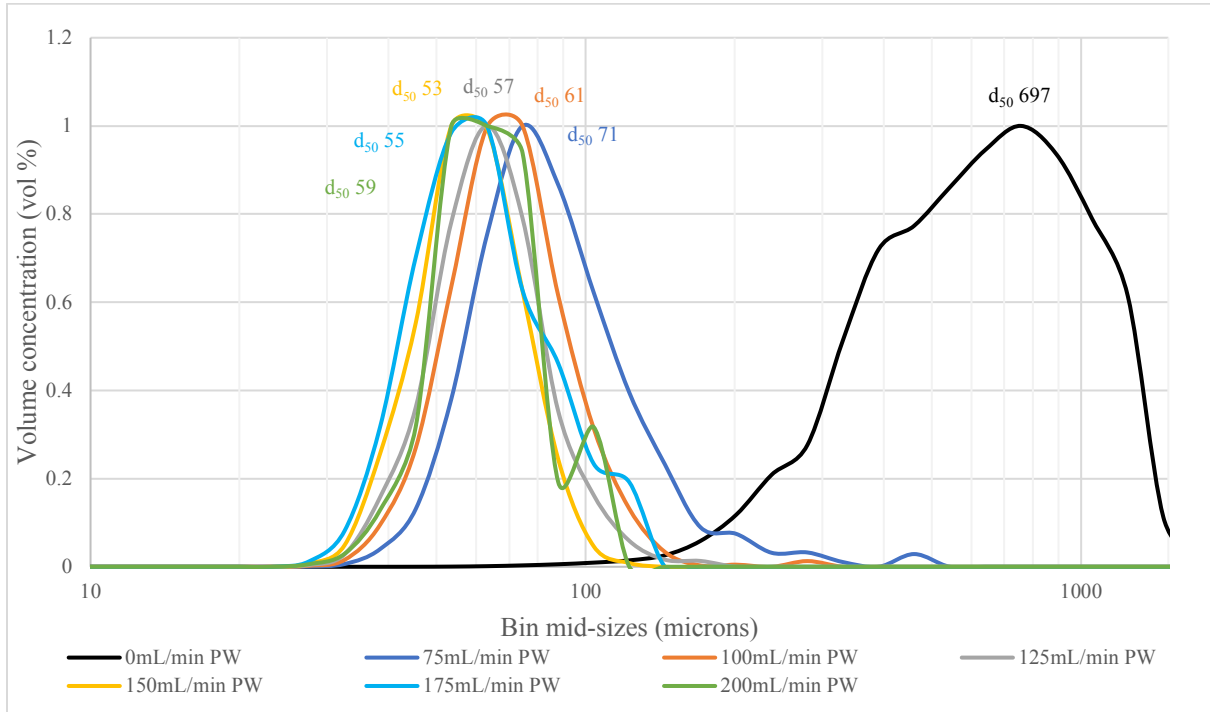
Figure 1 Oseberg Blend 2017, 0.50mm nozzle, oil flow 50mL/min, produced water flow 75-200mL/min.
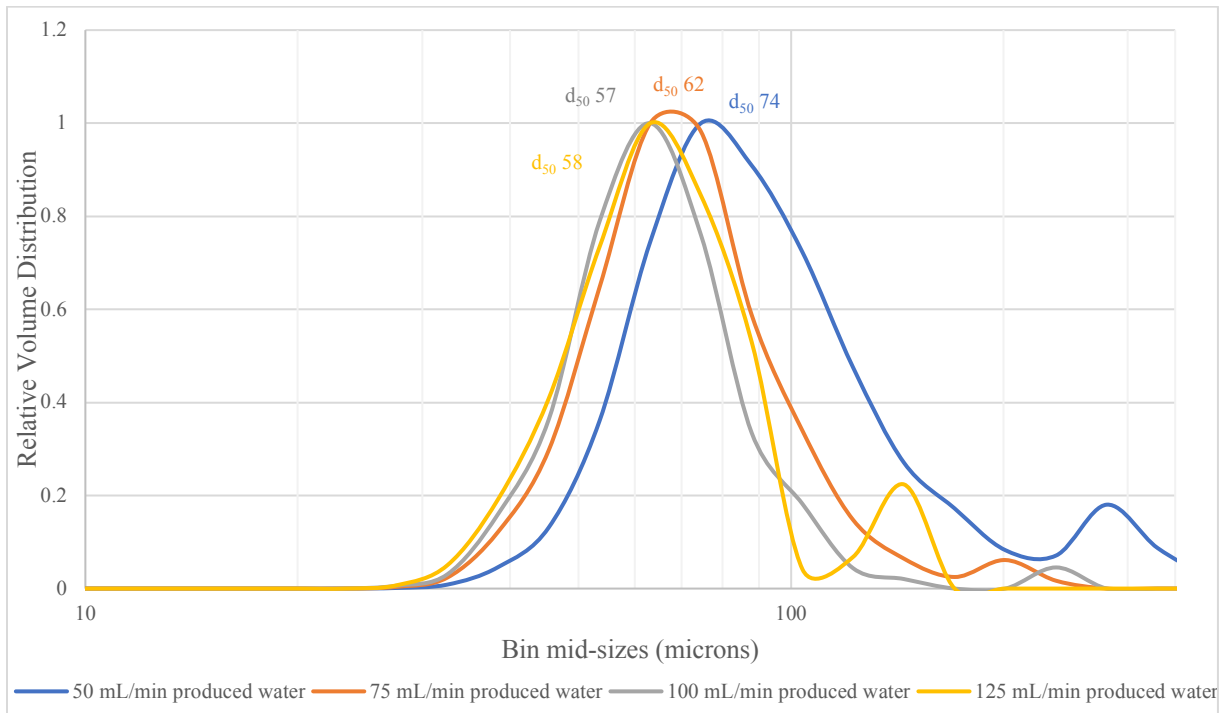
Figure 2 Oseberg 2017, 0.50mm nozzle, oil flow 100mL/min, produced water flow 50–125mL/min.

Appendix D

The following pages contain data from the OSCAR modelling scenarios. The figures describe the surface thickness time series.
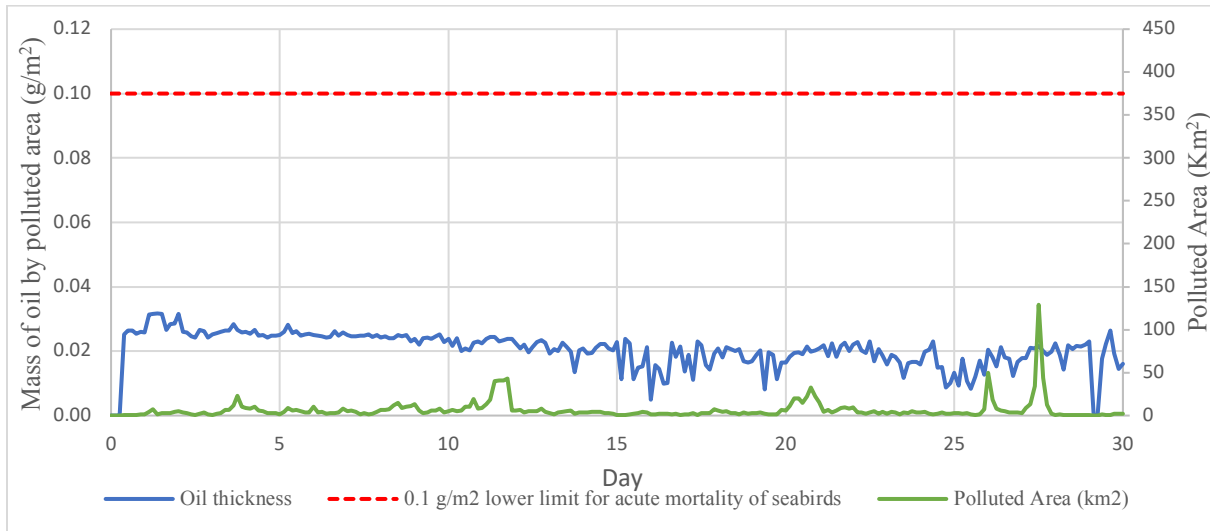
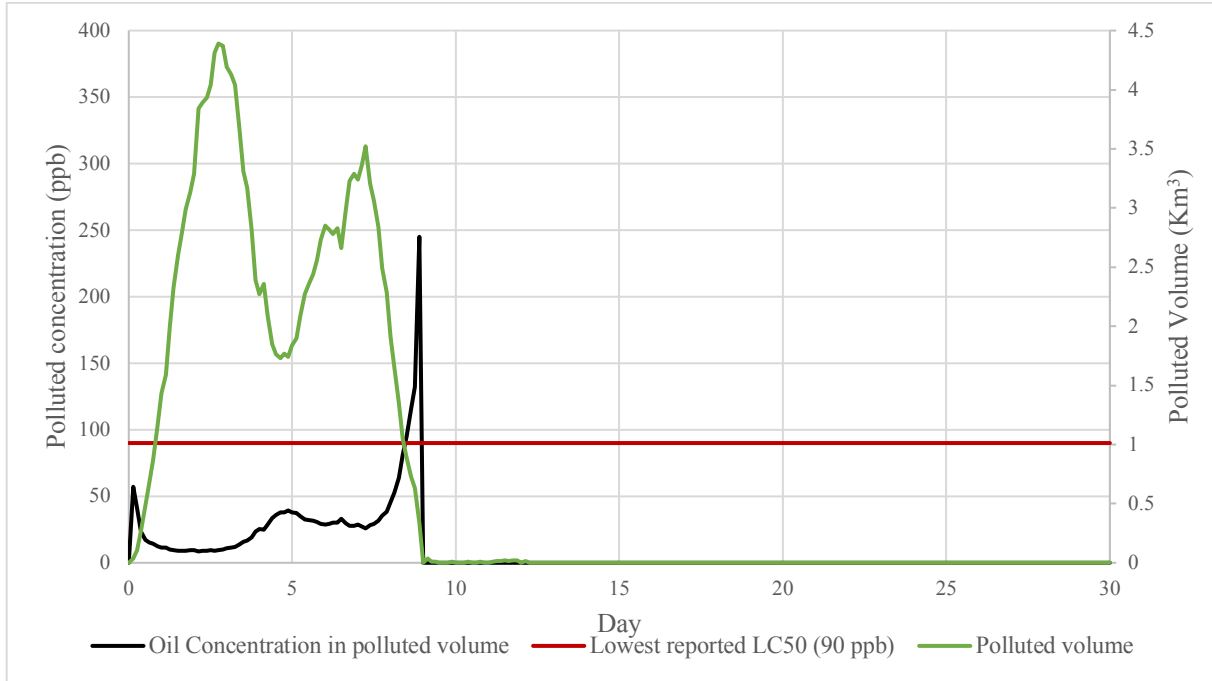*Figure 3 Surface thickness time series, small pipeline leak, winter.*
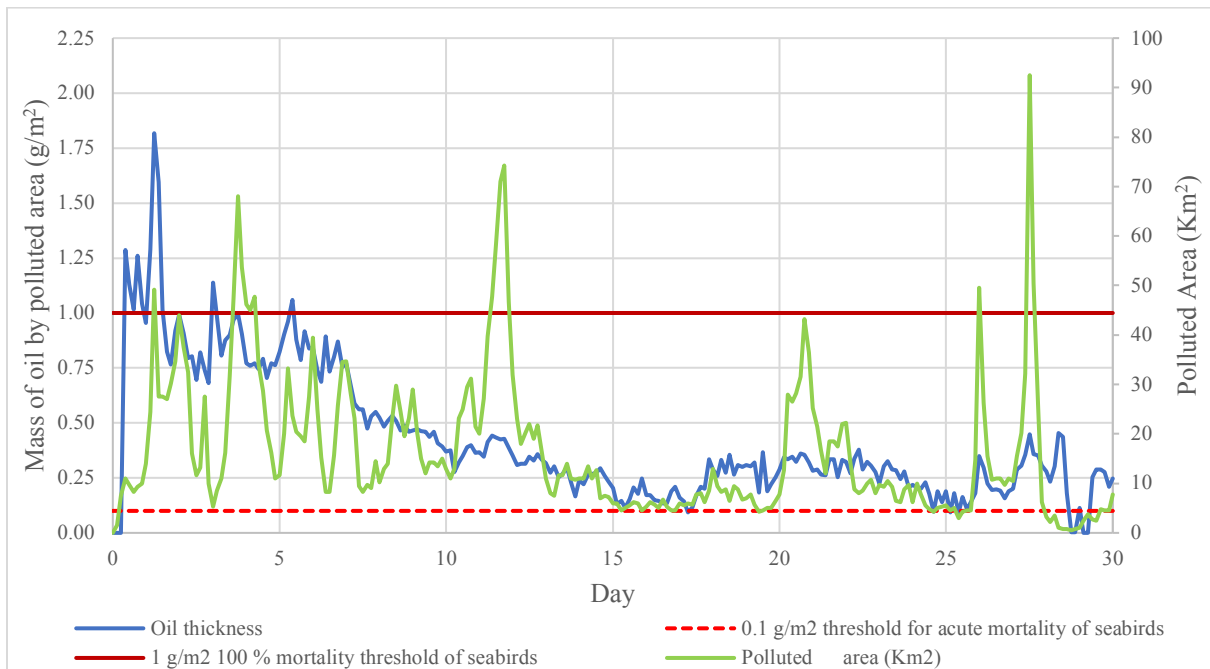
Figure 4 Surface thickness time series, medium pipeline leak, winter.
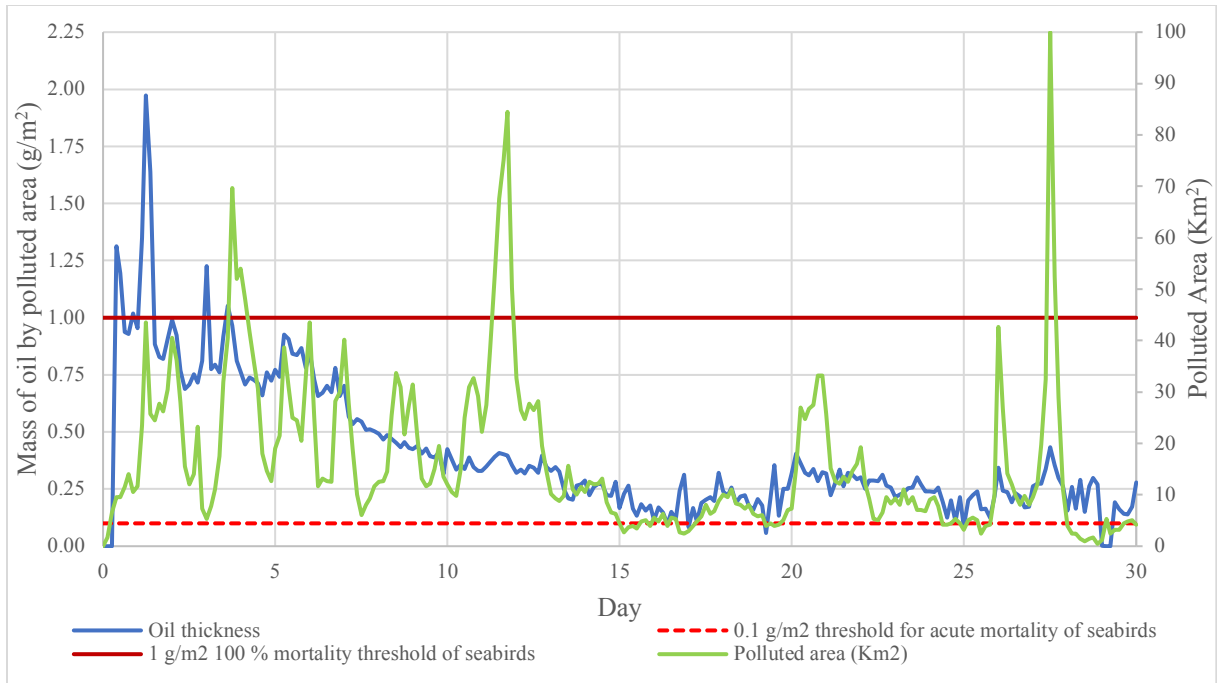
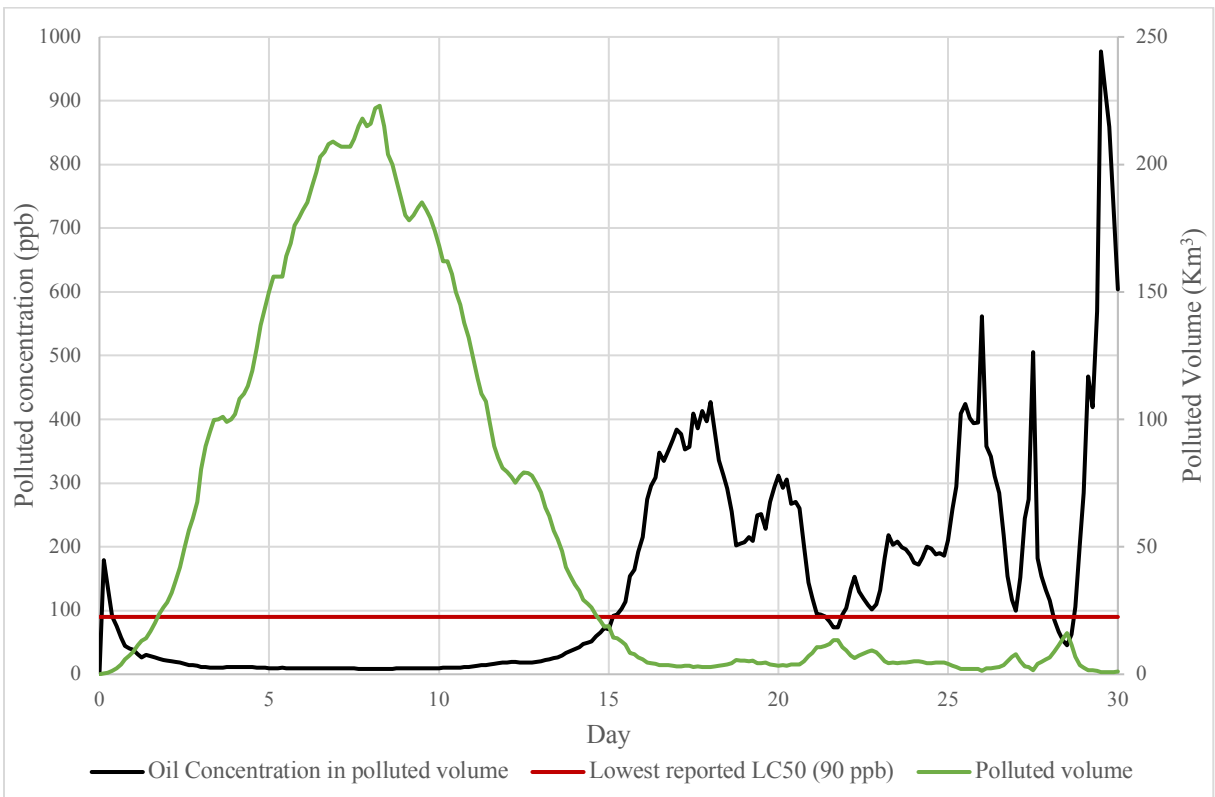*Figure 5 Surface thickness time series, medium pipeline leak, mechanical recovery, winter.*
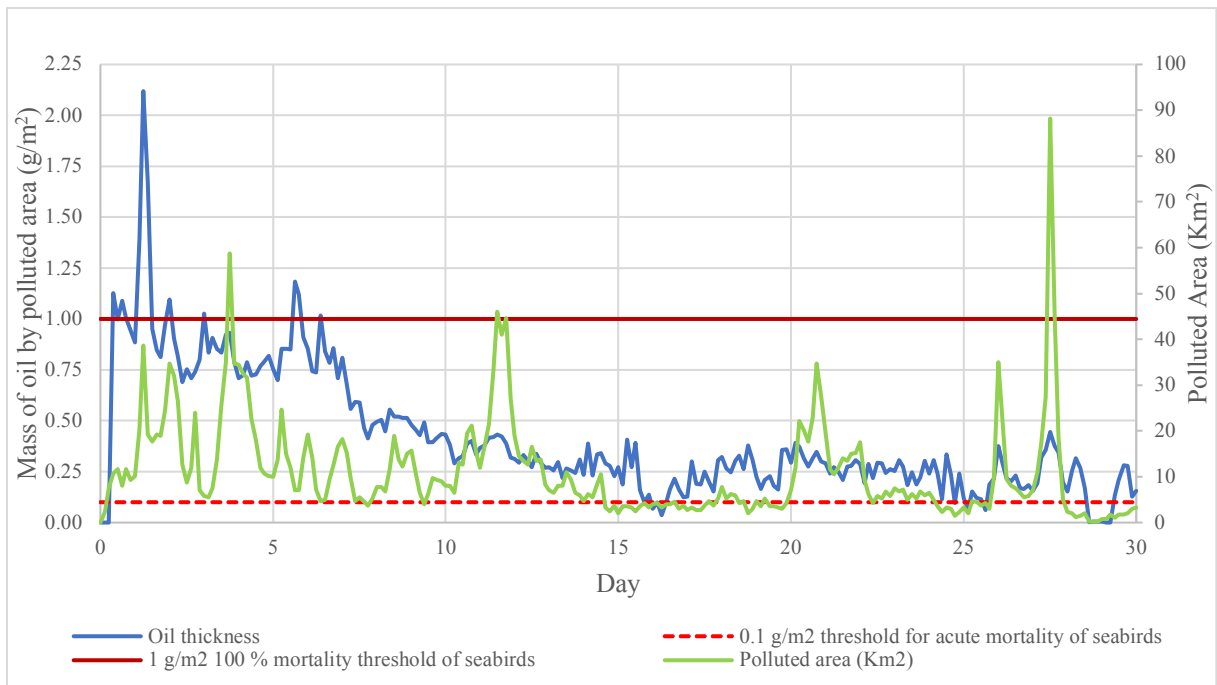
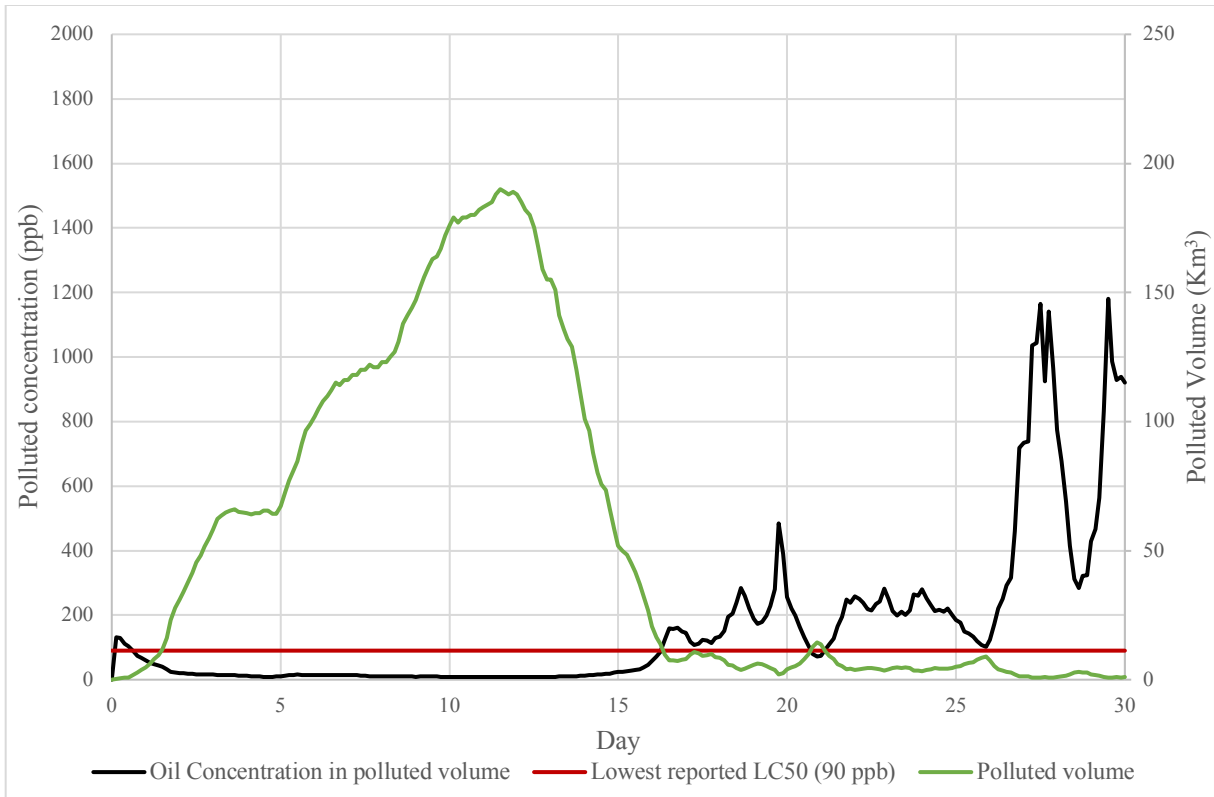*Figure 6 Surface thickness time series, medium pipeline leak, chemical response, winter*
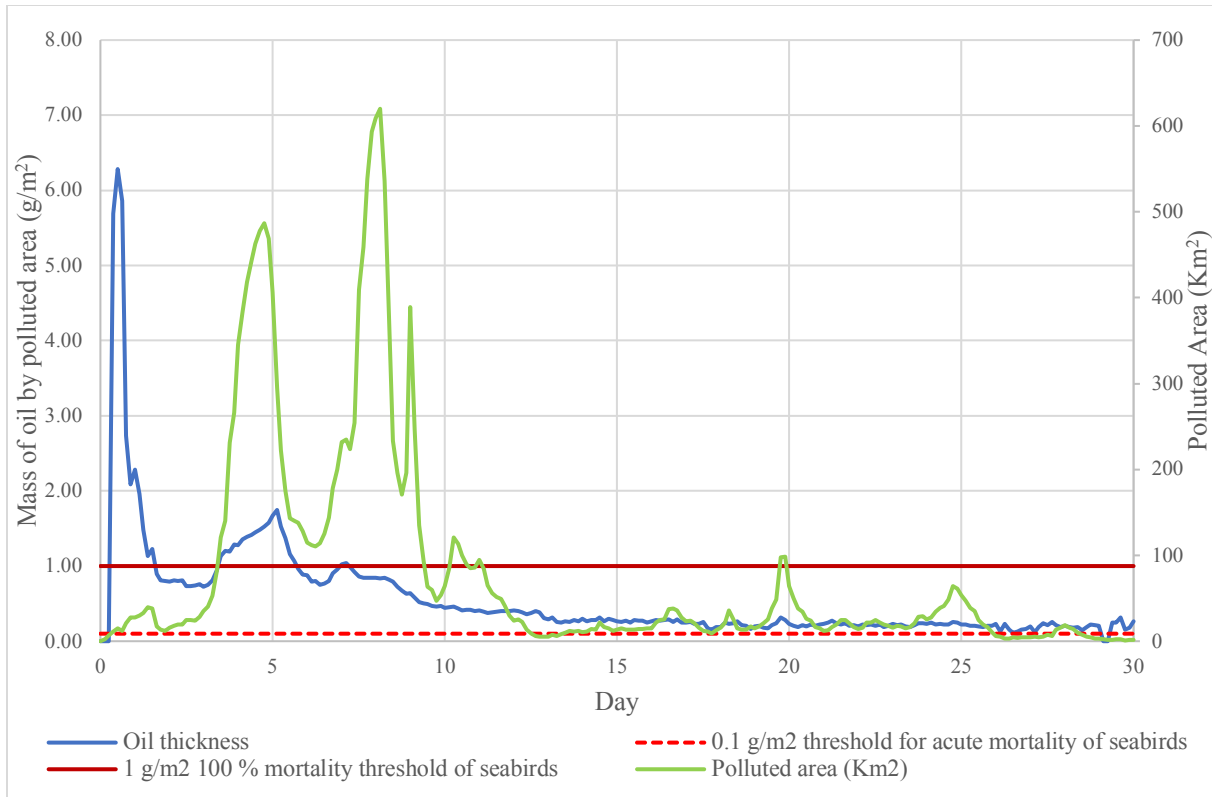
Figure 7 Surface thickness time series, medium pipeline leak, mechanical recovery, summer.
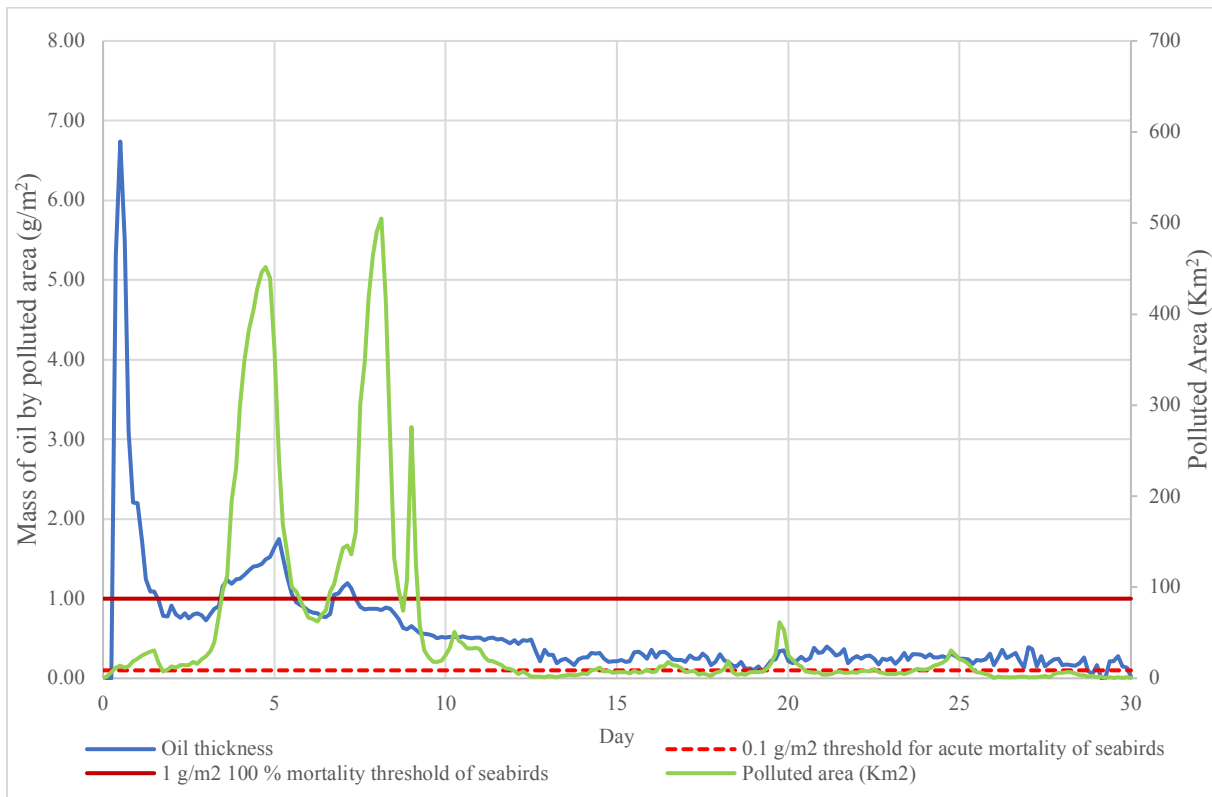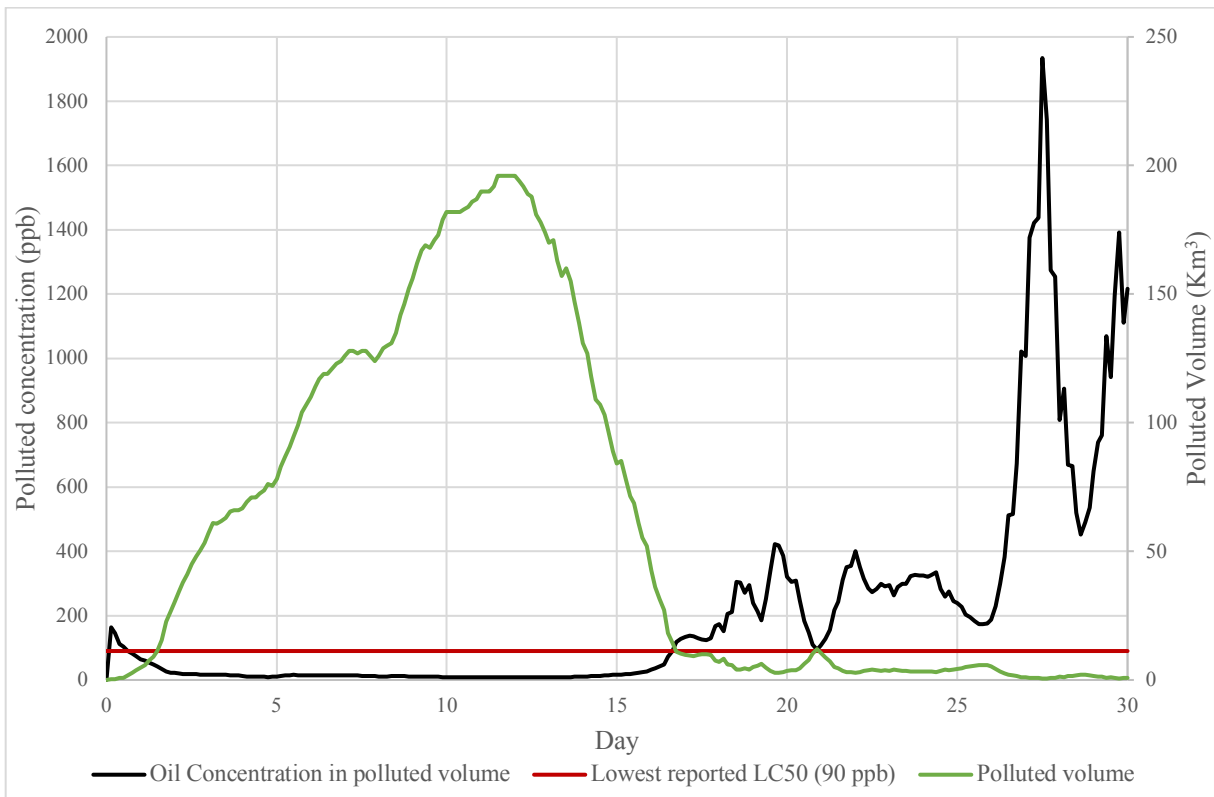

Figure 8 Surface thickness time series, medium pipeline leak, chemical response, summer
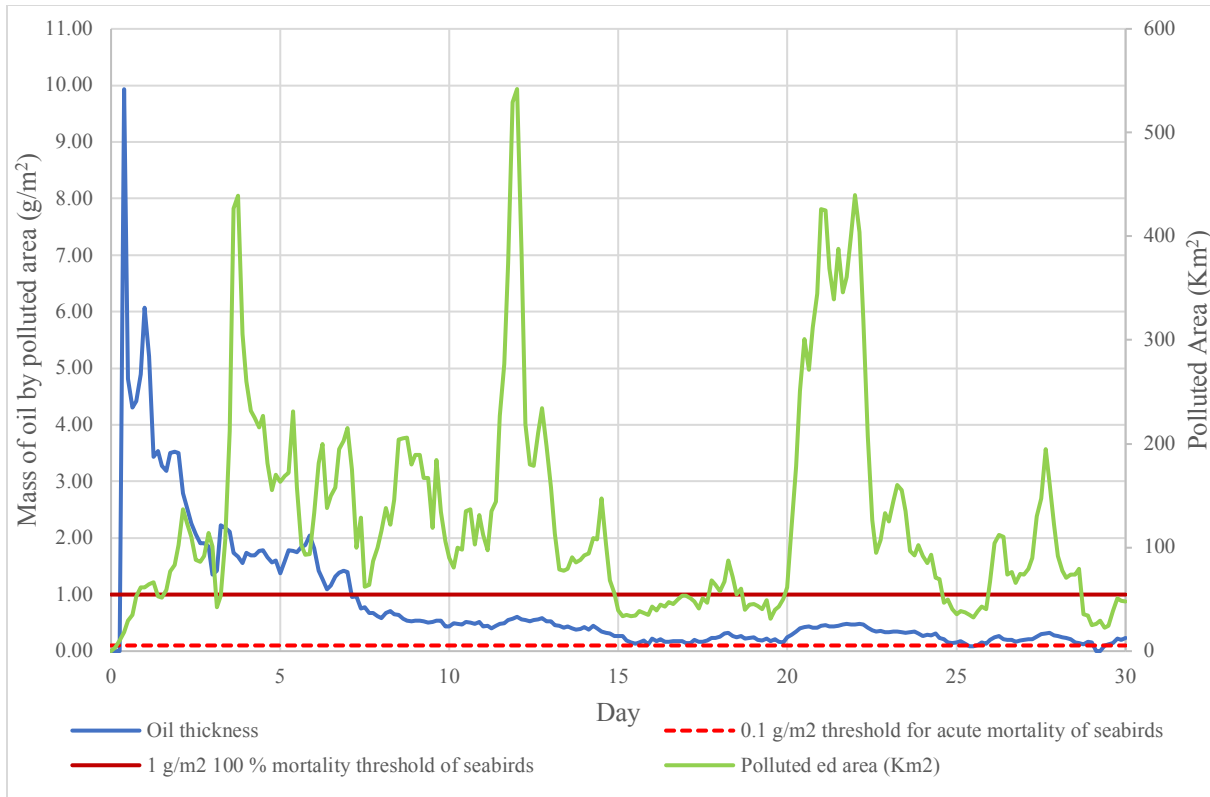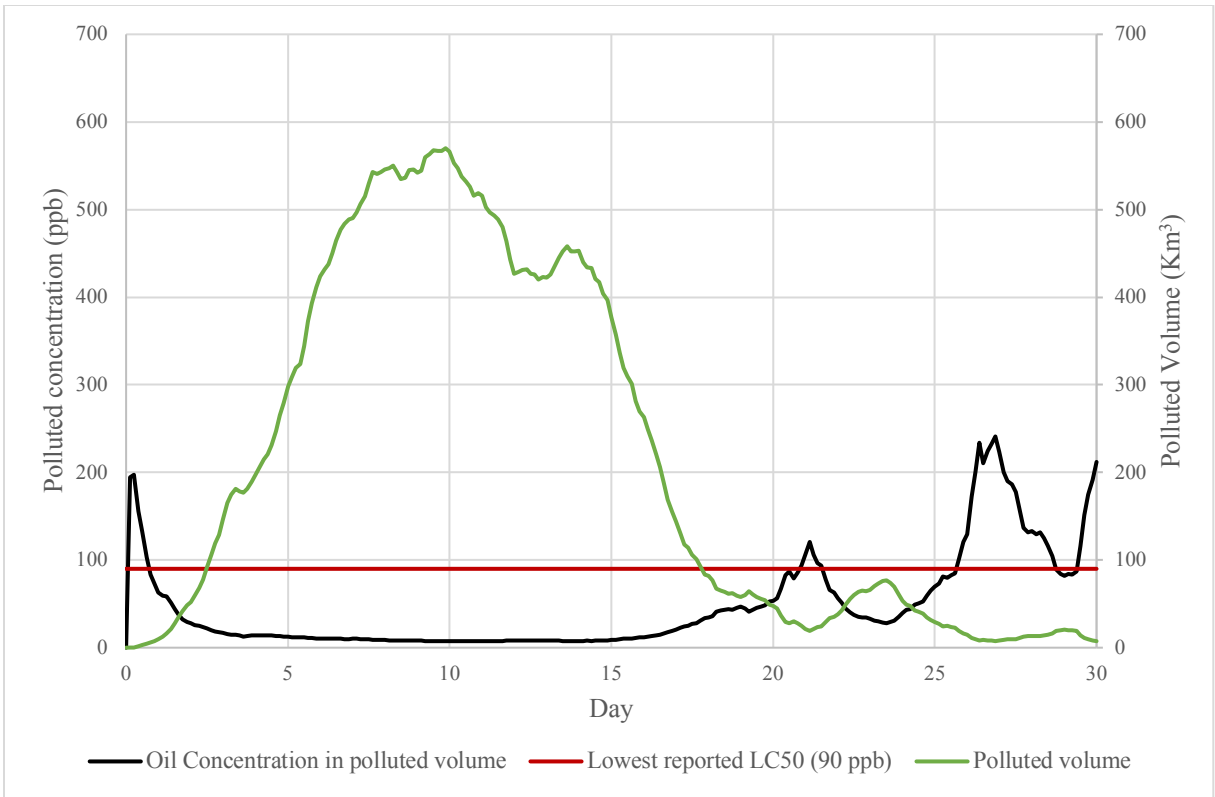
Figure 9 Surface thickness time series, blowout, winter.
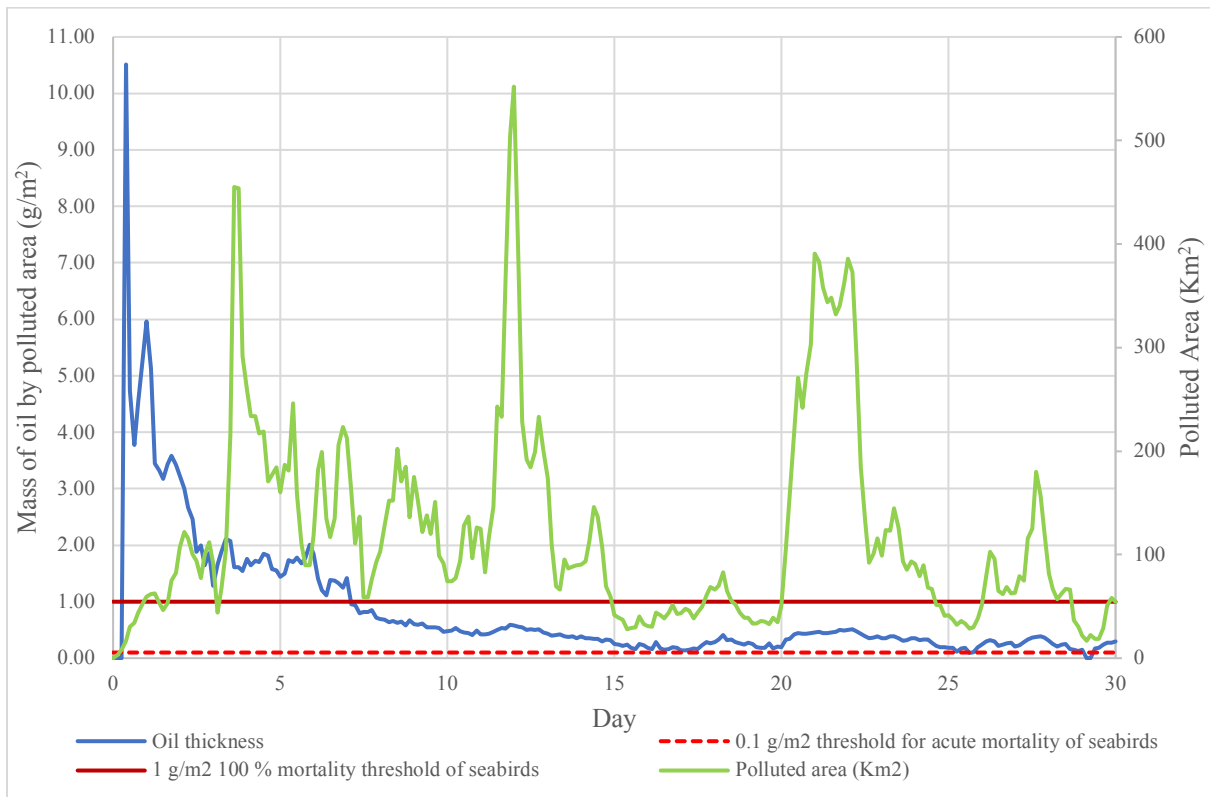
Figure 10 Surface thickness time series, blowout, mechanical recovery, winter.
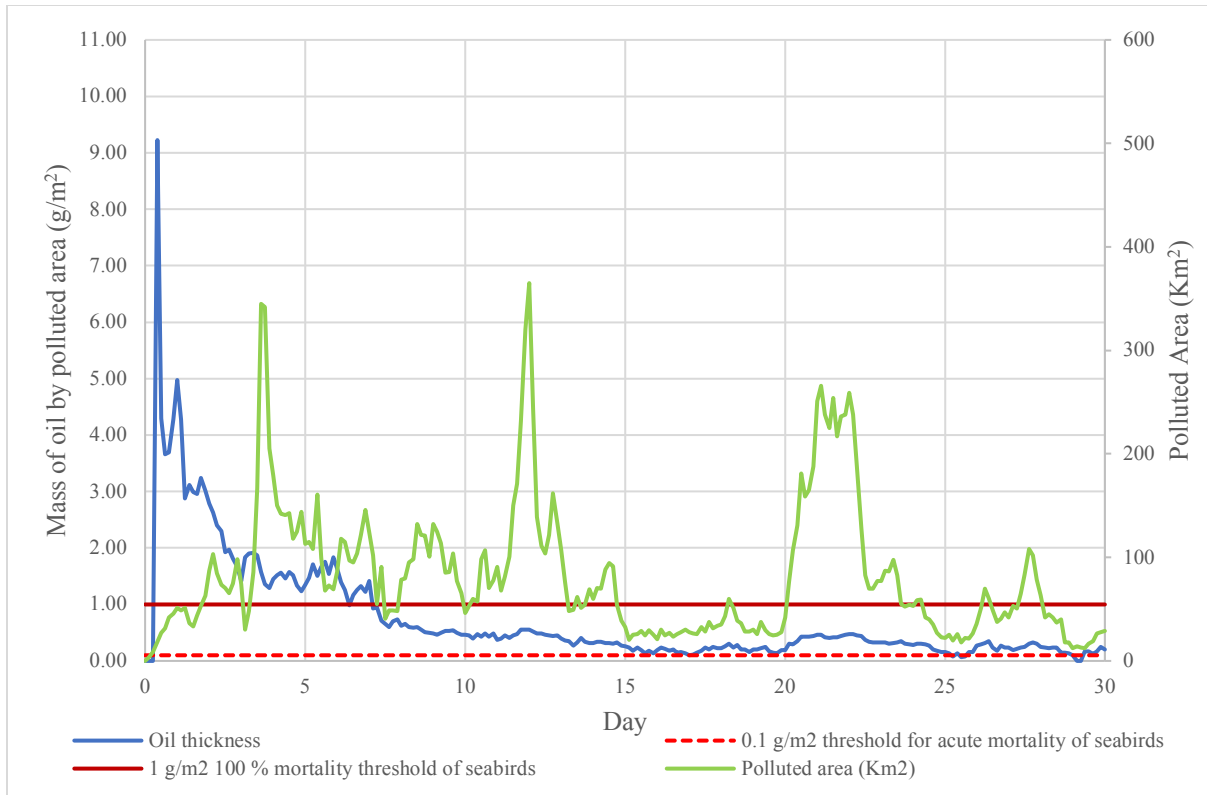
Figure 11 Surface thickness time series, blowout, chemical response, winter.
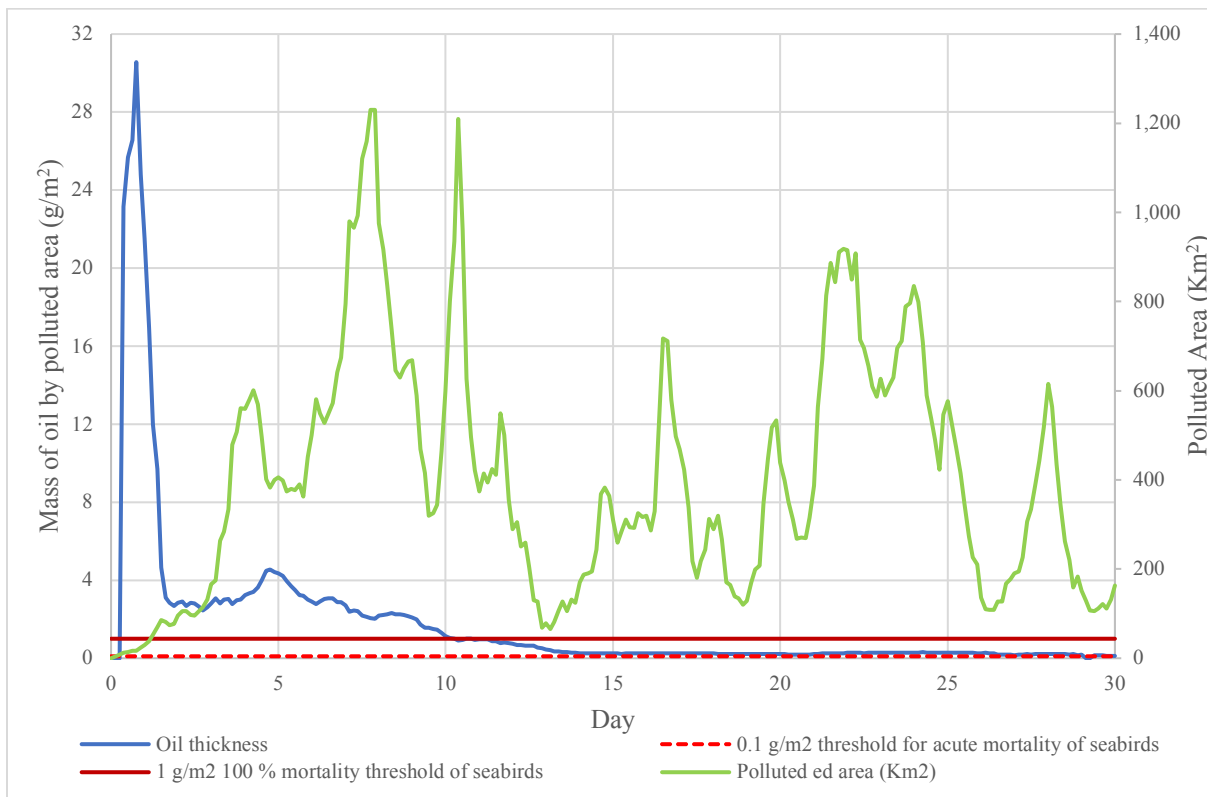
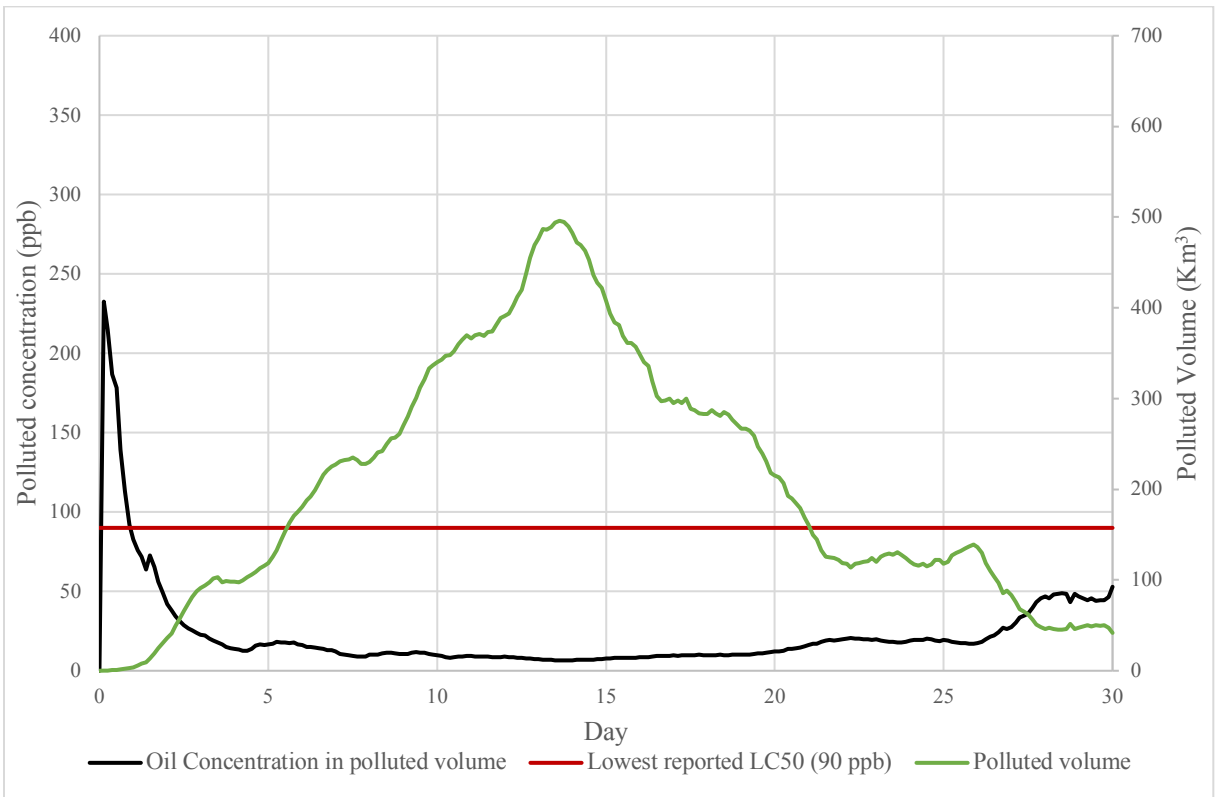*Figure 12 Surface thickness times series, blowout, mechanical recovery, summer.*

Appendix E

The following pages contain data from the OSCAR modelling scenarios. The figures describe the water column concentration time series.

Figure 13 Concentration time series, small pipeline leak, winter.
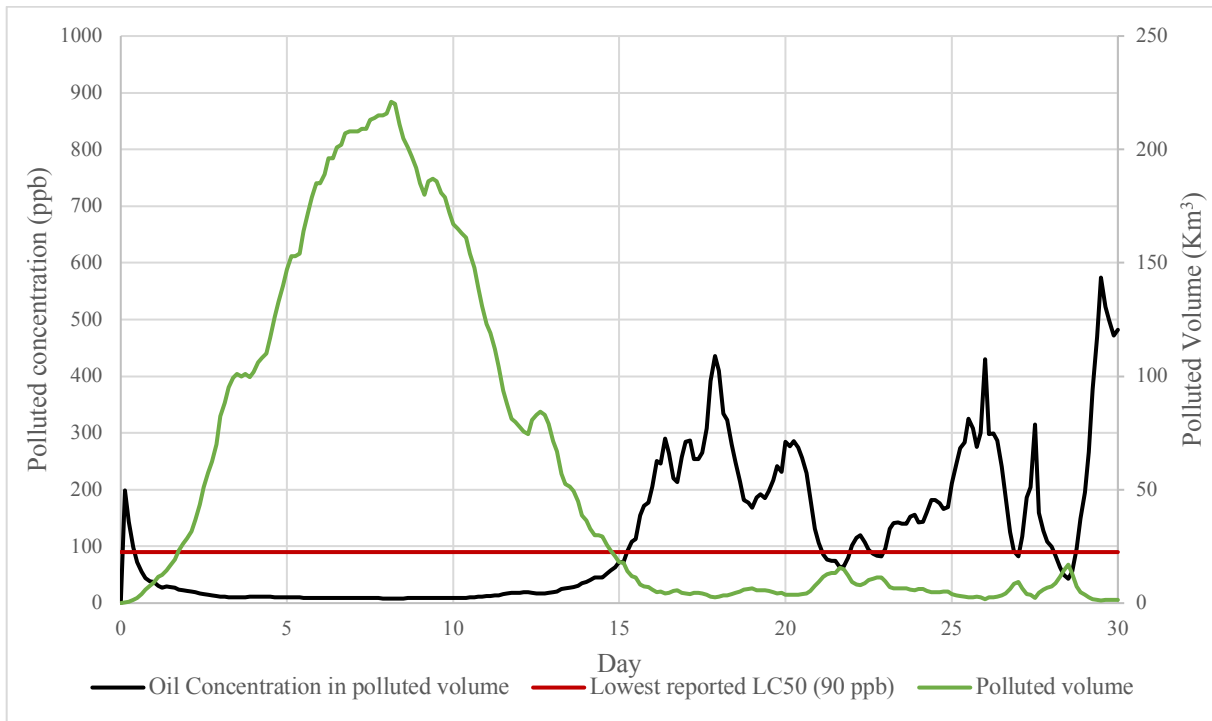
Figure 14 Concentration time series, medium pipeline leak, winter.
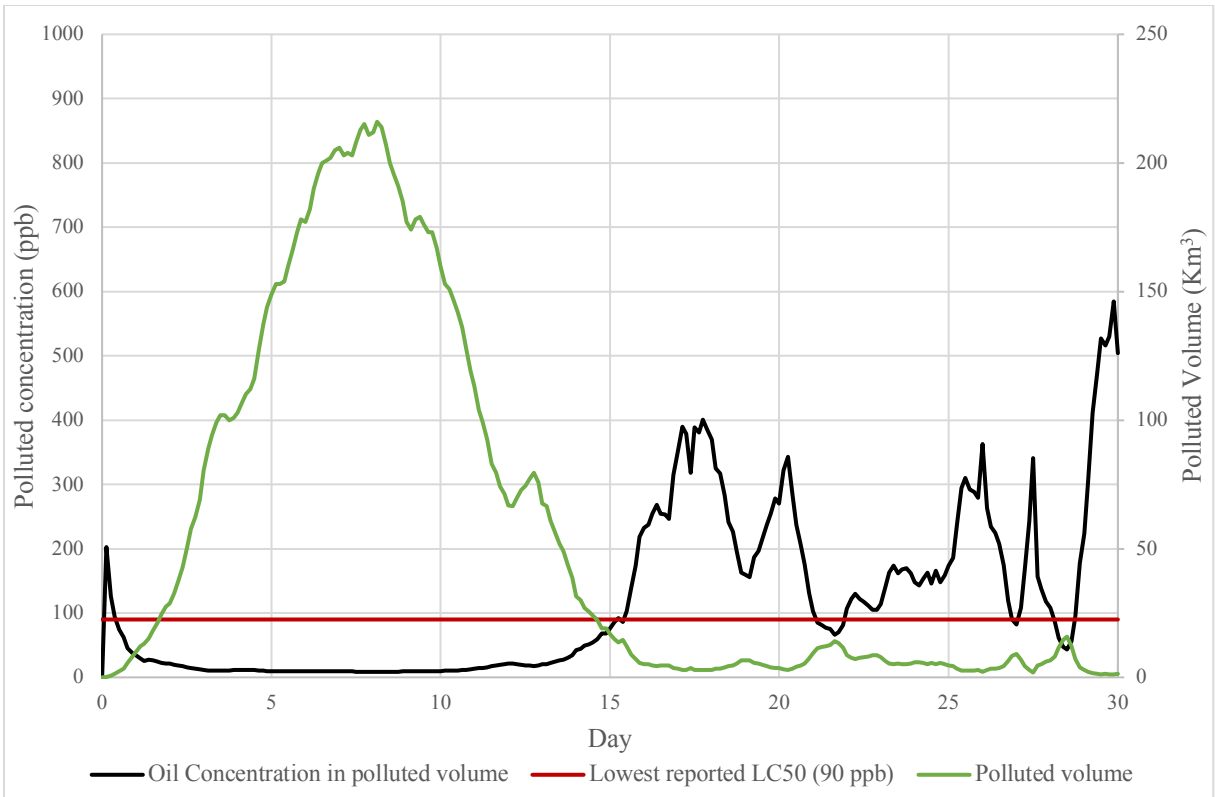
Figure 15 Concentration time series, medium pipeline leak, mechanical recovery, winter.

Figure 16 Concentration time series, medium pipeline leak, chemical response, winter.

Figure 17 Concentration time series, medium pipeline leak, mechanical recovery, summer.

Figure 18 Concentration time series, medium pipeline leak, chemical response, summer.

Figure 19 Concentration time series, blowout, winter.
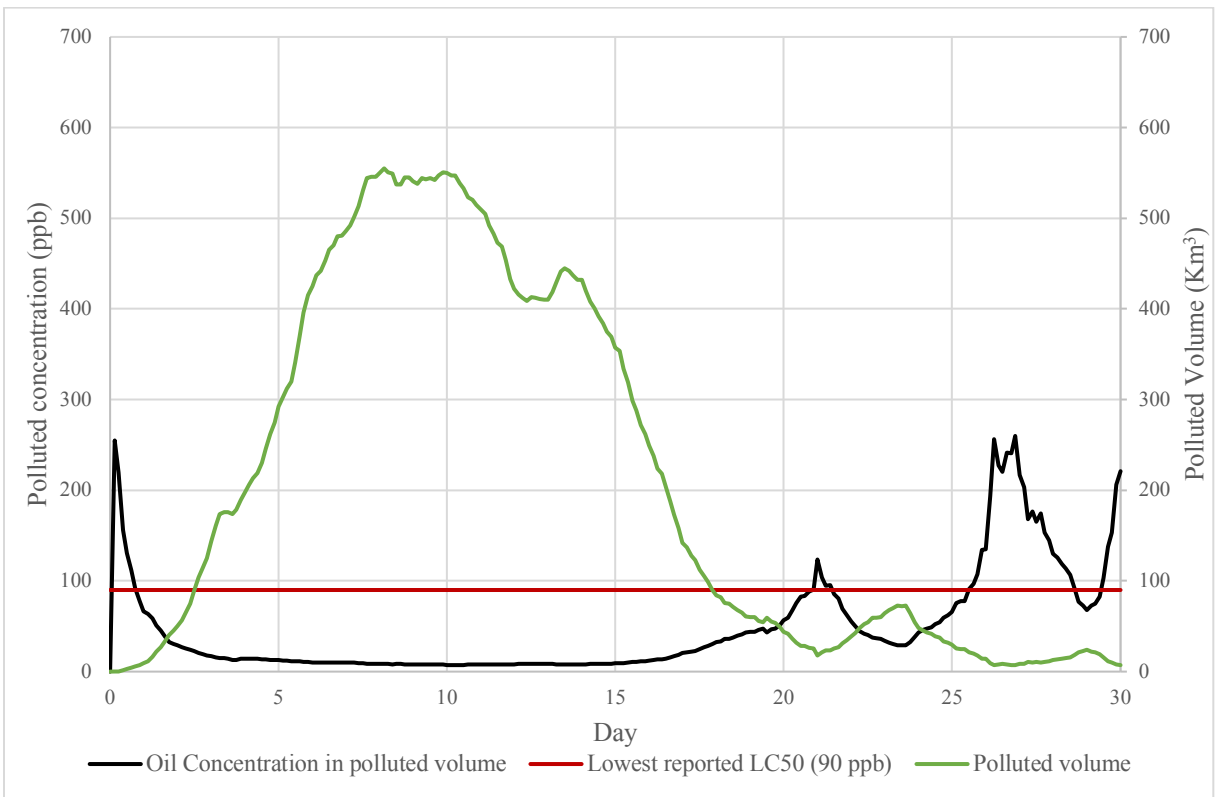
Figure 20 Concentration time series, blowout, mechanical recovery, winter.
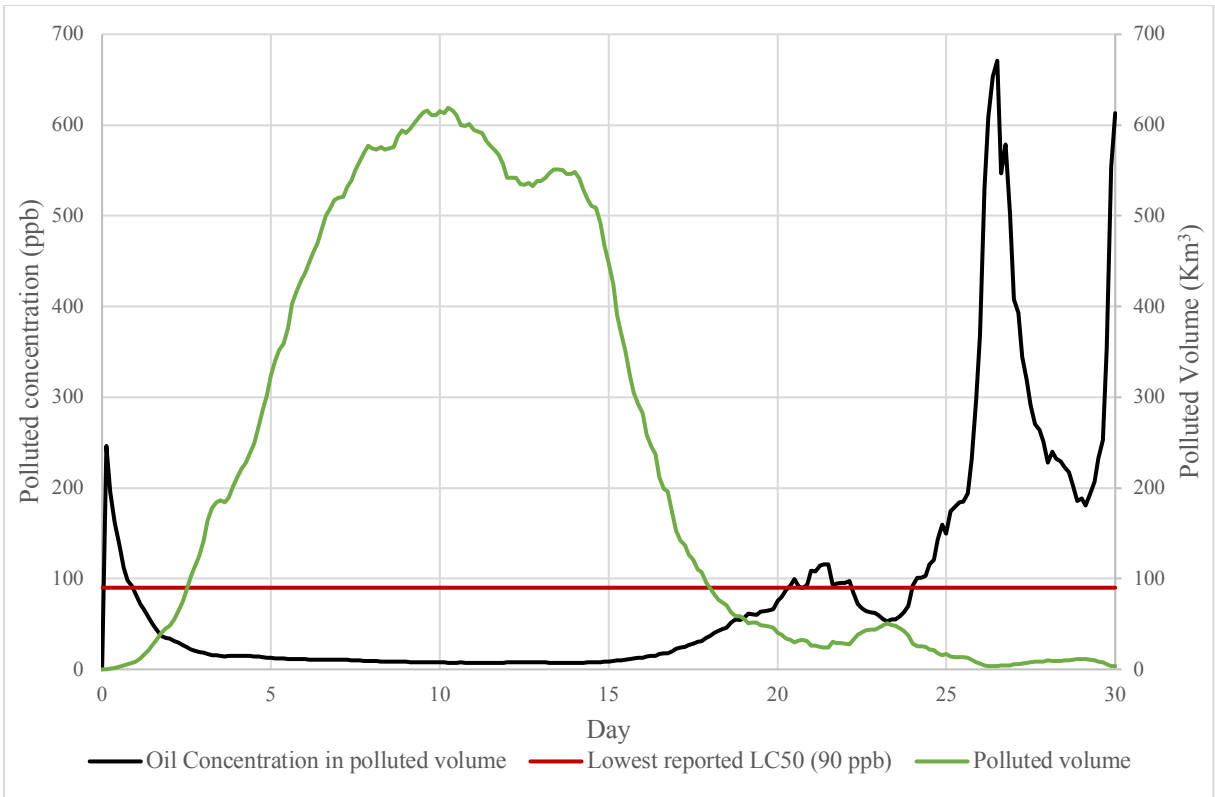
Figure 21 Concentration time series, blowout, chemical response, winter.

Figure 22 Concentration time series, blowout, mechanical recovery, summer.

Appendix F

The following pages contain images from the OSCAR modelling scenarios. The figures describe the shoreline hits for each scenario.
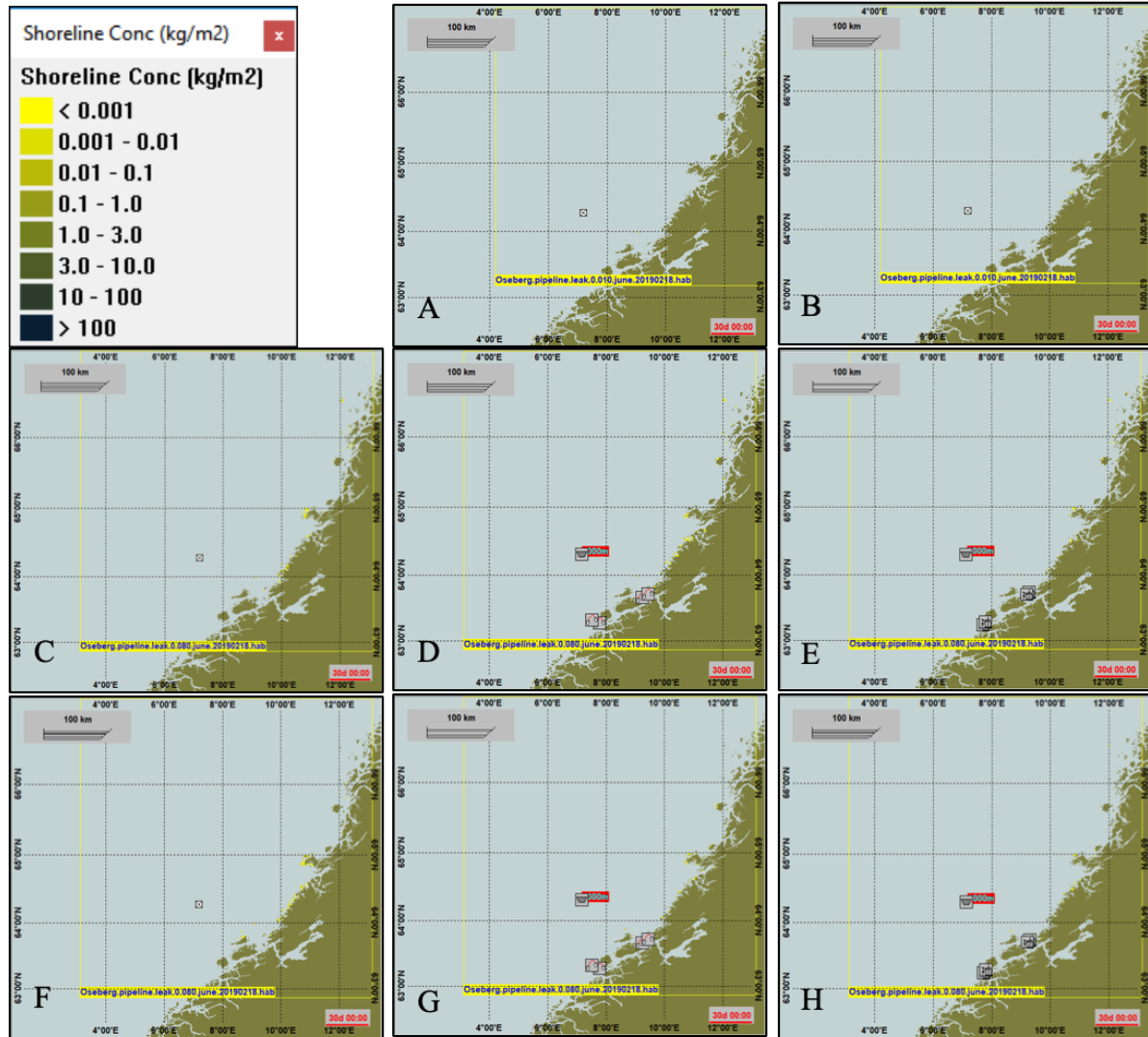

Figure 23 Shoreline concentration of oil in each scenario. The small pipeline releases had minimal shoreline hits, regardless whether the previous or new Weber constants were used for droplet sizes. A) small pipeline release, winter B) small pipeline release, summer C) medium pipeline release, winter D) medium pipeline release, winter, mechanical E) medium pipeline release, winter, chemical F) medium pipeline release, summer G) medium pipeline release, summer, mechanical H) medium pipeline release, summer, chemical
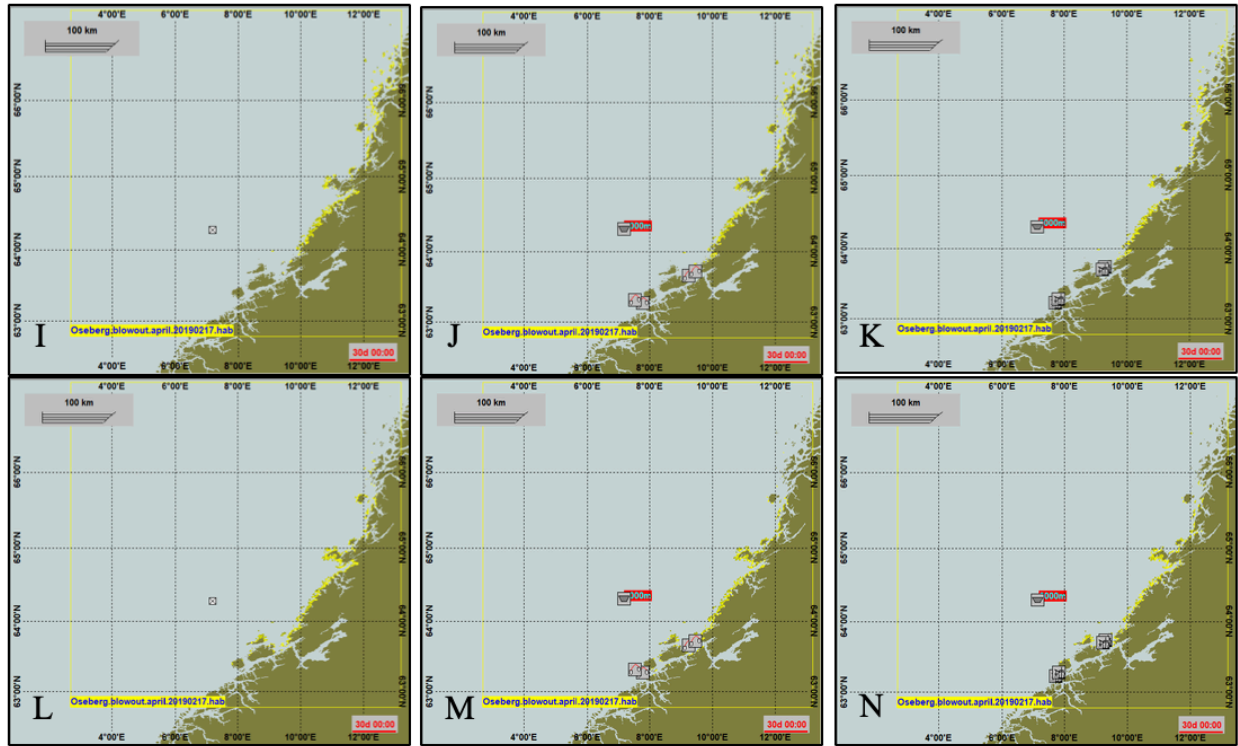
Figure 24 Shoreline concentration of oil in each scenario. I) Blowout, winter J) Blowout, winter, mechanical K) Blowout, winter, chemical L) Blowout, summer M) Blowout, summer, mechanical N) Blowout, summer, chemical

Appendix G

The following pages contain data from the OSCAR modelling scenarios. The figures describe the surface thickness and water column concentration time series for the Winter small pipeline releases using the new empirically obtained values for A and B.
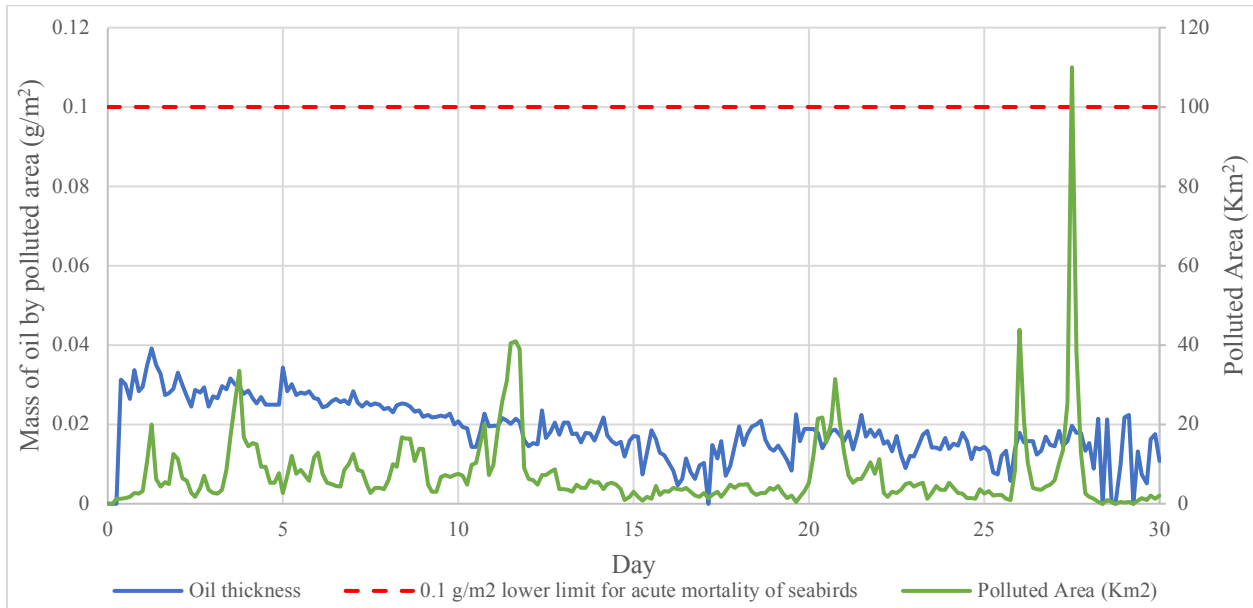

Figure 25 Surface thickness for winter small pipeline releases. Using the values of A and B obtained in the experimental portion of this thesis.
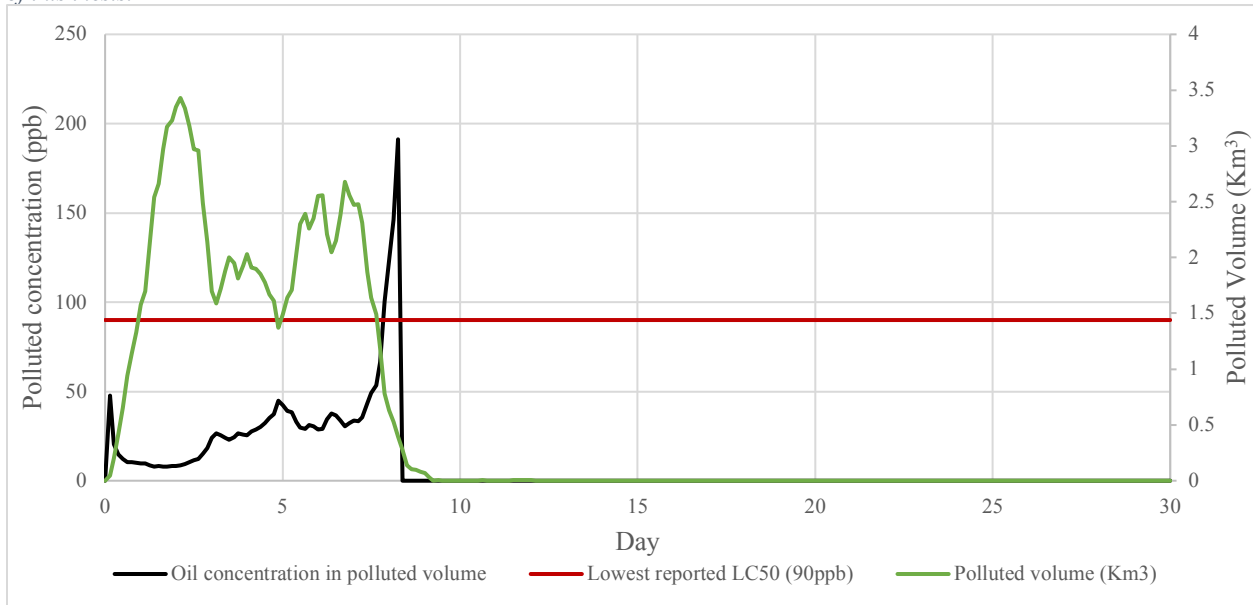

Figure 26 Polluted volume for winter small pipeline releases. Using the values of A and B obtained in the experimental portion of this thesis.

Appendix H

Residual plots for selected regressions of predicted vs. measured droplet sizes for different values of A and B.
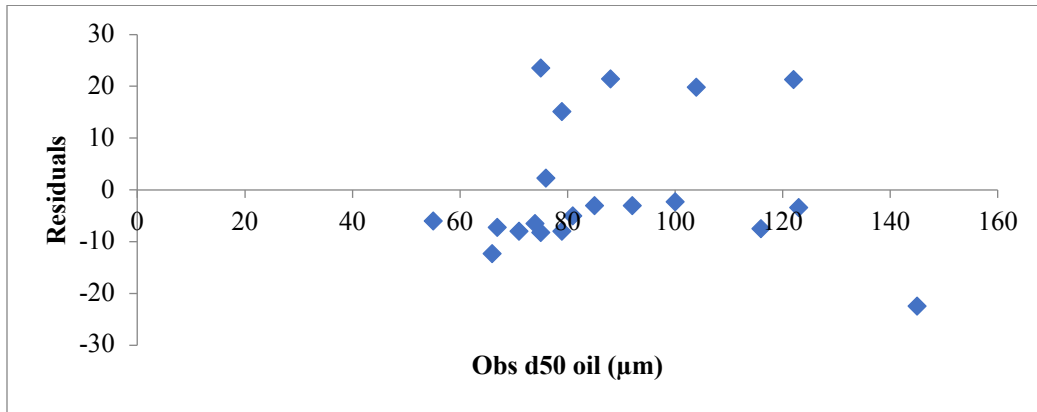

Figure 27 Residual Plot for regression of predicted vs. measured droplet sizes when A 8.5 and B 7.68.
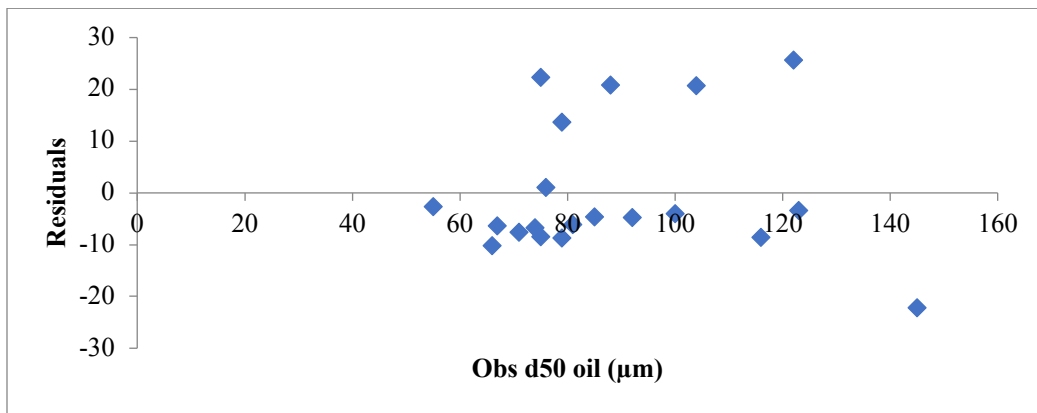

Figure 28 Residual Plot for regression of predicted vs. measured droplet sizes when A 24.6 and B 0.08.
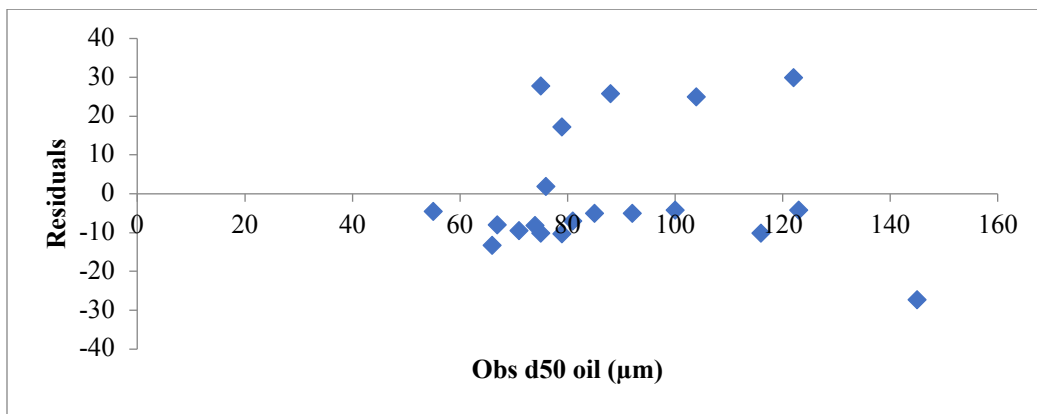

Figure 29 Residual Plot for regression of predicted vs. measured droplet sizes when A 24.6 and B 0.68.

Appendix I

Safe Job Analysis

<table>
<tr><td colspan="2">NTNU

HMS</td><td colspan="2">Hazardous activity identification processes</td><td>Risikovurderi</td><td>Nummer</td><td>Dato</td><td></td></tr>
</table>

NTNU HMS	Hazardous activity identification processes	Risikovurderi	Nummer	Dato
		HMS-avd.	HMSRV2601	2011-03-22
		Godkjent av	Side	Erstatter
		Rektor		2006-12-01

Unit: *Department of Chemistry*   **Date:**   9. October 2017

Line manager: *Hallstein Hemmer*

Participants in the risk assessment (incl.their fuction)

                 P.J. Brandvik (supervisor) & R. McKay (student)

Short description of main activity/main process   *Work under supervision in SINTEF laboratories*

Signatures

ID nr.	Activity/process	Responsible person	Existing documentations	Exisiting safty measures	Lows, regulations etc	Comments
1	Handling Chemicals	PJB	Lab Procedures	PPE (gogles/gloves)		will be given training at SINTEF
2	Operating lab equipment	PJB	Lab Procedures	PPE (gogles/gloves/coat)		will be given traing at SINTEF
3	Tripping & Falling	PJB	Lab procedures	PPE (helmet/shoes)		will be given training at SINTEF
4	Fire	PJB	SINTEF Evacuation Procedures	Fire exits and safety training		will be given training at SINTEF
5						
6						

Risk value = Liklihood + consequence, in the form we normally use the one for human, e.g. B2

Liklihood		Consequence				
Grading	Criteria	Grading		Human	External environment, Water, soil and air	Economy / materials
1	Minimal: Once every 50 year or less	E	Very critical	May produce fatality/ies	Very prolonged, non-reversible damage	Shutdown of work >1 year.
2	Low: Once every 10 years or less	D	Critical	Permanent injury, may produce serious serious health damage/sickness	Prolonged damage. Long recovery time	Shutdown of work 0.5-1 year.
3	Medium: Once a year or less	C	Dangerous	Serious personal injury	Minor damage. Long recovery time	Shutdown of work < 1 month
4	High: Once a month or less	B	Relatively safe	Injury that requires medical treatment	Minor damage. Short recovery time	Shutdown of work < 1week
5	Very high: Once a week	A	Safe	Injury that requires first aid	Minor damage. Short recovery time	Shutdown of work < 1day

Unit:
Line manager:
Participants in the risk assessment (incl.their fuction)

Short description of main activity/main process

Department of Chemistry **Date:** 9. October 2017

Hallstein Hemmer

P.J. Brandvik (supervisor) & R. McKay (student)
Work under supervision in SINTEF laboratories

Signatures

ID nr.	Activity from the identification process form	Potential undesirable incident/strain	Likelihood (1-5)	Consequence Human (A-E)	Enviroment (A-E)	Economy/ material (A-E)	Reputation (A-E)	Risk value human	Comments/ status Suggested measures
1	Handling Chemicals	exposure	1	B	B	A	A	B1	work under supervision
2	Operating lab equipment	damage	1	B	B	A	A	B1	work under supervision
3	Tripping & Falling	damage	2	A	B	A	A	A2	work under supervision
4	Fire	damage	1	B	B	C	A	B1	work under supervision
5									
6									

MATRIX FOR RISKASSESSMENTS at NTNU

Color	
Red	Unacceptable risk, action must be taken before work can start
Yellow	Action must be considered
Green	Acceptabel risk

Rosalie Dawn McKay

Experimental and modelling study of subsea oil releases

NTNU
Kunnskap for en bedre verden